Dose Constraints for important Organs at Risk in the Head and Neck Region for Carbon Ion Radiotherapy optimized with the Local Effect Model I (LEM I)

Jon Espen Dale

Thesis for the degree of Philosophiae Doctor (PhD)
University of Bergen, Norway
2021

UNIVERSITY OF BERGEN

Dose Constraints for important Organs at Risk in the Head and Neck Region for Carbon Ion Radiotherapy optimized with the Local Effect Model I (LEM I)

Jon Espen Dale

Thesis for the degree of Philosophiae Doctor (PhD)
at the University of Bergen

Date of defense: 25.03.2021

Year: 2021

Title: Dose Constraints for important Organs at Risk in the Head and Neck Region for Carbon Ion Radiotherapy optimized with the Local Effect Model I (LEM I)

Name: Jon Espen Dale

Print: Skipnes Kommunikasjon / University of Bergen

Erratum

For Paper I, in the process from manuscript to published article, an error has occurred in the *Introduction* section:

*"The properties of radiation therapy (RT) also seem to affect the risk of CB because rates as high as 8.4% to 15% are observed in reirradiation with hypofractionated stereotactic body RT (SBRT)[4-6] in contrast to **≥4%** with more conventional fractionated photon regimens.[2,7]"*

The correct sentence is as follows:

*"The properties of radiation therapy (RT) also seem to affect the risk of CB because rates as high as 8.4% to 15% are observed in reirradiation with hypofractionated stereotactic body RT (SBRT)[4-6] in contrast to **<4%** with more conventional fractionated photon regimens.[2,7]"*

Scientific environment

This project has been a collaborative work supervised by clinicians within the Department of Oncology and Medical Physics, Haukeland University Hospital, and leading clinicians within carbon ion radiotherapy at The National Center for Oncological Hadrontherapy (CNAO), Pavia, Italy, the National Institute of Radiological Sciences (NIRS), Chiba, Japan, and The Gunma University Heavy Ion Medical Center (GHMC), Gunma, Japan.

The candidate has been affiliated with the Ph.D. educational program of the University of Bergen, Norway, within the Department of Clinical Science, Faculty of Medicine.

About 15 months of the project period was spent at CNAO, for the purpose of acquiring an understanding of clinical particle therapy. At that time, more than 1000 patients had been treated with particle therapy there, the vast majority with carbon ions. CNAO has an ongoing close companionship/collaboration with the National Institute of Radiological Sciences in Chiba, Japan, which is the world's leading institution for carbon ion radiotherapy. CNAO has based most of their carbon ion radiotherapy protocols on the vast Japanese experience. Of particular importance to the PhD project, CNAO has a strong community of medical physicists and radiation oncologists with expertise on comparison of different RBE models for dose prescription in carbon ion radiotherapy and on treatment plan recalculations. The candidate has also had shorter visits at both NIRS and GHMC during the period.

Acknowledgements

I wish to express my heartfelt gratitude towards my main supervisor, Olav Dahl. I'm grateful that you invited me into your field of research many years ago. You have been enthusiastic and supportive since the dawning of this project through to its final conclusion. Your life-long dedication to cancer research and your academic merits are truly inspiring, as is your dauntless approach to engage in new fields of research.

I am forever grateful to Piero Fossati, for entrusting me with this project and for introducing me the world of particle therapy. Your vital and dynamic guidance has been essential. Your in-depth and wide understanding of the various technical, biological and clinical aspects of particle therapy is astonishing, so is your ability to communicate your knowledge to others.

I am sincerely thankful to Tatsuya Ohno and Tadashi Kamada for their efforts as co-supervisors for this project. Thank you for your immediate support for this project from its initiation, and for valuable advice along the way. Your openness in welcoming me to GHMC and NIRS has been essential for my understanding of the carbon ion therapy. Thank you for your dedication to share your vast experience.

I would like to thank everyone at CNAO for their meticulous efforts to collect the medical data used for this project. Additionally, I am grateful for the hospitality and friendliness offered to my family and me during our stay in Pavia. Cordial thanks to Silvia Molinelli for always being available and for providing substantial support without delay throughout the whole project. To Vivana Vitolo, Barbara Vischioni, Maria Bonora and Elisa Ciurlia I am grateful for fruitful discussions and day to day assistance. Thank you to Giuseppe Magro and Andrea Mairani for helping me understand more of the technical details related to the RBE models and recalculation methods. I am also grateful for the all the help and support, including pleasant conversations in the lunch canteen, provided by Mario Ciocca, Alessandro Vai, Edoardo Mastella, Kyungdon Choi and Alfredo Mirandola.

I am most grateful to Odd Harald Odland for your crucial role in facilitating the initiation of this project. It may never have started without you.

I truly appreciate the opportunity I was given by Olav Mella to execute this project through the support of the Department of Oncology and Medical Physics. Furthermore, I would like to thank Ása Karlsdottir and my colleagues in the clinic for extending me the opportunity to finish the thesis. Also I wish to thank Helge Pettersen, Liv Hysing, Camilla Stokkevåg and Sara Pilskog for support and discussions.

I am deeply grateful to my dear parents and brother for unconditional love throughout life. Special thanks to my father for persistent interest in the project.

Finally, a big embrace goes to my dear Anne-Grethe, and to our dear children, Mari and Torstein. I could not have done this without your understanding and support. You fill my heart with love and happiness, thus reminding me what really matters in life.

Abbrevations

CHO	Chinese Hamster Ovary cell
CIRT	Carbon ion Radiotherapy
CNAO	National Center for Oncological Hadrontherapy, Pavia, Italy
CNS	Central Nervous System
CT	Computed Tomography
CTCAE	Common Terminology Criteria for Adverse Events
$CumDmax_{EQD2}$	Cumulative maximum EQD2
$CumDmax_{nom}$	Cumulative nominal maximum dose
DICOM	Digital Imaging and Communications in Medicine
$D_{LEM\ I}$	RBE weighted dose optimized with LEM I
D_{NIRS}	RBE weighted dose optimized with the NIRS clinical dose model
DVH	Dose Volume Histogram
EQD2	Equivalent dose if given in fractions of 2 Gy
EUD	Equivalent uniform dose
FU	Follow-up
GHMC	Gunma University Heavy Ion Medical Center, Gunma, Japan
GSI	Gesellschaft für Schwerionenforschung, Darmstadt, Germany
HIT	Heidelberg Ion Beam Therapy Center, Heidelberg, Germany
HSG	Human Salivary Gland tumor cell
ICRU	International Commission on Radiation Units and Measurements
IMPT	Intensity Modulated Particle Therapy
IMRT	Intensity Modulated Radiotherapy
LEM I	Local Effect Model version I

LEM IV	Local Effect Model version IV
LET	Linear Energy Transfer
LKB	Lyman Kutcher Burman model
LQ	Linear Quadratic model
MKM	Microdosimetric Kinetic Model
mMKM	modified Microdosimetric Kinetic Model
MRI	Magnetic Resonance Imaging
NIRS	National Institute of Radiological Sciences, Chiba, Japan
NTCP	Normal Tissue Complication Probability
OAR	Organ at risk
OER	Oxygen Enhancement Ratio
PBS	Pencil beam scanning
QUANTEC	Quantitative Analysis of Normal Tissue Effects in the Clinic
RBE	Relative Biological Effectiveness
re-RT	Re-irradiation
RT	Radiotherapy
SBRT	Stereotactic Body Radiotherapy
SOBP	Spread out Bragg peak
SPHIC	Shanghai Proton and Heavy Ion Center, Shanghai, China
SRS	Stereotactic Radiosurgery
TD5	Tolerance dose threshold for 5% probability of toxicity
TD50	Tolerance dose threshold for 50% probability of toxicity
TPS	Treatment Planning System
V79	Chinese Hamster V79 cell
VMAT	Volumetric Arc Radiotherapy

Abstract

Carbon ion radiotherapy (CIRT) exhibits higher *relative biological effectiveness* (RBE), compared to photon and proton RT. However, there are substantial uncertainties regarding the clinical RBE of carbon ions. Therefore, prescription doses and organ at risk (OAR) dose constraints derived from experience with photon or proton RT may not be applicable to CIRT, and should preferably be derived and validated within the framework of this modality.

Two major approaches have been used for the clinical implementation of CIRT. Japanese centres typically use hypofractionated treatments (e.g. 16 fractions of 3.6 – 4.6 Gy [RBE]) in which prescription doses and OAR constraints initially were defined through carefully conducted dose-escalation trials at the National Institute of Radiological Sciences (NIRS, Japan). The NIRS clinical dose model, originally designed for a passively scattered carbon ion beam, is used to predict the RBE-weighted dose (D_{NIRS}). More than 22.000 patients have been treated at Japanese centres, resulting in several publications addressing tolerance doses or dose constraints for various OARs following D_{NIRS} optimized CIRT.

In contrast, CIRT at the Gesellschaft für Schwerionenforschung (GSI), Darmstadt, Germany, was initiated using moderately hypofractionated schedules (20-22 fractions of 3.0 - 3.5 Gy [RBE]) in which the Local effect model version I (LEM I) was used to predict the RBE. Trusting the LEM I to be sufficiently accurate, dose constraints derived from photon RT was applied. This strategy has been adopted by Heidelberg Ion Beam Therapy Center (HIT) and Marburg Ion Beam Center (MIT) in Germany.

When the National Center of Oncological Hadrontherapy (CNAO, Italy) started treating patients with LEM I optimized CIRT in 2012, it was decided to adopt the successful treatment approach developed at NIRS. However, comparative studies show that the LEM I predicts a 5-15% higher RBE in the spread out Bragg peak (SOBP) of a carbon ion beam, relative to the NIRS clinical dose model. In the entrance region, the RBE predicted by LEM I can be 60% higher. Consequently,

dependent on the clinical indication, prescription doses at CNAO (reported in LEM I weighted dose, $D_{LEM\ I}$) were increased by 5-15% relative to the prescription doses at NIRS (as reported in D_{NIRS}). However, dose constraints to OARs were not adjusted accordingly. This was a cautious approach aimed at avoiding unexpected toxicity due to the lack of validated $D_{LEM\ I}$ constraints. However, it may lead to suboptimal target coverage.

The aim of this thesis was to explore and update $D_{LEM\ I}$ constraints for important organs at risk in the head and neck region. Anonymized data gathered from medical records of consenting patients treated within prospective protocols at CNAO were used in this project. *Paper I* focused on the event of carotid blowout. This rare, but often fatal, complication occurs more frequently after re-irradiation (re-RT) than after primary treatment. High rates (8-15%) have been seen in hypofractionated re-RT using stereotactic body RT (SBRT). Detailed analysis of the relation between the cumulative dose to the carotid artery and carotid blowout has never been published. At CNAO the current practice has been to avoid cumulative equivalent dose in 2 Gy fractions (EQD2) > 120 Gy (RBE) in the re-RT setting. Thus, the medical records of 96 patients re-irradiated with particles (protons: n=17, carbon ions: n=79) at CNAO were analyzed. We found one confirmed, and one possible case of carotid blowout, both amongst the patients receiving proton re-RT. There were no cases recorded among the patients receiving carbon ion re-RT. An actuarial rate of 2.7% for the event was acceptable compared to other studies. For 51% of the patients the cumulative dose to the carotid artery could be calculated. Cases occurred at cumulative EQD2 of 129 Gy (RBE) for the confirmed event, and 107 Gy (RBE) for the possible event. Unfortunately, these data were insufficient to conclude firmly on the relation of cumulative dose and the risk of carotid blowout.

The focus of *Paper II* and *III* was to derive more optimal $D_{LEM\ I}$ constraints for the optic nerve and brainstem applicable for hypofractionated CIRT. For Paper II we analyzed the toxicity outcome and dose distributions of 65 optic nerves in 38 patients treated with CIRT. Visual decline developed in 3 cases, at $D_{LEM\ I|1\%}$>71 Gy (RBE) and $D_{LEM\ I|20\%}$ >68 Gy (RBE), thus far higher than the dose constraints adopted from

NIRS, i.e. $D_{NIRS|1\%} \leq 40$ Gy (RBE) and $D_{NIRS|20\%} \leq 28$ Gy (RBE), respectively. The patient treatment plans were recalculated to D_{NIRS}, and thus a dose translation model was obtained, showing that NIRS constraints of $D_{NIRS\,|\,1\%} \leq 40$ Gy (RBE) and $D_{NIRS\,|\,20\%} \leq 28$ Gy (RBE) corresponded to $D_{LEM\,|\,1\%} \leq 50$ Gy (RBE) and $D_{LEM\,|\,20\%} \leq 40$ Gy (RBE), respectively. However, due to uncertainties in the method, and to cohere with constraints used at GSI/HIT, a more moderate constraint escalation to $D_{LEM\,|\,1\%} \leq 45$ Gy (RBE)/$D_{LEM\,|\,20\%} \leq 37$ Gy (RBE) has been implemented in CNAO clinical routine since October 2018.

Paper III focused on the brainstem, in which CNAO has used the constraint $D_{LEMI|1\%} < 30$ Gy (RBE), in accordance with the original constraint used at NIRS. Due to this conservative approach, CNAO has not even observed asymptomatic brainstem injury following CIRT. A recent dose response analysis from Gunma University Heavy Ion Medical Center (GHMC), Japan, revealed that asymptomatic brainstem lesions did not occur when $D_{NIRS|0.1cm3} < 40$ Gy (RBE) and $D_{NIRS|0.7cm3} < 30$ Gy (RBE). Making use of 30 of the treatment plans recalculated to D_{NIRS} for Paper I, a dose translation model was derived also for these brainstem dose metrics, D_{NIRS} constraints corresponded to $D_{LEM\ I|0.7cm3} < 41$ Gy (RBE) (95% CI: 38-44 Gy [RBE]) and $D_{LEM\ I|0.1cm3} < 49$ Gy (RBE) (95% CI: 46-52 Gy [RBE]). The value corresponding to the lower bound of the 95% CI's were proposed as new constraints.

Overall, this thesis has contributed to knowledge of the risk of carotid blowout after particle re-RT. Moreover, we demonstrated a method to reliably calculate the cumulative dose to this OAR, which hopefully can inspire to future dose-response studies for this important endpoint. A novel approach of creating of a dose translation model to support the proposal of updated $D_{LEM\ I}$ constraints for the optic nerve and brainstem, proved useful, as detailed dose-response data for these OARs following $D_{LEM\ I}$ optimized CIRT is lacking. The new constraints can have an immediate clinical impact in regard to achieving more optimal treatments at CIRT centres applying the LEM I. Finally, the dose translation method can be used to compare and unify carbon ion treatments worldwide.

List of Publications

Dale, J. E., et al. (2017). "Risk of carotid blowout after reirradiation with particle therapy." Advances in Radiation Oncology **2**(3): 465-474.

Dale, J. E., et al. (2019). "Optic nerve constraints for carbon ion RT at CNAO - Reporting and relating outcome to European and Japanese RBE." Radiother Oncol **140**: 175-181.

Dale, J. E., et al. “Brainstem NTCP and dose constraints for carbon ion RT – application and translation from Japanese to European RBE-weighted dose” (accepted for publication in Frontiers in Oncology September 4th 2020).

Reprints of Paper I and II were made with permission from Elsevier Inc. Reprint of Paper III were made with permission from Frontiers Media.

Contents

1. Introduction

Radiotherapy (RT) is, together with surgery and chemotherapy, a cornerstone of modern treatment of malignant tumors. Evidence-based estimates suggest that approximately 50% of all cancer cases optimally should receive radiotherapy at least once after diagnosis (Barton et al. 2014). Of all radiotherapy courses administered in Norway in 2010, 50% were given as part of a curative treatment regimen (Asli et al. 2014), either as the sole treatment modality or in combination with surgery and/or chemotherapy. The key goal of curative radiotherapy is to administer a dose that is high enough to eradicate the malignant cells in the target volume, while at the same time minimizing the doses to the healthy tissues surrounding the target volume, i.e. achieving high conformity of the dose to the target. During the last decades, radiotherapy using photons has evolved from simple treatment fields guided by either anatomical reference points on the patient's surface or 2D X-ray imaging, through 3D conformal radiotherapy, to more sophisticated and highly conformal techniques, e.g. intensity- or volumetric modulated arc radiotherapy (IMRT or VMAT), see **Figure 1.** Stereotactic radiosurgery (SRS) and stereotactic body radiotherapy (SBRT) are other examples of highly conformal techniques, though their current indications are restricted by tumor site and/or extension (volume and shape).

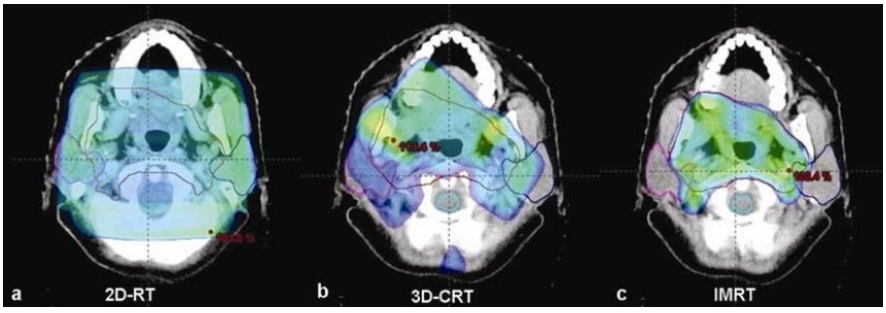

Figure 1: *Axial planning CT slice showing typical dose-wash of (a) conventional radiotherapy (2D-RT), (b) 3D conformal RT and (c) IMRT for a head and neck cancer patient. Note the progressive high-dose conformation to the target volume and sparing of surrounding normal structures. Figure from Tejpal, G., et al. (2010). Reused with permission.*

It is evident that the more conformal techniques have a superior ability to decrease mid-high doses to organs surrounding the target volume, thus decreasing the risk and/or magnitude of organ dysfunction and as a result improving quality of life (Staffurth 2010). However, the drawback of these techniques is that the radiation is given by an increasing number of fields, so that larger volumes of the tissues in the treated region receive a low dose bath. Whether or not this may cause more subtle, but important, long term effects on patients' morbidity and mortality has not been properly investigated, mainly due to the fact that detecting such small differences would require larger cohorts and longer follow-up than what is usually achievable. However, it has been estimated that IMRT, compared to 3D conformal RT, may almost double the incidence of secondary cancers for patients surviving 10 years (Hall and Wuu 2003).

On this background, the rationale for RT using charged particles emerges (i.e. protons or heavier ions), with its capability of delivering equally conformal high dose to the target volume, while minimizing the low dose bath to the healthy tissues. Alternatively, charged particle RT can deliver higher doses to the tumor, thus increasing the chance of cure, without increasing the risk of side effects (Durante, Orecchia, and Loeffler 2017).

In addition to the beneficial macroscopic dose profile, on the microscopic scale particles like protons and heavier ions deposit dose in a spatial and temporal pattern that leads to increased damage in biological systems relative to photon radiation, a phenomenon defined as increased *relative biological effectiveness* (RBE). However, the RBE of one type of radiation relative to another is highly variable, and is modified by changes in parameters such as absorbed dose, linear energy transfer (LET), cell-/tissue type and biological endpoint. For proton RT, the variability of the RBE is mostly so subtle that it is feasible to use a constant RBE of 1.1 (i.e. proton RT is 10% more effective than photon RT) for patient treatments, as recommended by the *International Commission on Radiation Units and Measurements* (ICRU) (ICRU 2007). Consequently, prescription doses to tumors, and dose constraints for organs at

risk (OARs) could be directly derived from the knowledge collected through many decades of clinical experience with photon RT.

Carbon ion RT (CIRT) has been successfully applied for cancers arising in the head and neck region, among other sites (Malouff et al. 2020). For a carbon ion beam, however, the RBE can be as high as 4, depending on the clinical situation or endpoint (Loeffler and Durante 2013). Moreover, the RBE varies significantly along the treatment beam, making it imperative to modulate the absorbed dose profile, in order to achieve a homogeneous biological effect. The CIRT centres therefore rely on models that predict the RBE within the treatment field. Currently, two different RBE models are applied clinically, in which one is applied exclusively in Japanese centres, while another is mostly applied in European centres. As currently applied in clinical treatments, they usually do not account for the fact that different tissues have diverging radiosensitivities, which in turn will modulate the RBE compared to photon RT. Therefore, it is questionable whether tolerance doses to the various OARs can be safely adopted from previous experience with photon RT. Most definitely, tolerance doses should at least be validated within the framework of this new treatment modality. This thesis aims at improving dose constraints applied for CIRT for various OARs in the head and neck region, to be used at centres applying the European RBE model.

2. Physics of radiotherapy

2.1 Ionizing radiation

The term ionizing radiation refers to radiation which has sufficient energy to remove electrons from atoms in the traversed material, producing ions and electrons, and thus ionizing the atom. Electrically charged particles (electrons, protons and heavier ions) interact mainly through direct ionization, while uncharged carriers of radiation (photons, neutrons) are indirectly ionizing; this refers to processes in which a primary interaction between the carrier and the traversed material produces a charged particle that, in turn, is capable of ionizing the material (e.g. a secondary electron or proton).

2.2 Interaction of photon RT with tissue

When photons traverse tissue, the energy of the photon is absorbed through several different interaction mechanisms with the atoms in the tissue that is being traversed; the most dominant mechanisms are; the Compton effect, the photoelectric effect and pair production (Khan and Gibbons 2014). The Compton effect is the prevailing mechanism in the energy range applied clinically. With photon energies between 6-20 MeV, the main product of the Compton process is the release of free electrons with adequate energy to form plural individual tracks of ionization in tissue. The range, of these tracks can be several centimeters long, and thus, the energy transferred from the initial photon is dispersed over a relatively large area, a significant part of the tracks ending some distance away from the location of the initial photon-tissue interaction. The direction of the electrons' tracks, although scattered and tortuous, is generally in the same direction of the photon beam, following conservation of momentum in the interactions. Initially after the photon beam enters a tissue, more and more electrons are produced, resulting in an increase of deposited dose within the first few centimeters of the irradiated tissue. However, following an exponential law, the photons are gradually attenuated. Therefore, after equilibrium is reached, the dose deposited decreases exponentially, see **Figure 2.**

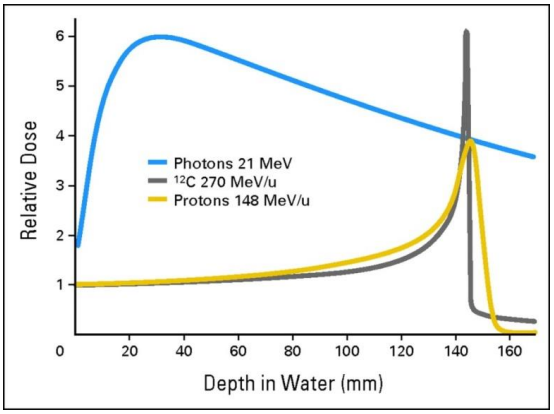

Figure 2: *Depth dose profiles of photons, protons and carbon ions. From Schulz-Ertner and Tsujii (2007). Reused with permission.*

2.3 Interaction of charged particles with tissue

Charged particles lose energy and thus speed through multiple consecutive interactions with the atoms of the tissue. As the particle slows down, there is a higher probability for interactions to occur per unit of length travelled, resulting in a marked increase in energy deposition as it reaches the end of its range, resulting in the so-called Bragg peak (Bragg and Kleeman 1904). Ions heavier than protons additionally undergo fragmentation events, in which either the projectile ion or an atomic nucleus of the tissue break up and form secondary particles. These secondary particles have lower mass and thus longer residual range, resulting in a "tail" of low dose after the Bragg peak in the depth dose curve for heavier ions, see carbon ion depth dose curve in **Figure 2**. However, the heavier ions have other dosimetric advantages over protons, e.g. less range straggling (producing a more distinct Bragg peak), and there is also less lateral scattering for the heavier ions, thus inherently producing a sharper lateral beam penumbra (Chen, Castro, and Quivey 1981).

For clinical applications, the millimeter wide Bragg peak needs to be widened in order to cover the whole extent of the tumor, typically several centimeters. This broadening of the high dose peak is done by creating a so called *spread out Bragg peak* (SOBP), which is composed of multiple pristine (monoenergetic) Bragg peaks of various energies. As a result, the dose in the plateau region proximally to the SOBP becomes higher as well, although it still remains lower than the dose in the

build-up/entrance dose region for a generic photon beam, see **Figure 3**.

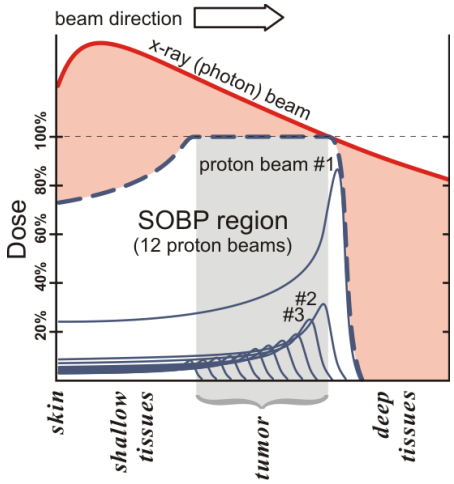

Figure 3: *Multiple proton beams of different energies and thus different range/penetration depths, are applied in order to produce a spread out Bragg peak (SOBP) that covers the extent of the tumor. The figure is adapted from Filipak (2012) with permission.*

A comparison of dose distributions in treatment plans for photon and proton RT, respectively, is shown in **Figure 4**. The different dose distribution is demonstrating the increased sparing of healthy tissues when applying charged particles in RT, while the high dose remains conformed to the planning target volume (PTV).

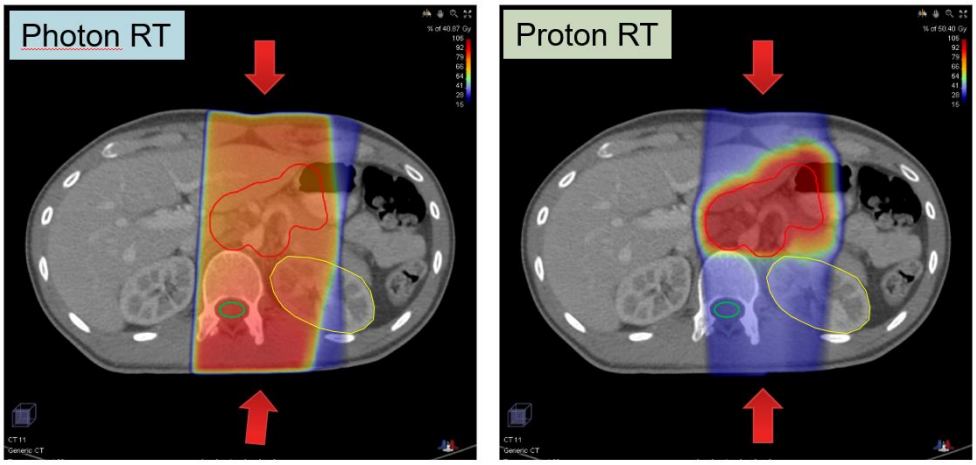

Figure 4: *Comparison of the dose distributions when applying a two field setup of either photon (left panel) or proton (right panel) radiotherapy. Red arrows indicate field direction. Red contour represents the planning target volume (PTV) needed to treat a tumor at the gastro-esophageal junction. Yellow contour represents the right kidney, and green contour represents the spinal canal harboring the spinal cord.*

2.3.1 Track structure of charged particles

On the microscopic scale, each ion species has a characteristic track structure, which describes the spatial and temporal pattern of the ion's interactions with an absorber. The ion track consists of a track *core* and *penumbra* (Blakely 1983). The core is produced by direct interactions between tissue atoms and the primary ion along its trajectory, while the track penumbra is a result of secondary electrons (δ- electrons). These electrons have enough energy to produce their own ionization track, thus allocating ionizations at distances farther away from the track core.

The rates of direct interactions in the track core, and the formation of secondary δ-electrons producing the penumbra, both increase with *increasing* charge of the ion and with *decreasing* velocity of the ion. Furthermore, as the ion speed decreases, the δ-electrons produced will have lower energies, thus becoming unable to travel far from the track core. The net result is that as the ion slows down, there is an increasing clustering of ionizations immediately along the track core, and there is also an increase in secondary electrons, though with lower energies, resulting in a simultaneous narrowing of the track penumbra (Conte et al. 2012). Therefore, on the micro- and nanometer scale, the dose deposition is condensed around the ion tracks, the magnitude increasing as the ion decelerates, see **Figure 5**.

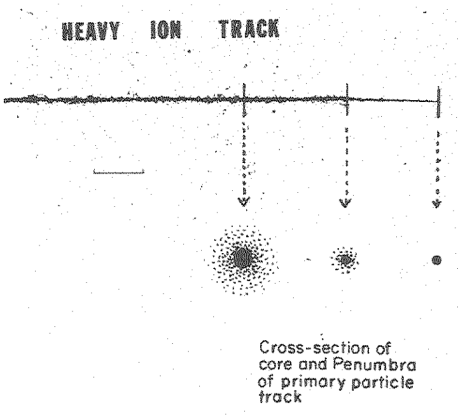

Figure 5: *Visualization of a heavy ion track as it traverses a nuclear emulsion, going from left to right. The cross-sections demonstrate the narrowing of the penumbra as the ion decelerates. The dots represent ionization events. The dense inner region of ionizations is the core, and the more diffuse peripheral region in each cross-section is the penumbra. From Benton & Tochilin (1966), figure reused with permission.*

2.4 Absorbed dose and specific energy

The absorbed dose, often also referred to as the physical dose, is a physical quantity describing the energy imparted by ionizing radiation to matter (ICRU 2011). The SI unit of absorbed dose is Gray (Gy), in which 1 Gy equals 1 Joule of energy absorbed per kilogram of matter (1 Gy = 1 J/kg). Conventionally, absorbed dose is used to report doses delivered to patients within radiation therapy using photon or electrons. However, for other radiation modalities, with a different pattern of dose deposition on the microscopic scale, e.g. for charged particles, the absorbed dose alone is not always adequate for quantifying the biological effect of the imparted physical dose within a treatment plan or field, and some additional parameters need to be incorporated in order to take the biological effectiveness of the imparted physical dose into account.

The term absorbed dose quantifies in RT the mean dose imparted to the tissue on a macroscopic scale. However, due to the stochastic nature of the interactions between traversing particles and tissue atoms, there will be large variations in the amount of deposited energy within small sub-volumes on the *microscopic* scale. Specific energy (z), is defined as the amount of energy *(E)* imparted by ionizing radiation in a volume of mass m ($z=E/m'$), and can be considered as the microdosimetric equivalent to the macroscopic quantity absorbed dose. Specific energy is therefore a more relevant quantity when dealing with biological effects that are dependent on amount of dose imparted into subcellular structures.

2.5 Linear energy transfer and lineal energy

As previously mentioned in chapter 2.3.1, each particle type has a unique track structure, defining the spatial pattern of energy deposition as it evolves throughout the tissue. Commonly, linear energy transfer (LET) is used to convert this three-dimensional structure into a one-dimensional quantity (Lindborg et al. 2013). LET describes the magnitude of energy transfer along the ion trajectory and is defined as the amount of energy (E) lost per unit of track length (x), $LET = \Delta E/\Delta x$. LET is usually expressed in units of kiloelectronvolts per micrometer (keV/µm). LET is

proportional to the square of the ion's charge divided by the square of its velocity (Joiner and van der Kogel 2009). Therefore, heavy ions have low LET at high speed, which changes to increasingly higher LET as the ion slows down. In contrast, photon RT, mediated through the highly tortuous tracks of the secondary electrons, is sparsely ionizing and has low-LET throughout the whole radiation field.

The radiation field of a therapeutic ion beam consists of primary ions of multiple energies (to produce a spread out Bragg peak) and a variety of secondary particles due to fragmentation events. Therefore, at any point in the field, the dose deposited stems from a mixture of particles species with a wide range of LET values. Commonly, the radiation quality in a given position of a beam is therefore described by the dose-averaged LET. As it follows, the radiation quality of an ion beam changes with depth. As seen in **Figure 6**, dose-averaged LET increases with depth and is also dependent of the ion type. It can also be seen that heavier ions (carbon and oxygen) exhibit substantially higher values of dose-averaged LET within the target/SOBP, while for protons increased LET values appear at a position beyond the target, which is not ideal (Tommasino, Scifoni, and Durante 2016).

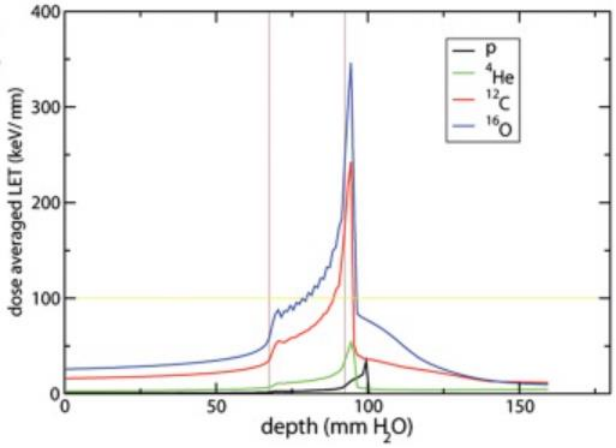

Figure 6: *Profiles of dose-averaged LET of different ions for the irradiation of an extended target of 2.5 x 2.5 x 2.5 cm^3 centered at 8 cm depth in water (vertical lines), with a field optimized on a uniform absorbed dose of 2 Gy. The yellow horizontal line indicates a LET level that can be associated to a significant reduction in the oxygen enhancement ratio. From Tommasino et al. (2016). Reused with permission.*

As for the relationship between specific energy and absorbed dose, lineal energy (y) is the microdosimetric equivalent of LET. Lineal energy is defined as the amount of energy imparted by single interaction event (E_s) to a volume with a mean chord length of $\bar{l}$ ($y = E_s/\bar{l}$).

3. Modelling radiobiological effects

Since the dawning of radiotherapy at the end of the 19th century, *in vitro* cell experiments have been used to explore and quantify the effects of radiation on biological systems. Most commonly, clonogenic assays have been used, where the radiation effect in a cell line is given by the *surviving fraction*, defined as the percentage of cells with ability to form colonies of at least 50 daughter cells, which in turn implies a capacity for unlimited proliferation (Puck and Marcus 1956). When the surviving fraction is plotted as a function of dose, the curve typically assumes a sigmoidal shape, or as a downward bending curve when survival is plotted on a logarithmic scale, as seen in **Figure 7**.

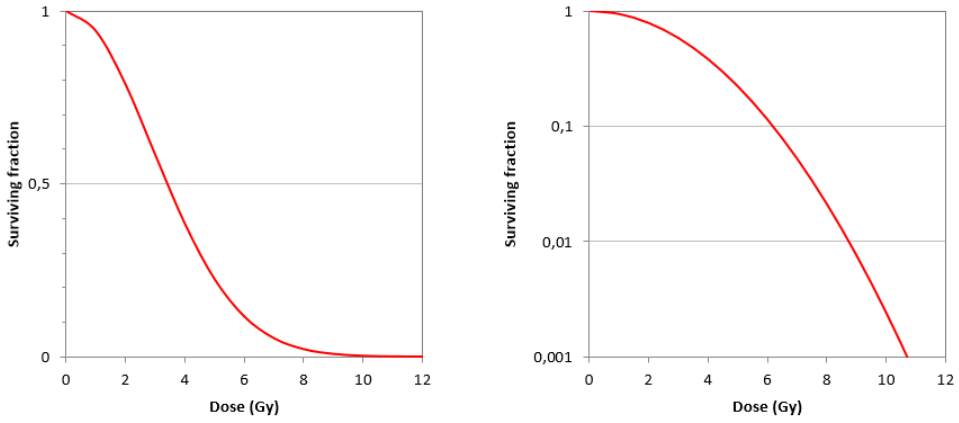

Figure 7: *Example of a typical cell survival curve, with survival plotted on a linear scale (left panel) and on a logarithmic scale (right panel).*

3.1 The linear quadratic model

Over the decades of radiotherapy, a plethora of different models with varying degree of complexity have been proposed in order mathematically describe and mechanistically explain the shape of the cell survival curve. One of them, the *linear quadratic (LQ) model*, is by far the most frequently applied model to analyze and

predict responses to ionizing radiation both in both in the laboratory and in the clinic. Although the first formulation of a LQ-like model often is attributed to Lea and Catcheside (Lea and Catcheside 1942), important contributions by Fowler (Douglas and Fowler 1976; Fowler 1989) and Barendsen (Barendsen 1982) paved the way for its pivotal role in radiotherapy. In its most common formulation, the LQ model describes the survival fraction (*S*) following a single dose of radiation (*D*) as:

$$S\,(D) = e^{-\alpha D - \beta D^2} \qquad \text{(Equation 1)}$$

where the α and β terms are derived by fitting to experimental data, and quantify the radiosensitivity of the investigated cell or tissue (McMahon 2018). The ratio of the parameters α and β (α/β ratio) determines the degree of the curvature, and corresponds to the dose at which the linear term ($-\alpha D$) and the quadratic term ($-\beta D^2$) equally contributes to cell inactivation, see **Figure 8**. The α/β-ratio is representative of how sensitive the cell is to fractionated radiation. A high α/β-ratio is typical for early responding tissues (e.g. skin and mucosa) and most tumors and implies a relative insensitivity to fractionation. A low α/β-ratio (i.e. 2-5 Gy) indicates higher sensitivity to fractionated treatment, which means that when fraction number increases (and dose per fraction decreases) a higher total dose can be applied while maintaining the same degree of cell survival. A low α/β-ratio is typically observed in late responding tissue (e.g. nervous tissues, lung and kidney) (Joiner and van der Kogel 2009). In radiotherapy, this difference in α/β-ratio for a typical tumor and the surrounding late responding tissues is utilized to achieve high radiation dose while preferentially sparing the late responding tissue from damage. The most common mechanistic interpretation of the LQ model is that the α term represents cell inactivation following a "single hit" event and that the β term reflects a "two hit" cell inactivation resulting from the interaction of damage from two different radiation tracks, the latter being more dominant at higher doses, see **Figure 8**. However, it is unlikely that the complex biological response of tumors, tissues and even cells lines to radiation can be encompassed by such a simple mechanistic explanation. Either way, the LQ model remains a practical empirical tool in radiation biology and physics.

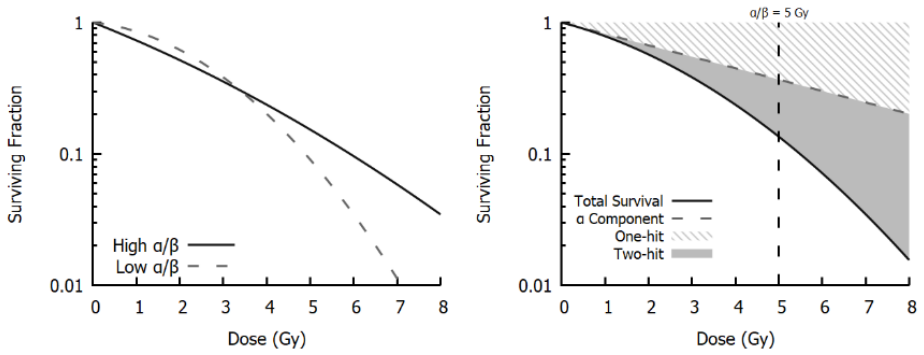

Figure 8: *Illustration of LQ curves. Left: Responses for cell lines with high and low α/β ratios. High α/β cell lines (10 Gy) have nearly-constant rates of cell killing with increasing dose, while low α/β lines (3 Gy) show a pronounced curvature, with greater killing per unit dose at higher doses. Right: Separation into one- and two-hit kinetics. At low doses, response is dominated by one-hit events, while at higher doses multi-hit killing is more important. These effects are equal when the dose matches the α/β ratio of the cell line (5 Gy). From McMahon (2018), reused with permission.*

The LQ model is also used to compare the efficacy of different fractionation regimens. Traditionally, radiotherapy has been given by dividing the total dose into fractions of 2 Gy. Hyperfractionation refers to applying smaller fraction doses, while hypofractionation is the use of larger fractional doses than the normally applied 2 Gy fraction doses. Therefore, differing dose-fractionation schedules can be compared, typically by converting them to *equivalent dose in 2 Gy fractions* (EQD2) by use of the LQ model.

3.2 Models for Normal Tissue Complication Probability

In clinical radiotherapy, avoiding potentially toxic doses to the body's organs is a major factor limiting the amount of dose one can apply to the tumor. The estimated risk for a given side effect will increase with increasing dose to and increasing volume within an OAR that receives a certain dose (Langendijk et al. 2013). The first compilation providing estimates of *normal tissue complication probability* (NTCP) for various organs was published by Emami et al. in 1991 (Emami et al. 1991). Focusing on conventionally fractionated photon radiotherapy, tolerance doses (TD)

for uniform irradiation of 1/3rd, 2/3rd and the whole organ volume, associated with 5% and 50% probability for toxicity within five years from treatment (TD 5/5 and TD 50/5, respectively) were proposed**.** It should be emphasized that due to the lack of strong evidence, many of the estimates provided in this paper, were based on the opinions and experience of the contributing authors.

However, with increasing use of more conformal dose delivery techniques, e.g. IMRT, the organs are usually partially irradiated with a highly *non-uniform* dose, thus reducing the validity of the arbitrary tolerance doses provided in the Emami paper.

A common approach to manage this issue, is applying the concept of *equivalent uniform dose* (EUD) (Luxton, Keall, and King 2008; Niemierko 1997) to the *Lyman-Kutcher-Burman* (LKB) NTCP model (Lyman 1985; Kutcher and Burman 1989). In summary, three parameters are fitted to the experimental data: *n*, *m* and *TD50*. *n*, the volume-effect parameter*,* represents the organ architecture (serial when $n \rightarrow 0$, and parallel when $n \rightarrow 1$), *m* represents the biodiversity in radiosensitivity amongst patients (steep dose-response curve when $m \rightarrow 0$), and *TD50* represents the dose (EUD) that would result in 50 % probability of toxicity if uniformly distributed over the organ's total volume. The volume-effect parameter, *n* is inversely proportional to the resulting individual patient's EUD; a small *n* will result in higher EUDs, closer to the maximum dose, and bigger *n* will result in lower EUDs overall.

The LKB and similar models require the use of more or less complex mathematical equations, and are not easily applicable in routine clinical practice. Therefore most publications on NTCP have focused on identifying a limited set of dose-volume reference points relating to a specific endpoint of organ dysfunction. These studies were collectively reviewed through the efforts of the *Quantitative Analysis of Normal Tissue Effects in the Clinic* (QUANTEC) initiative in 2010 (Marks et al. 2010). The most important dose-volume reference point(s) for an organ depends on the organ's functional architecture, and therefore varies widely between different toxic endpoints.

In order to make an NTCP model, the effect of a dose variable on the (often binary) outcome is fitted to a logistic regression function, resulting in a sigmoidal dose-

response curve, see **Figure 9.** Often, the model can be improved by incorporating patient related factors (age, sex, comorbidities) or treatment related factors (e.g. concomitant chemotherapy) (Tommasino, Nahum, and Cella 2017). However, a rule of thumb for logistic regression models is that one should have 10-15 events per parameter introduced in the model (Kong et al. 2007). As it follows, for more severe side-effects, optimally not occurring in more than 1% of patients treated, one would need at least 1000-1500 patients to derive a univariate NTCP model.

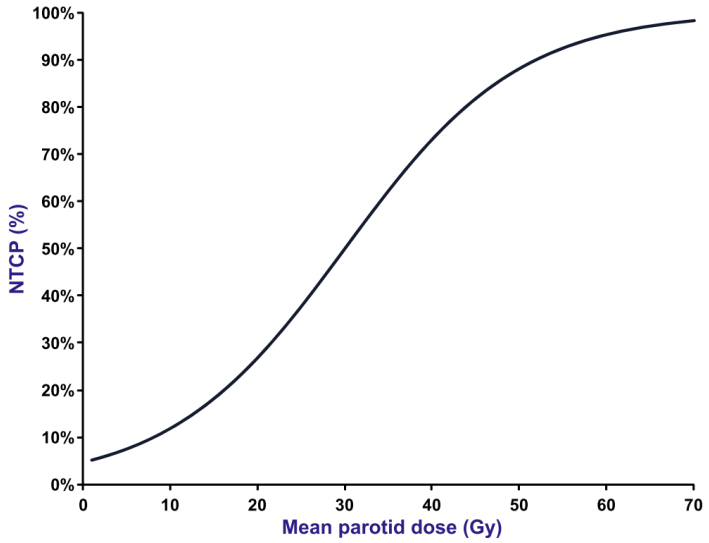

Figure 9: *Example of a Normal Tissue Complication Probability (NTCP) model describing the risk estimation on a given side effect (NTCP-value) as a function of the most relevant dose distribution parameter (in this case the mean parotid dose). From Langendijk et al. (2013), reused with permission.*

4. The biological advantage of charged particle therapy

The cellular response to ionizing radiation is very complex and many mechanisms remain to be uncovered. However, it is clear that the most important structure for radiation response in a cell is the DNA. It is the largest molecule within the cell, exist only in two copies and is crucial for all cell functions (Joiner and van der Kogel 2009). Due to its importance, the cells harbor highly sophisticated DNA repair systems which are activated when damage to the DNA occur. As previously described, compared to photons, the high LET radiation causes densely localized ionizations along its trajectory. Within the cell nucleus, this pattern of microscopic dose deposition increases the probability of causing so-called clustered damage to the DNA. This involves two or more closely associated DNA lesions involving both DNA strands, usually within one or two turns of the helically structured DNA molecule (Sutherland et al. 2001). Although one can expect the same absolute number of individual DNA lesions per unit of absorbed dose following low- and high-LET radiation, the proportion of *complex* DNA damage increases from 30-40% for low-LET to more than 90% for high-LET radiation (Semenenko and Stewart 2006). These complex DNA lesions are harder for the cell to repair properly, increasing the probability of cell inactivation through death, senescence or loss of reproductive capability.

4.1 Relative biological effectiveness

To compare the effect of different types of radiation, the concept of *relative biological effectiveness* (RBE) is applied. RBE is defined as *the ratio of absorbed dose of a reference radiation (usually photons) to that of a test radiation to produce the same biological effect, under otherwise identical conditions* (Joiner and van der Kogel 2009):

$$RBE = \frac{D_{reference}}{D_{test}} \qquad \text{(Equation 2)}$$

Therefore, radiation beams with higher RBE values are more effective at producing biological effects at equivalent doses. RBE is however a highly elusive quantity and is dependent on physical properties of the radiation (LET, ion type, dose), as well as the properties of the biological system (cell/tissue type, physiological status of the cell) (Karger and Peschke 2017). Therefore, a precise quantification of the RBE is only achievable within strict experimental conditions, where all factors affecting the RBE are fixed. Typically, basic characterization and quantification of RBE of ion beams has been performed under so-called "track segment" conditions. In these experiments, a monolayer of cells is irradiated and because this layer is extremely thin, one can exclude any variation of energy or LET within the layer. Such experiments are useful to systematically asses the dependence of RBE on physical and biological factors.

4.1.1 RBE dependence on LET and ion type

There is a clear trend in the relationship between LET and RBE as can be seen in **Figure 10**. With increasing LET, the RBE increases steadily up until LET values at about 100-200 keV/µm suggesting that at these values, the microscopic dose distribution is optimal for cell killing (Tsujii et al. 2014; Ando and Kase 2009).

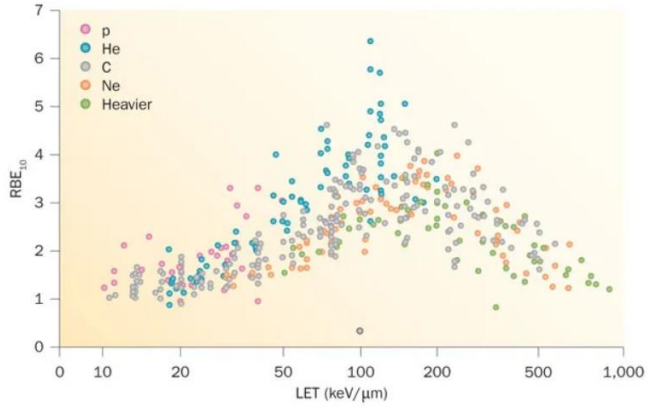

Figure 10: *RBE as a function of LET from published experiments on various in vitro cell lines. RBE is calculated at 10% survival. Colours indicate different ion types. From Loeffler and Durante (2013), reused with permission.*

At higher LET the RBE decreases, which is due to an overkill effect; at these levels, the density of ionizations around the track exceeds what is needed to kill the cell, and

thus some of the dose is "wasted". **Figure 10** also demonstrates the huge variability of in measured RBE-values according to the use of different cell types or due to different experimental or physiological conditions. Likewise, the figure shows a trend as the particle's charge increases, the maximum RBE shifts towards higher LET values. This observation highlights the fact that LET is a one-dimensional representation of the ion's three-dimensional track structure.

One of the main reasons for choosing carbon ions over other ions for radiotherapy is their beneficial LET distribution along the treatment beam; in the plateau region before the SOBP, the particles have relatively low LET, and thus low RBE, while in the SOBP LET values and RBE increases. Carbon ions therefore have the highest ratio of biological effect between the SOBP and the plateau region, as shown in **Figure 11** (Chu, Ludewigt, and Renner 1993)**.**

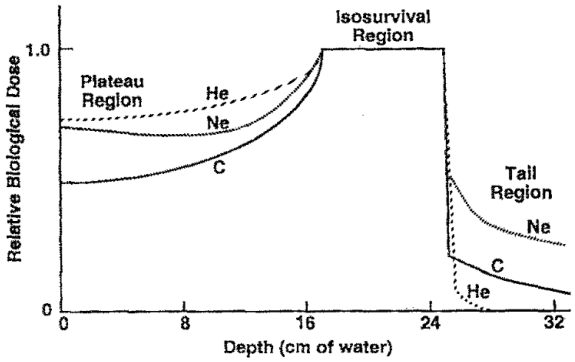

Figure 11: *The relative biological dose of SOBPs of helium-, carbon, and neon-ion beams as a function of penetrating depth in water are shown for comparison. These doses are normalized at the isosurvival region and the figure shows the different relative entrance, plateau and tail doses for these beams. From Chu et al. (1993), reused with permission*

4.1.2 RBE dependence on dose

Cells exposed to CIRT show higher α/β-ratios, and thus a steeper and more linear dose-response curve, than what is found for photon radiation. This change is mainly due to an increase in the radiosensitivity parameter α when high-LET radiation is used (Weyrather et al. 1999; Ando and Goodhead 2016). The phenomenon could be

explained by the increased ability of the high-LET particles to inflict complex, irreparable damage to the DNA also at lower doses. As a direct consequence of the different shape of the survival curves, the RBE is dependent on dose level, see **Figure 12**.

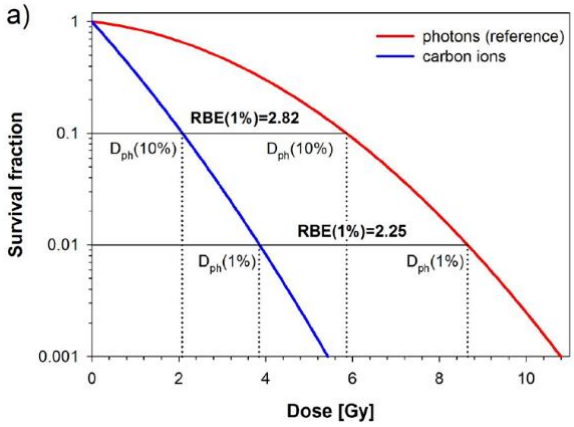

Figure 12: *Cell survival curves in vitro fitted by the LQ model. Irradiations with photons and carbon ions are considered as isoeffective if the survival fractions are the same. The dose dependence of the RBE results from the different shapes of the photon and carbon ion curve and leads to different RBEs at different survival levels. The different survival levels are considered as different endpoints. From Karger and Peschke (2018), reused with permission.*

4.1.3 RBE dependence on cell or tissue type

In general, the variation in radiosensitivity between different cell lines is reduced for high-LET radiation compared to low-LET radiation (Belli et al. 2008). Hence, the RBE of high-LET radiation is more dependent on the difference in radiosensitivity to photon radiotherapy. As an example, cells with deficient DNA repair systems are typically very sensitive to photon radiotherapy and will therefore exhibit rather low RBE when exposed to high-LET radiation (Weyrather et al. 1999). On the other hand, cells with high repair capacity are more resistant to photon radiation and show higher RBE values, see **Figure 13.**

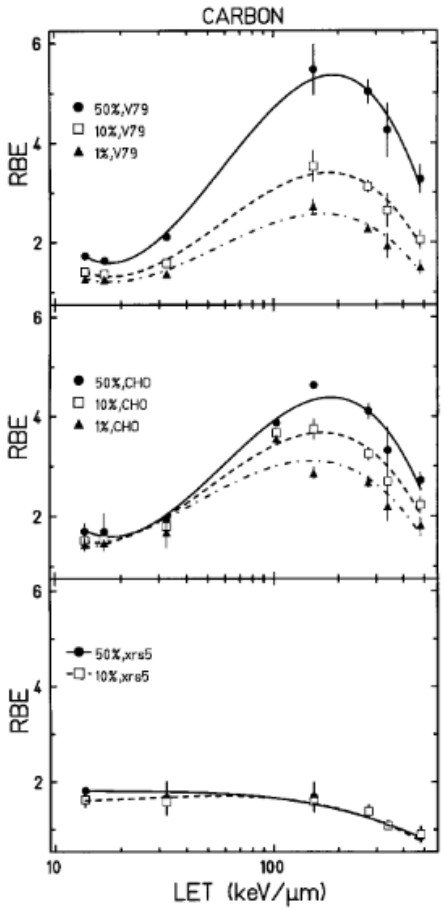

Figure 13: *RBE for carbon ion track-segment irradiation at a survival level of 50%, 10% and 1% for repair-efficient (V79 and CHO) and repair-deficient (xrs5) cells. From Weyrather et al. (1999), reused with permission.*

4.1.4 The oxygen enhancement effect

From experience with photon RT, it is well known that cells in hypoxic conditions are less radiosensitive (Gray et al. 1953). Tumors may outgrow their blood supply, or produce dysfunctional capillaries, causing a certain proportion of the tumor cells to be hypoxic. The effect of increased radiosensitivity observed when cells are reoxygenated is called the *oxygen enhancement effect* (OER). Typically, for photon RT, in vitro experiments have found the OER to be around 2.5 – 3.0, i.e. you would need a two- to threefold dose to get the same effect under hypoxic conditions relative to normoxic conditions (Hall and Giacci 2006). As with RBE, also the OER changes with LET, being equivalent with photons at low LET, decreasing to nearly 1.0 at LET

values of 200-300 keV/µm (Blakely and Chang 2009). As can be seen in **Figure 6** in chapter 2.5**,** LET values associated with a significantly reduced OER is only partially achievable within the SOBP of a carbon ion beam, which has caused an increasing interest in exploring the possibility of using even heavier ions (i.e. oxygen ions) instead of, or in conjunction with, other ions to treat hypoxic tumors (Tommasino, Scifoni, and Durante 2016; Inaniwa et al. 2017).

4.2 RBE of carbon ions

Due to its role as the only heavy ion currently applied in routine clinical treatments, the RBE of carbon ions has been extensively investigated. Examples of these experiments, uncovering different aspects of carbon ion RBE is presented in this section.

4.2.1 In vitro experiments

In a systematic analysis of cell survival experiments, Friedrich et al. demonstrated that carbon ions at optimal LET (100-200 keV/µm) can exhibit RBE as high as 14 (Friedrich et al. 2012). This was however at the limit of full survival level, i.e. at very low dose. At 10% survival, an endpoint considered more relatable to clinical tumor eradication, the RBE was found to be in the range 2-4. However, particles with these optimal LET-values are not dominant within the SOBPs of a therapeutic carbon ion beam, where the dose-averaged LET rather is in the range 40-100 keV/µm (Kanai et al. 2006). In experiments on human cell lines using dose-averaged LET values within this range, RBE values of 2-3 have been found for the 10% survival level using single fractions (Belli et al. 2008) and up to 3.5 for fractionated experiments (Suzuki et al. 2000).

4.2.2 In vivo experiments

While cell line experiments are useful to characterize fundamental properties of carbon ion beams, *in vivo* experiments are more helpful to examine clinical effects both on normal tissues and on tumors. As an example, Debus et al. (Debus et al. 2003) and Karger et al. (Karger et al. 2006) performed a series of experiments where the spinal cords of rats were exposed to carbon ion beams with dose-averaged LET of

either 13 keV/µm or 125 keV/µm. The irradiation was given in either 1, 2, 6 or 18 fractions. Radiation-induced myelopathy was used as endpoint. For the 13 keV/µm beam, representative of the LET in the plateau-region, the RBE remained constant at approximately 1.4, irrespective of the fraction number. In contrast, for the 125 keV/µm beam, representative for the LET in the distal SOBP, the RBE increased significantly, from 1.77 in the single fraction group, up to 5.04 in the 18 fraction group. The experiment demonstrated that in the plateau-region (low-LET), the tolerance dose of the rat spinal cord is dependent on the fraction number, similar to what is observed for photon radiation. Hence the RBE of carbon ions relative to photon RT remains constant, irrespective of fraction number. In contrast, in the high-LET SOBP of the carbon ion beam the spinal cord becomes insensitive to fractionation, i.e. the tolerance dose for CIRT remains constant irrespective of fraction number. The increase in RBE with fraction number in this region is therefore a result of the sparing effect exhibited by fractionated photon RT, see **Figure 14**.

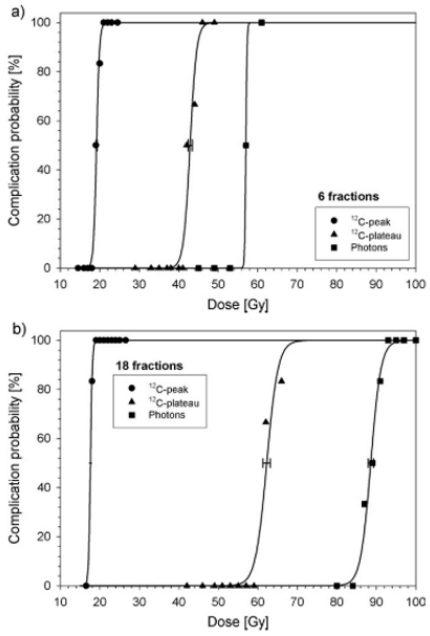

Figure 14: *Dose response for 6 (a) and 18 (b) fractions measured for irradiation with photons and carbon ions of LET 13 keV/µm (plateau) and 125 keV/µm (peak). Observe the indistinguishable the dose response curve of the high-LET carbon ion vs. the significant shift in dose response for the photon irradiation. From Karger et al. (2006), reused with permission.*

Determination of carbon ion RBE has also been performed in a few animal tumor models. Such models better mimic the complex dependencies of therapeutic effect in clinical radiotherapy, related to the interplay of a vast number of factors including tumor cell heterogeneity, physiological status, tumor stroma and immune cells (Karger and Peschke 2017). In studies on tumor growth delay, the RBE is defined as the ratio of reference radiation- to carbon ion dose needed to induce a certain amount of growth. In single fraction experiments on different tumor cell lines, applying carbon ion beams with dose-averaged LET in the range 74-80 keV/µm, RBE values up to 2.8 were found for 15 (Koike et al. 2002) and 20 day tumor growth delays (Tenforde et al. 1981).

5. Beam delivery techniques and treatment planning for particle therapy

5.1 Beam delivery techniques

From the particle accelerator a thin beam is extracted and guided towards the patient through the beam line. This thin beam needs to be broadened in both depth and width to cover the three-dimensional target volume. Two essentially different techniques are applied for this purpose (Chu, Ludewigt, and Renner 1993). Their main principals are presented here.

5.1.1 The passive scattering technique

As the name indicates, in this technique, the beam is broadened and shaped by a series of passive hardware components (Koehler, Schneider, and Sisterson 1977; Kanai et al. 1999). First the beam penetrates a scattering device causing the unidirectional particles to fan out. Thereafter the beam traverses a ridge filter (or similar device) which creates the SOBP. The exact design of the ridge filter dictates both the shape and the width of the SOBP in the beam direction. By varying the thickness of the range shifter, the penetration depth into the tissue is controlled. Finally the irradiation field is shaped laterally by a collimator and distally by a compensator so that the field matches the shape of the target volume, see **Figure 15** (upper panel).

5.1.2 The active scanning technique

This technique is also known as pencil beam scanning (PBS) (Kanai et al. 1980; Pedroni et al. 1995). Here, the thin beam extracted from the accelerator is not broadened, but rather deflected by two sets of scanning magnets, controlling the degree of deflection in the x- and y-direction. The Bragg peak is then deposited, either in a continuous sweep or spot by spot, across the most distal layer of the target volume. Then the energy of beam is decreased, either within the accelerator itself, and/or by a range shifter system so that the beam ends in a more proximal layer in the target volume which subsequently is swept by the beam. This process is repeated until every layer of the tumor is covered; see **Figure 15** (lower panel).

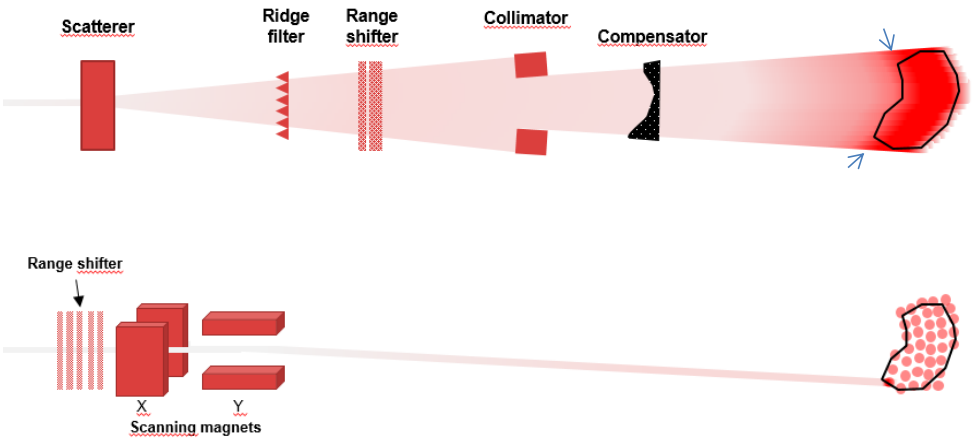

Figure 15: *Schematic illustration of the passive scattering (upper panel) and active scanning technique (lower panel). While the passive technique may conform the dose well to the distal edge of the target volume by use of a compensator, areas of high dose is given outside the proximal edge of the target volume (indicated by arrows).*

5.1.3 Comparison of the techniques

The passive technique has many disadvantages compared to the active scanning technique. Due to the hardware involved in the broadening and shaping of the beam, a higher proportion of the initially extracted particles are lost before reaching the patient. Additionally, the beam quality is deranged, due to interactions with the hardware components, creating contamination of fragmented ions and neutrons. The collimator and compensator have to be custom made for each field in each patient, adding to the cost and logistic complexity of the treatment (Tsujii et al. 2014). The active scanning technique is much more flexible, since the position and intensity of the beam can be modified for each spot position. High dose conformity can be achieved even for target volumes of complex geometric shape (Lomax et al. 2004), see **Figure 16**.

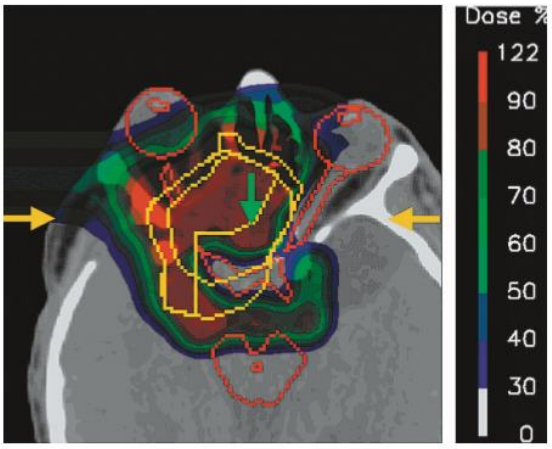

Figure 16: *A three field intensity-modulated proton therapy plan for a skull base chordoma, where the target volume is located between various organs at risk, e.g. brainstem, eyeballs, optic nerve and optic chiasm. From Lomax et al. (2004), reused with permission.*

A disadvantage of the active scanning technique is that the lateral penumbra may be less sharp than a collimated beam (Safai, Bortfeld, and Engelsman 2008), and that planned dose distribution is less robust in cases where the target volume is moving, i.e. due to respiratory motion. The latter may be mitigated by various techniques, such as rescanning, beam tracking, respiratory gating and 4D treatment planning (Bert and Durante 2011).

5.2 Treatment planning and optimization

The goal of radiotherapy is to deliver a dose that is high enough to eradicate the tumor cells, while delivering the lowest possible dose to the surrounding healthy tissues. More specifically, with the help of treatment planning systems (TPS) the dose distributions are optimized so that the prescribed dose covers as much as possible of the target volume, while the dose to the surrounding OARs is optimally kept below certain threshold values representing the accepted risk of organ toxicity for the specific treatment setting. These threshold values are referred to as *dose constraints*. For visualization of the dose distribution in both the target volume and the OARs, a dose volume histogram (DVH) is used, see **Figure 17**. Often there will be a trade-off between the risk of toxicity and the risk of tumor recurrence, especially in the case of tumors located close to important OARs. Therefore, it is utmost important to have accurate dose constraints and/or models to predict NTCP.

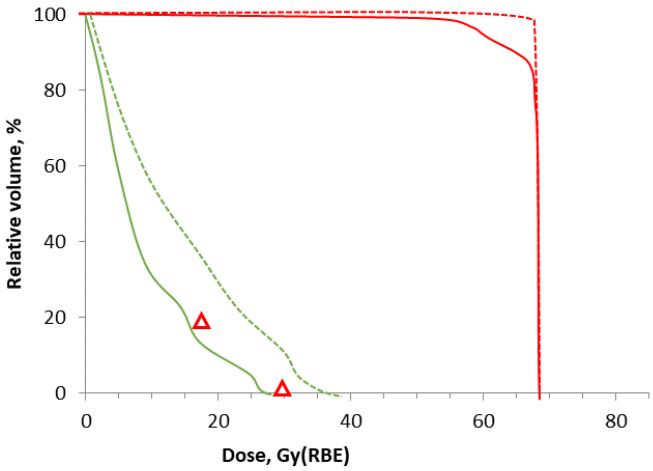

Figure 17: *Example of a dose volume histogram (DVH). Ideally, the DVH of the target volume (tumor) should be pushed towards the upper right corner, while the DVHs of the organs at risk (OARs) should be pushed towards the lower left corner. The red, broken line represents the optimal dose distribution for the target volume, e.g. nearly 100% of the target volume receives the prescribed dose of 64 Gy (RBE). However, to achieve this goal, the dose to an OAR (green, broken line) exceeds the recommended dose constraints (red triangles), putting the patient at risk of toxicity. The solid lines represent an alternative treatment plan, respecting the dose constraints of the OAR, while resulting in sub-optimal dose coverage of the target volume.*

For clinical treatment planning, there is a need for the TPS to be fast in order to secure a high through-put of treatment plans. Therefore, these often commercial TPS's predict and optimize the dose distribution using calculation algorithms that, although considered sufficiently accurate for their use, only partially depict the complex interactions between the particles of the beam and the tissues of the patients (Schuemann et al. 2015). For proton beams, the modelling of the lateral scattering of the beam in the presence of tissue heterogeneities is a particular weakness (Molinelli, Russo, et al. 2019). For heavier ions, like carbon ions, this lateral scattering is less pronounced. However, especially at greater depths, nuclear fragmentation events become more important in regards to reducing the sharpness of the lateral penumbra (ICRU 2019). Simulations based on Monte Carlo codes are more accurate, and are

considered the gold standard for dose calculations for particle therapy (Paganetti 2014; Mairani et al. 2010). However, the major drawback of Monte Carlo codes is that they demand high computational capacity and are time-consuming.

6. Dose prescription in CIRT

As covered in chapter 4, the RBE of the carbon ion beam is affected by factors such as dose per fraction, biological endpoint and by the penetration depth in the tissues (varying radiation quality). Due to these variations in RBE, the absorbed dose imparted in the tissue is not adequate to monitor the biological effect. *In vitro* and *in vivo* experiments can identify fairly precise RBE values for specific endpoints defined by the experimental set-up, and be of help to study the functional dependencies of the RBE. However, these "experimental RBE" values cannot truly reflect the complex variations in RBE encountered in patient treatments, where changes in irradiation conditions will modify the RBE of the multiple competing endpoints differently. The main purpose of RBE models in CIRT is to:

1) Achieve a homogeneous biological effect in the target area, by modulating the absorbed dose distribution in accordance with the depth dependent RBE.
2) Make the resulting RBE-weighted dose relatable to the biological effect observed for a reference radiation modality.

The lack of a universal RBE for CIRT has of historical reasons led to the development of two different methods to define the RBE-weighted dose for clinical patient treatments. As of yet, the ICRU does not give any recommendation as to which RBE model should be used to report the doses given in CIRT treatments (ICRU 2019).

6.1 The NIRS clinical dose

6.1.1 The mixed beam model (original NIRS clinical dose)

Kanai et al. developed the *mixed beam model* (also known as the NIRS clinical dose) for the passively scattered carbon ion beam of the HIMAC at NIRS (Kanai et al. 1999). Due to the advantageous effect of fast neutrons, another high-LET radiation, on malignant salivary gland tumors, the model was based on human salivary gland tumor (HSG) cells (Shirasuna, Sato, and Miyazaki 1981), in the belief that their moderate radiosensitivity was representative of the response of the tumor types one

expected to treat with CIRT (Tsujii et al. 2014). The α and β values of the LQ-model as a function of LET was examined in numerous studies for the HSG cells and many other cell lines using monoenergetic beams of carbon and helium. These values were thereafter used for the initial design of ridge filters that correctly weighted the absorbed dose as function of depth, in order to produce a homogeneous (flat) biological response (e.g. 10% HSG cell survival) over the entire SOBP (Kanai et al. 1997). Once SOBPs of various widths were designed – one had to connect the survival response of the HSG cells (biological effect in vitro) to the assumed clinical effect when treating patients. This was achieved by using NIRS's prior clinical experience with neutrons. In an 18 fraction regimen, an absorbed dose of 0.9 Gy of the NIRS neutron beam had a clinical RBE of 3.0. Planning to use the same fraction schedule initially, NIRS sought to find the neutron-equivalent point in the carbon ion beam SOBP. Various experiments showed that the NIRS neutron beam and the carbon ion beam were equiefficient at the point in the SOBP where the dose-averaged LET of the carbon ions beam was 80 keV/µm. For a 6 cm SOBP of a 290 MeV/nucleon beam, this *neutron-equivalent point* was located 8 mm upstream of the distal fall-off. Therefore, the clinical RBE at this point was defined to be 3.0 if an absorbed dose of 0.9 Gy was given by the carbon ion beam, thus resulting in an RBE-weighted dose of 2.7 Gy (RBE)[1] at this point in the SOBP, see **Figure 18**.

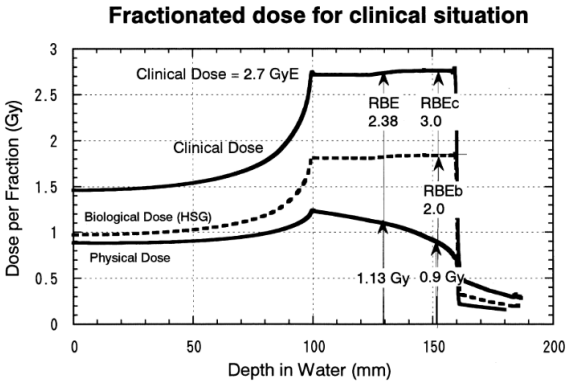

Figure 18: *Schematic method used to determine the RBE at the center of the SOBP for the clinical situation. From Kanai et al. (1999), reused with permission.*

[1] Originally, the RBE-weighted dose was reported as *Gy equivalents* (GyE)

Since the absorbed dose profile of the SOBP yielded a flat biological response for HSG cell survival *in vitro*, one could assume a flat biological response in clinical patient treatments as well. Thus, the clinical dose of 2.7 Gy (RBE) was attributed for the entire SOBP, thus defining the depth dependent RBE of the rest of the SOBP. For the 6 cm SOBP, the RBE in the SOBP center was defined to be 2.38. The same procedure was undertaken for multiple SOPBs with different widths. Since the neutron-equivalent point (80 keV/µm) will be at a different positions within SOBPs of different widths, the mid-SOBP RBE will be higher for the smaller SOBPs (3 cm = RBE 2.8) relative to the wider SOBPs (12 cm = RBE 2.1).

For every treatment in which 0.9 Gy was given to the neutron-equivalent point in these SOBPs, one could argue that the resulting RBE-weighted dose was approximately *photon-equivalent*, although derived through prior experience of the photon-related RBE of fast neutron therapy. However, from the initial modest doses given at clinical start-up in 1994, the NIRS gradually increased fraction doses within carefully monitored dose-escalation trials (Tsujii et al. 2004; Mohamad, Makishima, and Kamada 2018), keeping the RBE fixed dependent on the SOBP width, while disregarding that RBE will decrease with increasing fraction dose. Therefore, the NIRS clinical dose model is per design not reflecting true photon-equivalent doses.

6.1.2 The updated NIRS clinical dose

In conjunction with the implementation of an actively scanned carbon ion beam at NIRS in 2011, it was necessary to update the RBE model of the treatment planning system. This was also an opportunity to correct for oversimplifications embedded in the mixed beam model, particularly the lack of a dose-dependent RBE. At the same time, the new RBE model had to stay consistent with the old model, in order to ensure the continuity of the favorable clinical experience gathered over the prior decades (Inaniwa et al. 2015).

As basis for RBE-prediction, the *microdosimetric kinetic model* (MKM) developed by Hawkins (Hawkins 1994) was chosen. This model predicts cell survival after radiation from the specific energy (z) deposited in a subcellular structure referred to

as a *domain*. To account for the decrease in RBE due to the overkill effect in regions of very high specific energies, a saturation correction was included (Kase et al. 2006), hereby referred to as a *modified* MKM (mMKM). Thereafter, the radiosensitivity parameters required by the mMKM was fitted from experimental data, so that it correctly predicted the survival of the HSG cell within a carbon ion SOBP representative for patient treatments (Inaniwa et al. 2010). The radiation quality, defined as the *dose-averaged saturation-corrected specific energy*, found in the middle of this SOBP, was considered as the reference radiation quality for the updated dose system (Inaniwa et al. 2015). Lastly, a scaling factor of 2.41 was applied to unify the RBE-weighted dose with the former dose-fractionation regimens, see **Figure 19**.

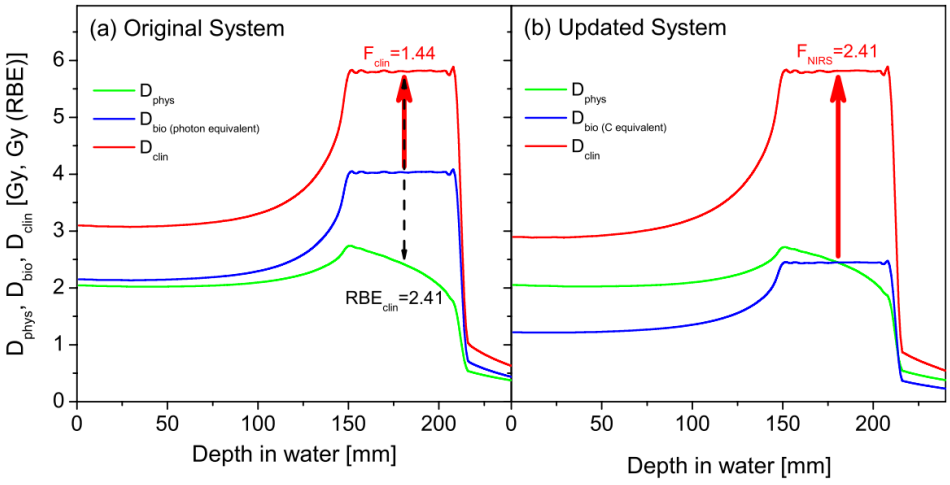

Figure 19: *Schematic designs of (a) the original and (b) the updated clinical-dose systems for a SOBP C-ion beam with a width and energy of 60 mm and 350 MeV u^{-1}, respectively. From Inaniwa et al. (2015), reused with permission.*

The NIRS clinical dose model, in either its original or updated form, is applied in almost all CIRT facilities in Asia and has been used for more than 20.000 patient treatments, see **Table 1**. In the following chapters, RBE-weighted doses predicted by the NIRS clinical model will be abbreviated as D_{NIRS}.

Table 1: Number of patients treated at sites applying the NIRS clinical dose model as of December 2018. Data from the Particle Therapy Co-Operative Group (www.ptcog.ch).

Country	*City (Site)*	*First patient*		*Patients total*
Japan	Chiba (NIRS)	1994		12649
Japan	Hyogo (HIBMC)	2002		2897
Japan	Gunma (GHMC)	2010		2711
Japan	Tosu (Saga-HIMAT)	2013		2583
Japan	Kanagawa (i-Rock)	2015		600
			SUM:	**21440**

6.2 The local effect model

The *Local Effect Model* version I (LEM I) was developed mainly by Scholz and Kraft at the Gesellschaft für Schwerionenforschung (GSI, Darmstadt, Germany) (Scholz et al. 1997; Scholz 1996). It is integrated in the treatment planning systems of every European CIRT facility, in addition to the Shanghai Proton and Heavy Ion Center (SPHIC, Shanghai, China), see **Table 2**.

Table 2: Number of patients treated at sites applying the LEM I as of December 2018. Data from the Particle Therapy Co-Operative Group (www.ptcog.ch).

Country	*City (Site)*	*First (-last) patient*		*Patients total*
China	Shanghai (SPHIC)	2014		723
Germany	Darmstadt (GSI)	1997-2009		440
Germany	Heidelberg (HIT)	2009		3016
Germany	Marburg (MIT)	2015		322
Italy	Pavia (CNAO)	2012		1307
			SUM:	**5808**

The purpose of the LEM I is to predict the biological response of a cell/tissue to any type of particle irradiation, based on the same cell/tissue type's response to photon irradiation, thus making use of the vast experience and data derived from photon RT.

The main assumptions of the LEM I are that *1*) the inactivation of an irradiated cell is governed by the amount of energy deposited in target structures within the cell nucleus, and *2*) that an equal amount of energy deposited in these structures will amount to the same degree of damage, irrespective of what kind of radiation that deposited the energy. The term "local" in local dose and local effect refers to infinitesimally small subvolumes of the cell nucleus. The LEM I uses the microscopic dose distribution along the ion track and the survival curves derived from photon RT to predict the RBE.

Therefore, the difference in the biological effect an equal absorbed dose of photon vs. particle irradiation at the macroscopic scale is attributed to the difference in the spatial distribution of the dose (e.g. track structure) at the nanometer scale (Friedrich, Durante, and Scholz 2013), see **Figure 20**.

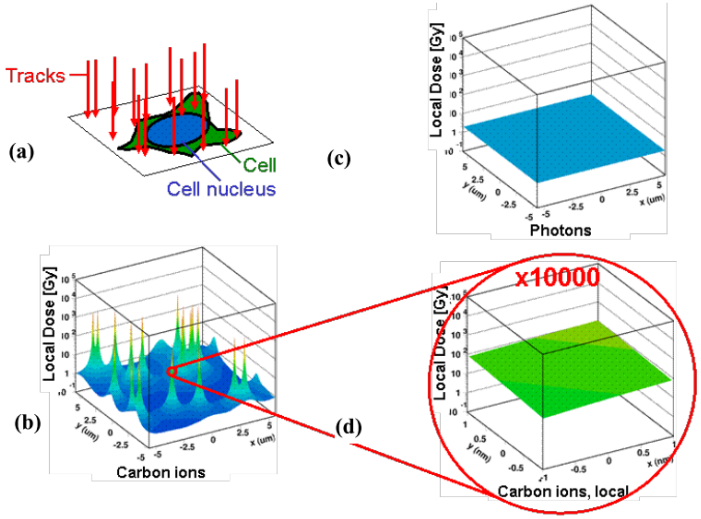

Figure 20: *Comparison of the microscopic local dose distributions of carbon ions and photons for the same macroscopic dose of 2 Gy. For a random distribution of particle traversals through a cell as depicted in (a) the corresponding local dose distribution is characterized by extremely high spikes close to the particle trajectory (b). In contrast, for photons the distributions is expected to be flat (c). Locally, i.e. in nm dimensions, the distributions of particles can also be approximated by a flat distribution (d), thus allowing the link to the photon distribution. From Friedrich et al. (2013), reused with permission.*

For clinical application, the LEM I has been used to predict the RBE of the carbon ion beam, relative to photon RT, using the photon dose-response curve of a late-responding, fraction-sensitive cell (α/β=2 Gy) as reference. The rationale for this strategy is that the dose-limiting factor for patient treatments is the late toxic effects of the surrounding normal tissues, and therefore, the RBE-model must be focused on the correct prediction of these effects (Jakel, Schulz-Ertner, and Debus 2007). Representative for this strategy, it has been shown that the LEM I can predict RBE (relative to photon RT) of skull base chordoma tumor control (Schulz-Ertner, Karger, et al. 2007) and temporal lobe reactions (Schlampp et al. 2011) with sufficient accuracy for clinical treatments.

However, in vivo and in vitro studies have indicated that LEM I overestimates the RBE for the low-LET carbon ions in the entrance-region of the beam (Karger et al. 2006; Elsässer, Krämer, and Scholz 2008). Therefore, the LEM has been updated through the years, the most recent being the LEM version IV (LEM IV). However, only the LEM I has been applied in the clinic so far. In the following chapters, RBE-weighted doses predicted by the LEM I will be abbreviated as D_{LEM}.

6.3 Comparison of the models from a clinical point of view

In the clinical setting, there are several important differences between the NIRS clinical dose model and the LEM I, as illustrated by **Figure 21**. Here, the depth dose curve has been optimized to result in a flat RBE-weighted dose of 3.6 Gy (RBE) in the SOBP, according to the NIRS clinical dose model (solid, red line). It is clear that the LEM I predicts RBE to be higher, relative to the NIRS clinical dose model, especially in regions of predominantly low-LET particles, e.g. the plateau-region and fragmentation tail. Moreover, when the RBE-weighted dose is calculated by the LEM I, based on the absorbed dose distribution defined by the NIRS clinical dose model, it does not remain homogeneous (flat) along the SOBP-region, but slightly higher proximally, compared to the distal part (Magro et al. 2017).

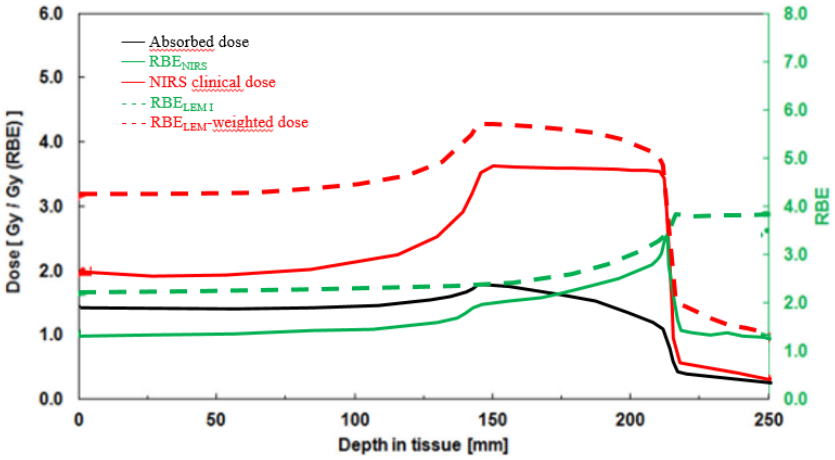

Figure 21: *Comparison the NIRS clinical dose and the LEM I. The absorbed dose (black line) has been optimized by using the NIRS clinical dose model to achieve a homogeneous RBE-weighted dose in the SOBP (red line). The red, dashed line is the resulting RBE-weighted dose if the LEM I is applied as RBE model for the same absorbed dose profile. The RBE predicted by the two models are presented as a continuous green line (for NIRS clinical dose) and a dashed green line (for the LEM I). Adapted from Magro et al. (2017), with permission.*

6.3.1 Comparison of prescription doses for CIRT

Comparisons of the models has been undertaken by several studies, both in silico (Steinstrater et al. 2012), by comparing dose distributions in a phantom set-up (Fossati et al. 2012) and by recalculation patient treatment plans using a in a sophisticated FLUKA Monte Carlo set-up reproducing the NIRS beamline (Molinelli et al. 2016). All these studies have focused on comparing the prescribed dose of the target volume. Although using different approaches, the conclusions are rather similar. Compared to the prescription doses used in the most common clinical protocols at NIRS, CIRT facilities applying the LEM I need to increase their respective RBE-weighted prescription doses by 5% - 15%, depending on the dose level, in order to expect equal tumor control rates, see **Figure 22**. Systematic analysis on the relationship of D_{NIRS} and D_{LEM} *outside* the target region, which is important in regards to comparing doses to OARs, has not been performed.

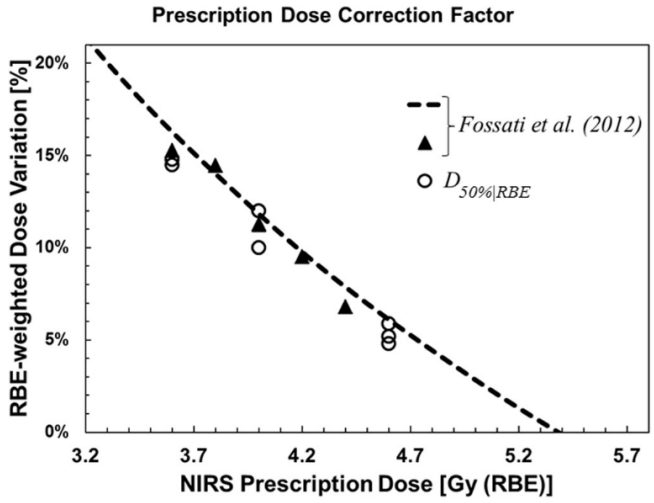

Figure 22: *Prescription dose correction factor as estimated by Fossati et al. (2012) and RBE-weighted target median dose variation between MC + LEM_I and NIRS calculations, as a function of NIRS prescription dose, for all cases analyzed. From Molinelli et al (2016), reused with permission.*

6.4 Status of dose constraints for CIRT

While proton RT can rely heavily in the prior decades of experience with photon RT, CIRT institutions need to proceed with caution in order to provide safe and effective treatments due to the radically different biological effect. The safety of the patients, primum non nocere, should always have first priority, and therefore, trustworthy dose constraints for OARs are of utmost importance. So far more than 27.000 patients with a variety of different diseases have been treated with CIRT worldwide. By comparing **Table 1** and **Table 2** one can see that the almost 80% of these patients have been treated at centres applying the D_{NIRS}. **Table 3** presents an overview of current publications addressing dose-volume response of various OARs treated with CIRT. As can be seen, validation of dose constraints for CIRT is still in its dawning, since there is a general lack of publications on the topic. Especially, at the time of initiation of this PhD project, there was only one publication addressing OAR toxicity following LEM I optimized CIRT, namely Schlamp et al.'s report on temporal lobe reactions (Schlampp et al. 2011). Therefore, this thesis focuses on toxicity after CIRT for three important OARs: 1) the carotid artery, 2) the optic nerve and 3) the brainstem.

TABLE 3: Overview of publications focusing on OAR toxicity following carbon ion radiotherapy, grouped by institutional RBE model. The table presents which institution the patient cohort was derived, year of publication and the reference.

Organ at risk	Endpoint	Institution (reference)	Events/ patients	Institutional RBE-model	
				NIRS clin	LEM I
Brain	Injury/reaction	NIRS (Koto et al. 2014) GSI (Schlamp et al. 2011)	*/39 10/59	X	X
Brainstem	Asymptomatic necrosis	GHMC (Shirai et al. 2017)	3/85	X	
Optic nerve	Optic neuropathy	NIRS (Hasegawa et al. 2006)	11/30	X	
Maxillary bone	Osteoradio-necrosis	NIRS (Sasahara et al. 2014)	26/63	X	
Oral mucosa	Acute mucositis	GHMC (Musha et al. 2015)	*/39	X	
Lung	Pneumonitis	NIRS (Hayashi et al. 2017)	9/65	X	
Skin	Late reaction	NIRS (Yanagi et al. 2010)	*/35	X	
Skin	Acute reaction	GHMC (Takakusagiet al. 2017)	*/22	X	
Upper GI tract	Ulceration	SAGA HIMAT (Shinoto et al. 2016)	12/58	X	
Rectum	Late reaction	NIRS (Fukahori et al. 2016) SPHIC (Wang et al. 2019) CNAO (Choi et al. 2019)	163 **/10 **/63	X	X

*multiple endpoints analyzed. **No events, dose constraints derived from translation from NIRS constraints

6.4.1 Carotid blowout

The carotid arteries are a pair of major blood vessels in the neck, responsible for most of the blood supply to the brain, neck and face. The common carotid arteries arise in the thorax and subsequently divide into the internal- and external carotid arteries. Carotid blowout refers to the rupture of the carotid artery or one of its main branches

and is a feared complication to treatment of neoplasms in the head and neck region (McDonald, Moore, and Johnstone 2012), as it can lead to life-threatening or disabling morbidity e.g. hypovolemic shock, threatened airways and/or cerebral stroke. Approximately 2 of 3 events occur in the common carotid artery or the internal carotid artery (Powitzky et al. 2010; Liang et al. 2016). Grading according to the *Common Terminology Criteria of Adverse Events* (CTCAE) version 4.03 is found in **Table 4.**

Table 4: Excerpt from CTCAE version 4.03

	Grade				
Adverse Event	**1**	**2**	**3**	**4**	**5**
Injury to carotid artery	-	-	Severe symptoms; limiting self care ADL (e.g., transient cerebral ischemia); repair or revision indicated	Life-threatening consequences; urgent intervention indicated	Death
Definition: A finding of damage to the carotid artery.					
Optic nerve disorder	Asymptomatic; clinical or diagnostic observations only	Limiting vision of the affected eye (20/40 or better)	Limiting vision in the affected eye (worse than 20/40 but better than 20/200)	Blindness (20/200 or worse) in the affected eye	-
Definition: A disorder characterized by involvement of the optic nerve (second cranial nerve).					
Central nervous system necrosis	Asymptomatic; clinical or diagnostic observations only; intervention not indicated	Moderate symptoms; corticosteroids indicated	Severe symptoms; medical intervention indicated	Life-threatening consequences; urgent intervention indicated	Death
Definition: A disorder characterized by a necrotic process occurring in the brain and/or spinal cord.					

Carotid blowout is perceived to result from pathologic alterations in or loss of the soft tissues surrounding the artery and/or of alterations in the vessel wall itself (Powitzky et al. 2010). Therefore, ulceration or infection in soft tissues adjacent to the artery, radiation to lymph node regions, dose to neck > 70 Gy, re-RT, radical neck surgery, nutritional status (BMI<22,5kg/m^2), osteonecrosis and to which degree the artery is involved by the tumor have been proposed as risk factors (Yamazaki et al. 2015; Chen, Wang, et al. 2015; Chen, Yen, et al. 2015; Cengiz et al. 2011). Although there are case reports of the event occurring after definitive chemoradiation in the primary treatment setting, it is more common following re-RT (Esteller et al. 2012). In this setting, relevant studies report median time to event to be around 6 months (range 0-

69 months) (McDonald, Moore, and Johnstone 2012; Cengiz et al. 2011; Yamazaki et al. 2013).

Correctly identifying the endpoint may be challenging, as f.ex. tumor regrowth may infiltrate the arteries and cause bleeding more or less unrelated to previous therapy. Furthermore, profuse bleeding from smaller arteries in the nasal cavity may mimic a carotid blowout event (Yang et al. 2018). Therefore, the diagnosis should preferably be based on angiographic and/or endoscopic findings.

Concerning the general risk of carotid blowout in patients re-irradiated with photons, McDonald et al. performed a pooled analysis of studies from the years 1996-2009 (McDonald, Moore, and Johnstone 2012). Within 1554 patients, the crude rate of carotid blowout was 2.6%. The outcome was fatal in as many as 76% of the events. Dionisi et al. recently published a review of the most recent literature (publications from 2002-2019) addressing general toxicity after re-RT to the head and neck with *photon*- or *proton* radiotherapy. Although treatment related death was not to frequent (<5%), most of the fatalities were caused by carotid blowout (Dionisi et al. 2019), emphasizing the importance of focusing on this endpoint.

Furthermore it may seem that properties of the RT affects the risk of carotid blowout, as rates as high as 8.4 – 15% have been reported after re-RT with hypofractionated SBRT (Cengiz et al. 2011; Yamazaki et al. 2013; Kodani et al. 2011) in contrast to less than 4% in more conventionally fractionated photon regimens (Chen, Wang, et al. 2015; McDonald, Moore, and Johnstone 2012).

CIRT is considered a promising radiation modality in the re-RT setting, since its high dose conformity minimizes excess dose to tissues that already are partially damaged by prior radiotherapy. In addition, the high-LET particles may overcome the resistance to low-LET radiotherapy that recurring tumors evidently may inhibit. Prior to this PhD project, there was only one publication mentioning the event of carotid blowout following re-RT using carbon ions: in a general outcome study of 52 patients with recurrent adenoid cystic carcinoma, Jensen et al. (Jensen et al. 2015) found 2 cases of grade IV carotid hemorrhage, within a cohort of 52 patients retreated for

adenoid cystic carcinoma. The cumulative lifetime dose (i.e. the summation of prescribed doses to the patient throughout his/her life) expressed in EQD2, was high for these two patients, i.e. 149 and 182 Gy (RBE).

An interesting common feature of the all publications mentioned in this section, is that none of them have investigated the event of carotid blowout in relation to the cumulative dose to the organ. Rather, the cumulative lifetime dose has been used as a surrogate, although this metric in many instances probably will overestimate the cumulative dose received by the same segment of the carotid artery. Subsequently, a tolerance dose threshold for this OAR has not been validated. However, in the re-RT protocols at CNAO the current practice has been to avoid cumulative EQD2 > 120 Gy (RBE) to the carotid artery.

6.4.2 Radiation induced optic neuropathy

The optic nerve is another important organ at risk when treating tumors in the head and neck region with radiotherapy, since visual impairment from radiation-induced optic neuropathy is very disabling. It usually presents as a painless loss of vision occurring between 3 months and 9 years following radiotherapy, although peak incidence is between 1 and 1.5 years after treatment (Danesh-Meyer 2008). Applying the CTCAE grading system, radiation induced optic neuropathy would be graded according to the subheading *Optic nerve disorder*, as shown in **Table 4.**

The precise diagnosis of radiation induced optic neuropathy may be challenging, since a plethora of other conditions may cause loss in visual acuity, e.g. dry eye, cataracts and retinopathy (Mayo et al. 2010). Furthermore, tumor recurrence may affect the nerve and cause optic neuropathy unrelated to prior radiotherapy. Therefore, the diagnosis of radiation induced optic neuropathy should be based on thorough ophthalmological evaluation and radiological investigations.

In the review of radiation dose-volume effects published after the QUANTEC-effort (Mayo et al. 2010), the risk of damage to the optic nerve were rare for maximum doses < 55 Gy, but increased markedly (>7-20%) at doses > 60 Gy at ~1.8 Gy/fraction when using photons or protons. Currently, the recommended dose

constraint applied for photon and proton treatments is therefore a maximum dose < 54 Gy (Mayo et al. 2010; Lambrecht et al. 2018).

For LEM I based facilities the only unambiguous case of radiation-induced optic neuropathy is reported by Schultz-Ertner et al. (Schulz-Ertner, Karger, et al. 2007), in which a patient developed bilateral blindness after receiving a maximum dose of 54 Gy (RBE) in 20 fractions to the optic pathways. In 2014, Uhl et al. reported on long term outcome of 155 patients treated with CIRT for chordoma of the skull base (Uhl, Mattke, Welzel, Roeder, et al. 2014). They described 3 cases (2%) of "decreased visual field" in relation to a discussion concerning dose constraints to optic *structures*. Probably, the nature of the toxicity scoring during follow-up, which was "based on medical records and questionnaires" did not allow for a detailed description of the underlying pathology. Therefore it is unknown whether these cases are linked to radiation induced damage optic neuropathy; they may as well be a result of damage to the cornea, lens or retina, or even completely unrelated to the radiotherapy. Applying the same methodology in data collection, Uhl et al. (Uhl, Mattke, Welzel, Oelmann, et al. 2014) and Mattke et al. (Mattke et al. 2018) reported long term outcome of collectively 158 patients treated for skull base chondrosarcoma, without describing any cases of visual field dysfunction. All these publications originate from GSI or HIT, and when explicitly stated, the dose constraint applied for the optic pathway has been a maximum EQD2 of < 54 Gy (RBE) (Schulz-Ertner, Karger, et al. 2007; Uhl, Mattke, Welzel, Roeder, et al. 2014).

For CIRT at Japanese centers applying D_{NIRS} a maximum dose of 40 Gy (RBE) has been used as the dose constraint for the optic nerve (Koto et al. 2014). In 2006, Hasegawa et al. published outcomes of visual acuity after CIRT optimized with the NIRS clinical dose model (Hasegawa et al. 2006). The patients had at least 4 years of follow up, which consisted routine MRI, clinical examination of ophthalmologists and even an electrophysiological test (visual evoked potential), the latter being able to detect occult (asymptomatic) neuropathy. No toxicity was seen in patients were maximum dose to the optic nerve was < 57 Gy (RBE). In multivariate analysis, the dose received by 20% of the optic nerve volume (D20%) was the only significant

predictor of toxicity. NTCP modelling showed that visual acuity could be preserved with a probability of 95% when D20% did not exceed 28 Gy (RBE). Onset of decline of visual acuity was on average by 19.6 months, with a range of 5 - 39 months, with the progression to complete visual loss occurring at 26 months (range 10-41 months).

Using the same dose/fractionation scheme as defined in the NIRS protocols, and in the lack of dose constraints validated for LEM I, CNAO adopted the dose constraints from NIRS at par value, i.e. maximum dose < 40 Gy (RBE) and D20% < 28 Gy (RBE).

6.4.3 Radiation-induced brainstem damage

The brainstem is an important organ acting as a relay between the cerebrum, cerebellum and the body. Furthermore, nine of the twelve cranial nerves arise within the brainstem. Damage to this organ, resulting in necrosis, may therefore result in symptoms ranging between cranial nerve deficiency, ataxia, cognitive disorders, coma and death (Guimas et al. 2016). Due to the potential severity of this injury, dose constraints for radiotherapy are seldom transgressed, and therefore the incidence of injury is generally low (Mayo, Yorke, and Merchant 2010). Radiation-induced brainstem damage is usually graded according to the CTCAE term *Central nervous system necrosis*, as shown in **Table 4.**

For photon and proton treatments using conventional fractionation, it is commonly acknowledged that the dose to the brainstem in general should be < 54 Gy (RBE) although smaller volumes may be treated to <60 Gy (RBE) (Mayo, Yorke, and Merchant 2010; Lambrecht et al. 2018).

Similar constraints ($D_{LEM\ I|1\%}$< 54 Gy (RBE) and $D_{LEM\ I|max}$ <60 Gy (RBE)) have been utilized for CIRT at GSI/HIT in Germany (Nikoghosyan et al. 2010). Various publications from this institution have explicitly reported an absence of brainstem toxicity (Schulz-Ertner, Karger, et al. 2007; Uhl, Mattke, Welzel, Oelmann, et al. 2014). Consequently, these constraints are considered safe for CIRT under HIT's current treatment paradigm, which consists of 20-22 fractions of 3.0-3.5 Gy (RBE) and 5-7 fractions per week. However, it is worth mentioning that a *potential* case of

brainstem toxicity is reported by Mattke el al. in their paper on 101 patients with skull base chondrosarcomas treated with either carbon ions (n=79) or protons (n=22) (Mattke et al. 2018). Here, under the subheading "Radiation necrosis", in which tolerance doses to both brainstem and temporal lobes is mentioned, they describe that *"1 patient developed radiation necrosis 1 year after irradiation with consecutive worsening of her walking abilities"*. The exact location of the damage was not stated, although the described symptoms maybe would be more consistent with damage to the brainstem than to a temporal lobe (Lee et al. 1988; Guimas et al. 2016). Unfortunatley, whether or not this particular patient received proton or CIRT was not stated.

In Japanese centers applying the D_{NIRS}, a maximum dose to the brainstem of 30 Gy (RBE) has been used as constraint (Koto et al. 2014). This constraint was hence adopted at par value by CNAO for their 16 fraction treatment regimes.

Recently, a dose-response analysis of brainstem toxicity following D_{NIRS} optimized CIRT at *Gunma University Heavy Ion Medical Center* (GHMC) was published by Shirai et al. (Shirai et al. 2017). None of the 85 patients included in this analysis experienced symptomatic brainstem toxicity. However, four cases of focal brainstem contrast enhancement were detected on routine Magnetic Resonance Imaging (MRI) during follow up, which by the authors were defined as CNS necrosis grade 1. The lesions were stable or reversible although no therapeutic intervention was administered. These asymptomatic events did not occur before the maximum dose exceeded 48 Gy (RBE). Thus, the former constraint of <30 Gy (RBE) was probably conservative even when applied for D_{NIRS}. In a multivariate analysis, the brainstem volume receiving more than 30 Gy (RBE) ($V_{30\ Gy(RBE)}$) and 40 Gy (RBE) ($V_{40\ Gy(RBE)}$) were independent risk factors for this endpoint. Brainstem toxicity of any grade did not occur before $V_{30\ Gy(RBE)}$ exceeded 0.7 cm^3 and $V_{40\ Gy(RBE)}$ exceeded 0.1 cm^3. Shirai et al. also fitted their data to the LKB NTCP model (Lyman 1985; Burman et al. 1991; Niemierko 1997), resulting in the following model parameters: volume-effect parameter (n) = 0.08, biodiversity parameter (m) = 0.08 and the EUD corresponding to 50% probability of toxicity (TD50) = 32.4 Gy (RBE).

7. Objectives and purpose

A general challenge when applying radiotherapy for cancers is to limit the dose to various organs at risk, often located in immediate proximity to the tumor. Within the head and neck area, the optic pathways and brainstem are among the most important organs to preserve in order to avoid disabling or life-threatening toxicity. In the setting of re-RT, the risk of an acute hemorrhage from the carotid artery increases, an event which is most often fatal. In order to balance the competing aims of high tumor control probability and low risk of severe toxicity, it is imperative to obtain the most exact information on risk factors and dose-response for the development of toxicity in these organs. In general, tolerance doses and dose constraints for CIRT are not well established. The general aim of this work was to improve CIRT for institutions applying the LEM I for treatment planning, by improving dose constraints to various important organs at risk in the head and neck district.

7.1 Paper I

Carotid blowout is a feared complication after re-RT to the head and neck area. Experience from photon radiotherapy has suggested that rates of carotid blowout increase when re-RT is given by hypofractionated schedules compared to conventionally fractionated schedules. The aim of this study was to evaluate the rate of carotid blowout under the current practice for re-RT with particle therapy at CNAO, were fraction doses ranging from 2 Gy (RBE) to 5 Gy (RBE) are applied. Also, we aimed at exploring the potential relationship between this event and the cumulative dose to the carotid artery, a relationship which has not been thoroughly investigated for any type of radiation.

Research questions Paper I:

1. Does re-RT with particle therapy at CNAO result in an acceptable rate of carotid blowout?

2. Is there a correlation between the event of carotid blowout and the cumulative dose received by the carotid artery i.e. can a dose constraint be defined?

7.2 Paper II and Paper III

Dose constraints for the brainstem or optic pathways have never been validated for LEM I optimized CIRT. As a cautious approach, CNAO has therefore adopted constraints from NIRS at par value, although these constraints were defined in a completely different RBE system. Within the clinically most commonly applied dose range, the LEM I overestimates the RBE of CIRT, relative the NIRS clinical dose model. Therefore, in certain clinical situations this strategy would lead to excess sparing of the optic nerve and/or the brainstem, on the cost of adequate target dose coverage. The aim of these studies was therefore to confirm that the original dose constraints applied at CNAO are too conservative in regard to the constraints used at NIRS, and to propose new constraints that can be applied for 16 fraction CIRT treatments that are optimized with the LEM I.

Research questions Paper II:

1) At which dose threshold is radiation induced optic neuropathy observed at CNAO following CIRT?
2) How does the current dose constraints applied for the optic nerve at CNAO relate to the practice at Japanese centres?
3) Can the dose constraints be improved by translating Japanese dose constraints to the LEM I weighted dose?

Research questions Paper III

1) How does the current dose constraints applied for the brainstem at CNAO relate to the practice at Japanese centres?
2) Can the dose constraints be improved by translating Japanese dose constraints to the LEM I weighted dose?

8. Materials and methods

8.1 Paper I

8.1.1 Patients

Paper I included all patients re-irradiated at CNAO in the period September 2012 to March 2016 within the protocols:

- CNAO S05/2011/P: *Treatment with protons for recurrent tumors in the head and neck district*
- CNAO S14/2012/C: *Treatment with carbon ions for recurrent tumors in the head and neck district*

Patients were excluded from the analysis if they had not returned for any follow-up, if records of doses from their previous radiotherapy were missing and in the cases where the treatment fields of the prior irradiation(s) and the re-RT at CNAO did not overlap in any segment of the carotid arteries.

8.1.2 Calculation of cumulative dose to the carotid arteries

For as many patients as possible we calculated the cumulative dose received by their carotid arteries. For the patients were *Digital Imaging and Communications in Medicine* (DICOM) files from previous treatments were available, the Computed Tomography (CT) images, structure set files and dose files from all RT courses were imported to a workstation with the RayStation® version 5.0 TPS (RaySearch Laboratories AB, Stockholm, Sweden). For the treatment course at CNAO, also the Magnetic Resonance Images (MRI) in treatment position was imported and co-registered with the planning CT and used as support in the contouring of the carotid arteries on the CNAO planning CT. For the purpose of this study the carotid artery OAR structure was defined as the common carotid artery and internal carotid artery, with distal limit at the origin of the medial cerebral artery. Thus we excluded smaller branches and the external carotid artery, because these arteries were impossible to contour in many of the patients, and because the current practice at CNAO has been

to delineate only the common carotid and internal carotid artery. All contouring was done by the same radiation oncologist, and only the segment of the carotids which had received re-RT was contoured. In order to obtain the cumulative dose statistics to the carotid artery, the dose from the patient's previous RT course(s) was deformed to the planning CT of the final RT course (CNAO CT) in the following procedure: A rigid registration was made between the patients different planning CTs, with a focus on achieving the best possible match in the section were the carotid arteries had been re-irradiated. Secondly, with the goal of providing the best estimates of cumulative doses for the carotid artery, we applied the hybrid deformable registration function of the RayStation®. It combines image information, f. ex. Hounsfield intensities, with anatomical information provided by the structures (OARs) contoured on the images. Specifically, the carotid artery was defined as a "controlling organ" for the deformation process. This feature allows the software algorithm to prioritize the correct deformation of the carotid artery, while suppressing the obligation to correctly deform the other structures in the image. Furthermore, in order to allow the software to ignore irrelevant parts of the carotid artery (e.g. the subsections that were not irradiated), we defined only the subsection of the artery in which re-RT had occurred as the *region of interest* for the deformable registration. **Figure 23** presents an example of a carotid artery segment deformed using the Raystation TPS.

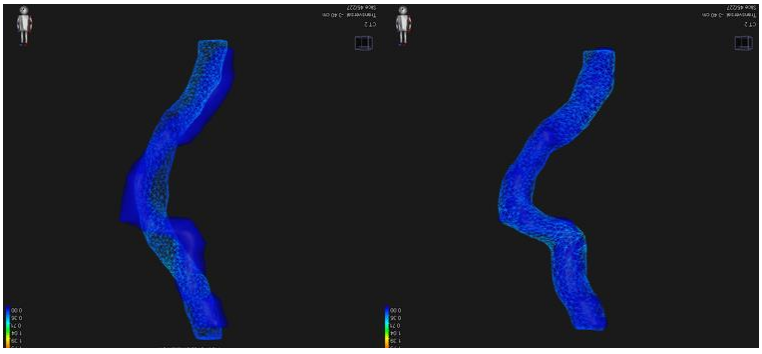

Figure 23: *Left panel: 3D visualization of the path of the same segment of a carotid artery at 1st (sky blue mesh structure) and 2nd course of radiotherapy (solid blue structure) aligned by rigid registration. Right panel: corrected alignment of the carotid artery by deformable registration.*

After the deformable registration was performed, we confirmed that the dose distribution to the carotid artery from the prior radiotherapy course was correctly reproduced on the CNAO treatment planning CT by comparing the original DVH from the prior radiotherapy, with the DVH reproduced on the CNAO treatment planning CT, see **Figure 24**.

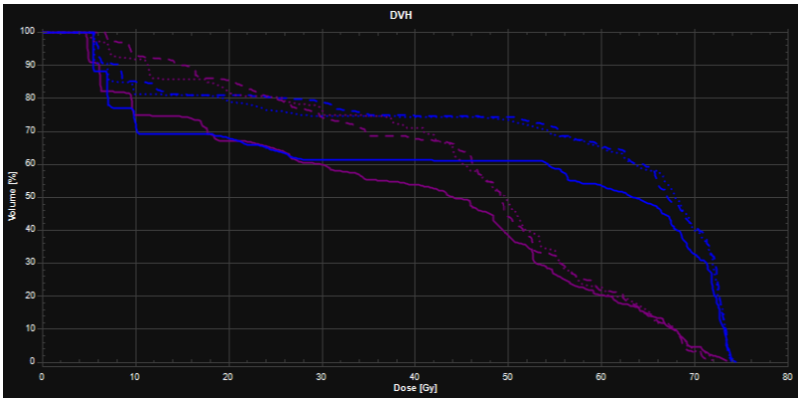

Figure 24: *DVH of left (blue) and right CA (purple). Dashed line DVH represents the original dose distribution from original treatment plan CT. Solid line represents the reproduced dose distribution on CNAO treatment plan using rigid registration. Dotted line represents reproduced dose distribution on CNAO treatment plan CT using deformable registration and dose deformation. Note the far better reproduction of the original dose distribution when deformed deformation is used.*

A cumulative nominal dose distribution was then created with the RayStation TPS by summing the deformed dose(s) with the dose from the final RT on the CNAO CT. The cumulative nominal maximum dose to the carotid artery ($CumDmax_{nom}$) .Since many of the treatments were given with fraction doses well above 2 Gy/Gy (RBE), we also calculated a cumulative maximum EQD2 to the carotid artery ($CumDmax_{EQD2}$) by the following equation:

$$CumDmax_{EQD2} = \frac{D_{1st}\left(\frac{D_{1st}}{Fx_{1st}}+\frac{\alpha}{\beta}\right)}{\left(2+\frac{\alpha}{\beta}\right)} + \frac{D_{2nd}\left(\frac{D_{2nd}}{Fx_{2nd}}+\frac{\alpha}{\beta}\right)}{\left(2+\frac{\alpha}{\beta}\right)} + \frac{D_{3}\left(\frac{D_{3rd}}{Fx_{3rd}}+\frac{\alpha}{\beta}\right)}{\left(2+\frac{\alpha}{\beta}\right)} \qquad \text{(Equation 3)}$$

where D_{1st} was the dose from the 1st RT course contributing to the cumulative nominal maximum dose and Fx_{1st} was the fraction number of the same course. The

second term of the equation was used for patients whom had more than one previous RT, and the third term represented the final re-RT at CNAO. Due to the lack of published data on the α/β-ratio of the carotid artery, an α/β-ratio of 3 Gy was chosen, in coherence with other publications concerning toxicity to arteries induced by radiation (Yazici et al. 2013; Evans et al. 2013).

For some patients the dose distribution from the prior radiotherapy courses was only obtainable from printed CT-slices. In this situation the dose statistics had been collected by the following procedure: the segment of the carotid artery where the highest $CumDmax_{nom}$ would be located was identified by visually comparing the dose plan from the particle therapy course at CNAO with the printed CT-slices from the previous RT courses. The doses (D_{1st}, D_{2nd},...) contributing to the $CumDmax_{nom}$ were then collected from the prints for the respective segment of the carotid artery. If for example the carotid artery in the 1st radiotherapy course was situated between the 50 and 60 Gy isodose curves, an approximation of the D_{1st} was set to 55 Gy. Thereafter, the dose given to the same segment in the particle therapy course at CNAO (D_{3rd}) was derived directly from the *Syngo* TPS installed at CNAO. In this way, an approximation of the $CumDmax_{nom}$ had been collected. A $CumDmax_{EQD2}$ was calculated according to Equation 3.

8.2 Paper II

8.2.1 Patients

Paper II included patients treated in the period January 2013 to December 2014 within the protocols:

- CNAO S09/2012/C: *Treatment with carbon ions for adenoid cystic carcinoma of the salivary glands*
- CNAO S12/2012/C: *Treatment with carbon ions for sarcomas (of bone or soft tissues) in the head and neck district*
- CNAO S15/2012/C: *Treatment with carbon ions for mucosal melanomas of the head and neck district*

Among these, the patient data was analyzed if they had:

- at least 2 years of follow-up
- maximum dose ($D_{LEM|1\%}$) > 20 Gy (RBE) to optic nerve
- available records of visual acuity before and after CIRT

and did not have:

- radiotherapy before or after CIRT at CNAO
- higher dose to the chiasm than to the optic nerve
- preexisting visual impairment
- development of visual impairment in the follow-up period due to other causes than radiation induced optic pathway neuropathy (e.g. recurrent

8.2.2 Recalculation of CNAO treatment plans to D_{NIRS}

An essential method applied for Paper II was to relate the LEM I optimized treatment plans from CNAO to the alternate RBE model, the NIRS clinical dose model. Therefore, the patients' CT image files, structure set files, dose files and plan files were exported from the *syngo*® TPS and imported to the *matRad* open source multimodality radiation TPS (Cisternas et al. 2015). It has been shown to produce absorbed- and RBE-weighted doses consistent with the treatment planning systems used clinically at these institutions (Syngo TPS) for head and neck cases (Wieser et al. 2017). Therefore, it was suitable to reproduce the absorbed doses of CNAO's head and neck treatment plans, and subsequently recalculate the LEM I-weighted doses and the NIRS clinical doses. The input parameters used clinically for LEM I were applied, i.e. $\alpha_\gamma = 0.1$ Gy^{-1}, $\beta_\gamma = 0.05$ Gy^{-2}, $D_t = 30$ Gy, $s_{max} = 3.1$ Gy^{-1}, $R_n = 5$ µm (Kramer and Scholz 2000). The DVHs of targets and OARs were compared with the corresponding DVHs of the dose distribution from the *syngo*® TPS to ensure correct reproduction of both absorbed doses and $D_{LEM\,I}$. Secondly, NIRS clinical dose model was implemented in the *matRad* TPS code using the input parameters used clinically ($R_d = 0.32$ µm, $R_n = 3.9$ µm, $\alpha_0 = 0.172$ Gy^{-1}, $\beta = 0.0615$ Gy^{-2}, $\alpha_r = 0.764$ Gy^{-1}, $F_{Clin} = 2.39$) (Inaniwa et al. 2015; Magro et al. 2017) and D_{NIRS} was thus derived from the

exact same absorbed dose and LET spectra as the $D_{LEM\ I}$. **Figure 25** presents the process of obtaining the RBE-weighted doses according to the LEM I and the NIRS clinical dose model.

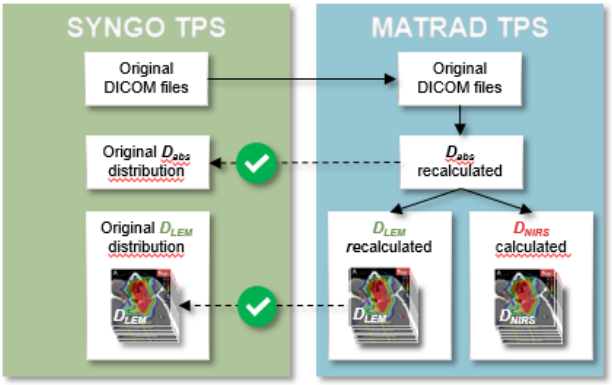

Figure 25: *Process of recalculation. DICOM files from the Syngo TPS were imported to the matRad TPS, in which the absorbed dose was reproduced. Subsequently, the LEM I-weighted (D_{LEM}) and NIRS clinical (D_{NIRS}) doses were calculated. Correct reproduction was ensured by comparing the dose distributions to the original dose distributions in Syngo.*

8.2.3 Data analysis

NTCP was calculated for both $D_{LEM\ I}$ and D_{NIRS} for the DVH variables $D_{1\%}$, $D_{10\%}$, $D_{20\%}$ through $D_{50\%}$ and were used to derive the dose that would result in 5% (TD5) and 50% (TD50) probability of radiation induced optic neuropathy according to the equation:

$$NTCP\ (Dx\%) = 1 - \frac{1}{1+e^{a+b*d}} \qquad \text{(Equation 4)}$$

where d is the RBE-weighted dose to $x\%$ of the optic nerve volume and a and b are constants estimated to provide the best fit to the data set, using binary logistic regression.

Furthermore, for each optic nerve, the D_{NIRS} received by 1% and 20% of the optic nerve volume ($D_{NIRS|1\%}$ and $D_{NIRS|20\%}$) were plotted as a function of respective dose metrics in $D_{LEM\ I}$. A curve fitting procedure performed with the software IBM SPSS Statistics for Windows, Version 24.0 (IBM Corp., Armonk, NY, U.S.A.) in order to produce a dose translation model. The model could then be used to translate D_{NIRS} constraints to $D_{LEM\ I}$ constraints.

By assessing the results from NTCP modelling and the dose translation models possible new $D_{LEM\ I}$ constraints were be proposed. As a final step, five of the treatment plans were re-optimized applying this new set of $D_{LEM\ I}$ constraints. Subsequently, these re-optimized plans were recalculated to D_{NIRS} to ensure that the new $D_{LEM\ I}$ constraints still were in compliance with the D_{NIRS} constraints. These procedures, which were conducted exclusively to confirm the relationship of the RBE models, were performed with the RayStation® 6.99 TPS (RaySearch Laboratories AB, Stockholm, Sweden), where both the LEM I and the NIRS clinical dose were implemented with the respective model input parameters as mentioned earlier in chapter 8.2.2. The process of data analysis and verification of the dose translation model is summarized in **Figure 26.**

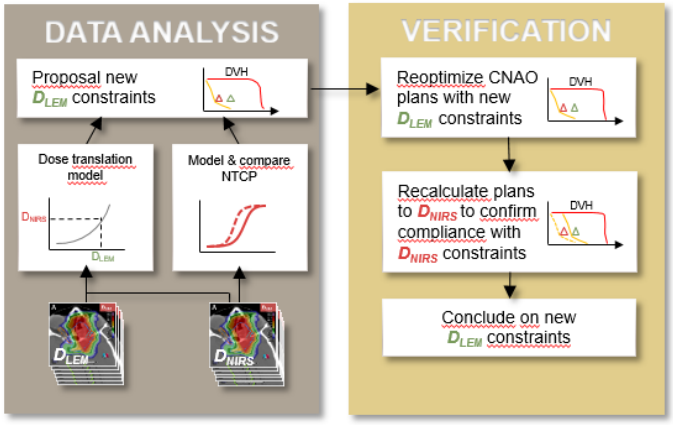

Figure 26: *Overview of process of data analysis and verification of dose translation model.*

8.3 Paper III

In this study we made use of 30 of the 38 patient treatment plans already recalculated to D_{NIRS} for Paper II. In the remaining eight patient treatment plans the maximum $D_{LEM\ I}$ to the brainstem was less than 10 Gy (RBE), and thus the information from these plans would not contribute to achieve the goal of Paper III.

The D_{NIRS} recalculated treatment plans were used to estimate NTCP of asymptomatic brainstem injury for these 30 patients treated at CNAO, based on the NTCP-model published by Shirai et al. as presented in chapter 6.4.3.

Dose translation models were produced, as described for Paper I, for the brainstem dose metrics $D_{0.07cm3}$ and $D_{0.01cm3}$, in order to translate the D_{NIRS} constraints proposed by Shirai et al. into $D_{LEM\ I}$.

Finally, to verify that the dose translation models predicted correctly also at dose levels higher than our original data set, five of the treatment plans were re-optimized applying this new set of $D_{LEM\ I}$ constraints. Subsequently, these re-optimized plans were recalculated to D_{NIRS} to ensure that the new $D_{LEM\ I}$ constraints still were in compliance with the D_{NIRS} constraints, as described in Paper II.

8.4 Statistical methods

All statistical procedures were performed with the software IBM SPSS Statistics for Windows, Version 24.0 (IBM Corp., Armonk, NY, U.S.A.). Descriptive statistics were used to summarize the characteristics of the patient population and treatment. Differences in frequencies between cohorts were compared using the Chi-Square test or the Fischer's exact test. The Shapiro-Wilk test with an alpha level of 0.05 was applied to evaluate whether or not a variable was normally distributed. Non-parametrical distributions were compared with the Mann-Whitney U-test, while normally distributed data were compared with the independent samples T-test. Bivariate correlations between skewed data were analyzed with Spearman's rho. The Kaplan-Meier method was used to estimate rates of toxic events or overall survival. Univariate binary logistic regression was used to fit the relation of a continuous

independent variable (dose) to a dichotomous dependent outcome variable (toxicity: "Yes" or "No") to produce models for NTCP. All p-values were obtained from two-sided tests. P-values <0.05 were considered significant.

8.5 Ethics, approvals and grants.

All patients included in this analysis of medical record data were treated at CNAO within the framework of prospective protocols. The treatment protocols were approved by the institutional ethics committee (*Comitato Etico Fondazione CNAO, references for approval: CE EMEND. n.1 al 9_2012, CE 19.12.2012 S15_2012C, CE 09.09.2011 S5/2011/P, CE 19.12.2012 S14/2012/C and CE 19.15.2012 S_12/2012C*).All patients gave written, informed consent before inclusion, which included that the clinical data could be used for research purposes. All patient data were anonymized before transmission to the Ph.D. candidate for analysis. The studies were supported by grants (grant no: BFS2015PAR02) from the *Trond Mohn Foundation, Ytrebygdsvegen 215, Kokstad, Postboks 7150, 5020 BERGEN, Norway, Phone: +47 479 00 111, org.nr: 988 029 327.*

9. Results

9.1 Paper I

Patient and disease characteristics are presented in **Table 5.** The median follow-up was 13.4 months (range 0.8 – 49.2 months). The actuarial 1 year overall survival for the whole cohort (n=96) was 81.5%. We found one confirmed and one probable case of carotid blowout, i.e. in 2.1% of the investigated population. The 1 year actuarial rate of carotid blowout was 2.7% (95%CI: 0.01-11.0%), see **Figure 27.**

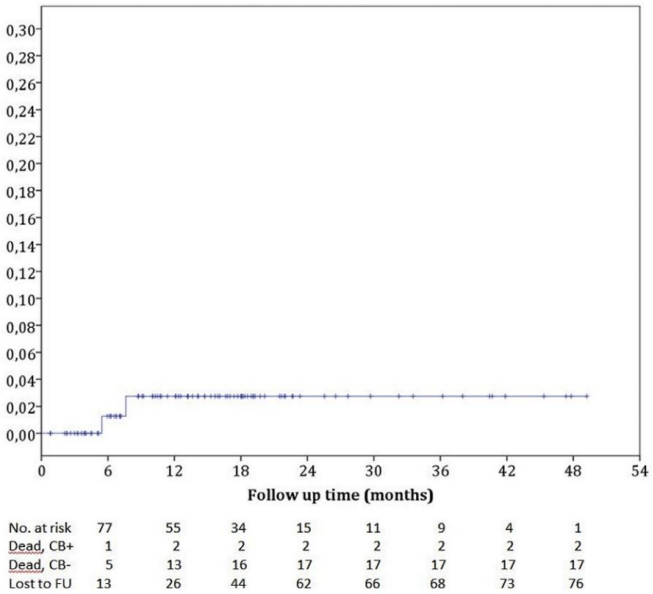

Figure 27: *Cumulative carotid blowout (CB) rate. The table displays the absolute number of patients who were at risk of CB, death due to CB, death due to other causes than CB, and loss to follow-up at the end of each 6 month interval.*

Table 5: *Patient and disease characteristics*

	Quality of Final Re-RT			*P* value
	All (n = 96)	Proton RT (n = 17)	CIRT (n = 79)	
Median age (range), y	61 (24-88)	55 (24-75)	63 (24-88)	
Sex, male:female	56:40	8:9	48:31	NS
Comorbidity, n (%)				
Hypertension	26 (27.0)	2 (11.8)	24 (30.4)	NS
Diabetes mellitus	6 (6.3)	2 (11.8)	4 (5.1)	NS
Cardiovascular disease	5 (5.2)	3 (17.6)	2 (2.5)	.037
Histology, n (%)				
Adenoid cystic carcinoma	28 (29.2)	0 (0.0)	28 (35.4)	.003
Squamous cell carcinoma	27 (28.1)	13 (76.5)	14 (17.7)	
Sarcoma	11 (11.5)	0 (0.0)	11 (13.9)	
Mucoepidermoid carcinoma	5 (5.2)	0 (0.0)	5 (6.3)	
Undifferentiated carcinoma	5 (5.2)	1 (5.9)	4 (5.1)	
Pleomorphic adenoma	5 (5.2)	0 (0.0)	5 (6.3)	
Adenocarcinoma	3 (3.1)	0 (0.0)	3 (3.8)	
Myoepithelial carcinoma	3 (3.1)	0 (0.0)	3 (3.8)	
Meningioma	3 (3.1)	1 (5.9)	2 (2.5)	
High grade glioma	2 (2.1)	2 (11.8)	0 (0.0)	
Other[a]	4 (4.2)	0 (0.0)	6 (7.8)	
Site of Primary Tumor, n (%)				
Parotid gland	18 (18.8)	0 (0.0)	18 (22.8)	.003
Paranasal sinuses	17 (17.7)	0 (0.0)	17 (21.5)	
Rhinopharynx	15 (15.6)	6 (35.3)	9 (11.4)	
Oropharynx	10 (10.4)	3 (17.6)	7 (8.9)	
Oral cavity	7 (7.3)	2 (11.8)	5 (6.3)	
Brain/meninges	5 (5.2)	3 (17.6)	2 (2,5)	
Nasal cavity	5 (5.2)	1 (5.9)	4 (5.1)	
Skull base	5 (5.2)	0 (0.0)	5 (6.3)	
Skin of scalp or face	4 (4.2)	1 (5.9)	3 (3.8)	
Submandibular gland	3 (3.1)	0 (0.0)	3 (3.8)	
Larynx	2 (2.1)	1 (5.9)	1 (1.3)	
Lacrimal gland	2 (2.1)	0 (0.0)	2 (2.5)	
Other[b]	3 (3.1)	0 (0.0)	3 (3.8)	
Site of Highest Dose to CA, n (%)				
Neck	50 (52.1)	9 (52.9)	41 (51.9)	NS
Skull base	34 (35.4)	4 (23.5)	30 (38.0)	
Sinus cavernosus	10 (10.4)	3 (17.6)	7 (8.9)	
Intracranial	2 (2.1)	1 (5.9)	1 (1.3)	
Tumor Involvement Grade, n (%)				
No involvement	24 (25.0)	6 (35.3)	18 (22.8)	NS
<1/3 of CA circumference	14 (14.6)	2 (11.8)	12 (15.2)	
≥1/3 < 2/3 of CA circumference	9 (9.4)	2 (11.8)	7 (8.9)	
≥2/3 of CA circumference	49 (51.1)	7 (41.2)	42 (53.2)	
Surgery, n (%)				
Any surgery	80 (83.3)	10 (58.8)	70 (88.6)	.007
Neck dissection	26 (27.1)	6 (35.3)	20 (25.3)	NS
In vicinity of highest dose to CA	46 (47.9)	5 (29.4)	41 (51.9)	NS
High-Risk Features[c], n (%)				
0 risk factors	28 (29.2)	8 (47.1)	20 (25.3)	NS
1 risk factor	41 (42.7)	6 (35.3)	35 (44.3)	
2 risk factors	27 (28.1)	3 (17.6)	24 (30.4)	

CA, carotid artery; CIRT, carbon ion radiation therapy; NS, not significant; RT, radiation therapy.

[a] Esthesioneuroblastoma, sinonasal carcinoma, carcinoma ex pleomorphic adenoma, oncocytoma.

[b] Mandible, hyoid bone, lymph node metastasis neck.

[c] Risk factors: Tumor involvement grade ≥2/3 and surgery in high-dose areas.

Interestingly, these carotid blowout events were found within the subgroup reirradiated with protons (n=17). Therefore, for the proton subgroup exclusively, the 1 year actuarial rate was 14.4% (95%CI: 0.11-19.0%), compared to 0% in the carbon ion group, a difference that was significant according to the log-rank test ($p<0.003$). Both cases were re-irradiated at the nasopharyngeal site due to recurrent squamous cell carcinoma within 20 months following primary photon RT. The cumulative maximum EQD2 received by their carotid arteries were 107 and 132 Gy (RBE). A significantly higher proportion had undergone surgery in the carbon ion group compared to the proton group (88.9% vs. 58.8%, $p=0.007$). Median cumulative nominal lifetime dose was 120 Gy (RBE) for the whole cohort, with no significant difference in the distribution between the carbon ion and proton group. However, due to significantly higher fraction doses used in the carbon ion group compared to the proton group, the cumulative prescribed lifetime doses were generally higher in the carbon ion group when evaluated in EQD2, median 132 (range 46-296) Gy (RBE) vs. 122 (range 67-140) Gy (RBE), respectively ($p<0.005$). However, there was no significant difference between the groups in regard the cumulative maximum EQD2 *received by the carotid artery*, which was median 109 (range 25-167) Gy (RBE) among the 49 patients in which these data were available. The correlation between the cumulative nominal lifetime dose and cumulative maximal dose to the carotid artery was poor, as demonstrated by a Spearman's rho coefficient of 0.363 ($p=0.010$). **Figure 28** presents the cumulative maximum EQD2 for the 74 carotid arteries. There was no obvious correlation between this dose metric and the event of carotid blowout.

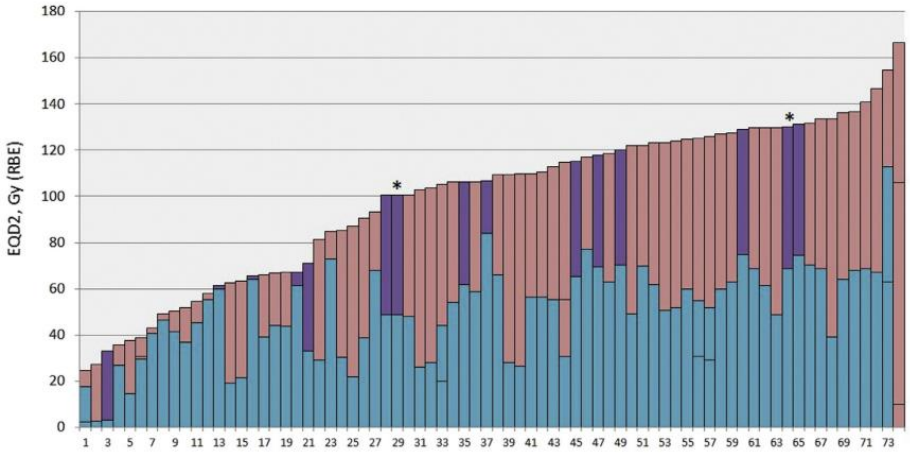

Figure 28: *Cumulative maximum EQD2 for all 74 carotid arteries, displaying the contribution from photon RT (blue), carbon RT (pink) and proton RT (purple). * Carotid arteries of the 2 patients who developed oronasal haemorrhage.*

9.2 Paper II

A total of 141 patients had been treated in the relevant protocols within the years 2013-2014. The majority of patients treated were excluded because the dose to the optic nerve was less than 20 Gy (RBE), see **Figure 29.** Further analysis was therefore based on 65 optic nerves from 38 patients. Patient and disease characteristics are presented in **Table 6.**

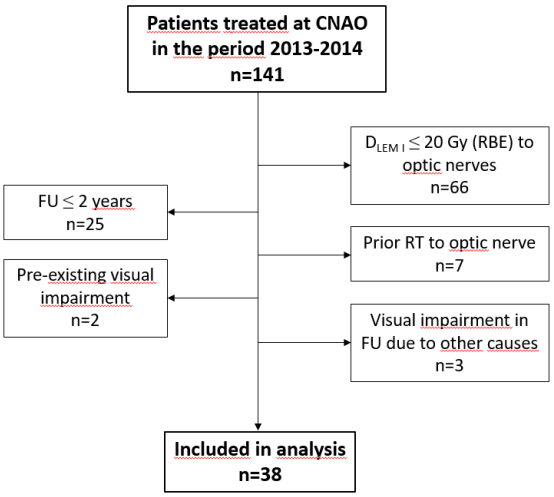

Figure 29: *Overview of patient selection and reasons for exclusion from the analysis.*

Table 6: Patient and disease characteristics for all patients and grouped by patients that developed (RION=yes) or did not develop (RION=no) radiation induced optic neuropathy.

	All (n=38)	RION=Y (n=3)	RION=N (n=35)	*P* value
Sex, female:male	18:20	2:1	16:19	1.0
Median age (range), y	59 (16-81)	62 (54-68)	54 (16-81)	0.44
Comorbidity, n (%)				
Hypertension	9 (23.7%)	1 (33.3%)	8 (22.9%)	1.0
Diabetes mellitus	8 (21.1%)	1 (33.3%)	7 (20.0%)	0.59
Cardiovascular disease	4 (10.5%)	1 (33.3%)	3 (8.6%)	0.29
Histology, n (%)				
Adenoid cystic carcinoma	14 (36.8%)	2 (66.7%)	12 (34.3%)	0.48
Chordoma	14 (36.8%)	0 (0.0%)	14 (40.0%)	
Chondrosarcoma	3 (7.9%)	0 (0.0%)	3 (8.6%)	
Other sarcoma	5 (13.2%)	1 (33.3%)	4 (11.4%)	
Acinar cell carcinoma	1 (2.6%)	0 (0.0%)	1 (2.9%)	
Mucosal malignant melanoma	1 (2.6%)	0 (0.0%)	1 (2.9%)	
Site, n (%)				
Clivus	12 (31.6%)	1 (33.3%)	11 (31.4%)	0.67
Paranasal sinus	9 (23.7%)	2 (66.7%)	7 (20.0%)	
Skull base	9 (23.7%)	0 (0.0%)	9 (25.7%)	
Nasal cavity	4 (10.5%)	0 (0.0%)	4 (11.4%)	
Nasopharynx	2 (5.2%)	0 (0.0%)	2 (5.7%)	
Other	2 (5.2%)	0 (0.0%)	2 (5.7%)	

The median follow-up was 47 (range 26-67) months. We observed three events of unilateral radiation induced optic neuropathy (all CTCAE grade 4), occurring at LEM I-weighted doses of ≥71 Gy (RBE) and ≥68 Gy (RBE) to 1% ($D_{LEM|1\%}$) and 20% ($D_{LEM|20\%}$) the optic nerve volume, respectively. In addition, 10 other optic nerves received doses exceeding the former CNAO dose constraints of $D_{LEM|1\%} \leq 40$ Gy (RBE) and $D_{LEM|20\%} \leq 28$ Gy (RBE) without developing toxicity, see **Figure 30**. After recalculation of the dose distribution to the NIRS clinical dose (D_{NIRS}), only 6 of these 10 optic nerves still exceeded these constraints, highlighting that equal constraints become more restrictive when applied at CNAO.

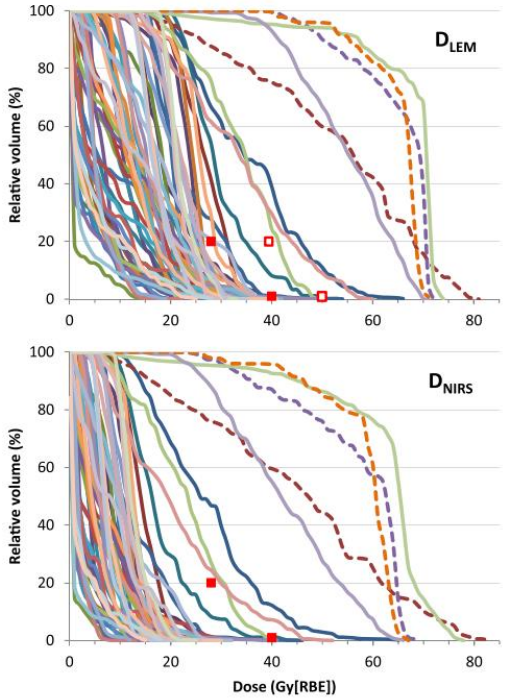

Figure 30: *Cumulative DVH of all 65 optic nerves in D_{LEM} (upper panel) and D_{NIRS} (lower panel). Dashed DVH-lines represents optic nerves that developed neuropathy. Red, filled squares indicate the current dose constraints of $D_{1\%} \leq 40$ Gy(RBE) and $D_{20\%} \leq 28$ Gy(RBE). Red, open squares in upper panel represents possible new D_{LEM} constraints for CNAO based on RBE-weighted dose translation.*

For the dose metrics $D_{1\%}$ and $D_{20\%}$, the D_{NIRS} value was plotted as function of the corresponding value in $D_{LEM\ I}$. A quadratic function fit well with the data pairs, showing high coefficients of determination (R^2), as seen in **Figure 31**. From these plots, the NIRS dose constraint of $D_{NIRS|20\%} \leq 28$ Gy (RBE) corresponded to $D_{LEM\ I|20\%} \leq 40$ Gy (RBE), and $D_{NIRS|1\%} \leq 40$ Gy (RBE) corresponded to $D_{LEM\ I|1\%} \leq 50$ Gy (RBE). These values were below, and thus not in conflict with the threshold for 5% risk of

toxicity (TD5) suggested from the NTCP-modelling, which was found to be at 55 Gy (RBE) for $D_{LEM\ I|20\%}$ and at 62 Gy (RBE) for $D_{LEM\ I|1\%}$.

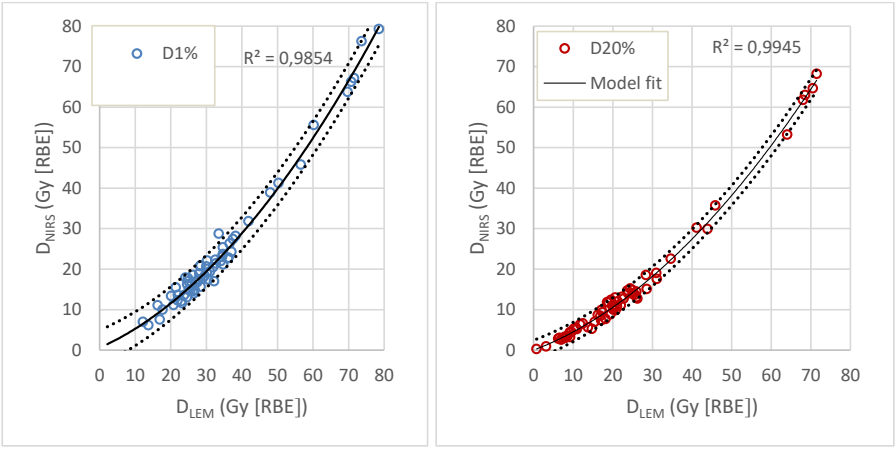

Figure 31: *Relationship of D_{NIRS} and D_{LEM} for $D_{1\%}$ (left panel) and $D_{20\%}$ (right panel). Solid line represents the quadratic regression model fit with 95% confidence intervals (dotted lines). The corresponding coefficients of determination (R^2) are also provided.*

9.3 Paper III

The disease and treatment characteristics of the 30 cases used in this analysis are presented in **Table 7.** The recalculation of these $D_{LEM\ I}$ optimized treatment plans optimized in to D_{NIRS} (in this paper referred to as D_{MKM}) confirmed that the RBE-weighted dose distributions to the brainstem are predicted to be lower when D_{NIRS} is applied, see **Figure 32a** and **32c.**

TABLE 7: Disease and treatment characteristics

Case no.	*Histology*	*Site*	*Total D_{LEM} Gy(RBE)*	*Fraction D_{LEM} Gy(RBE)*
1	Chordoma	Skull base	70.4	4.4
2	Mesenchymal tumor	Frontal sinus	76.8	4.8
3	Chordoma	Skull base	70.4	4.4
4	Chordoma	Skull base	70.4	4.4
5	MPNST	Clivus	76.8	4.6
6	Chordoma	Skull base	70.4	4.4
7	ACC	Meckel's cave	68.8	4.3
8	Chondrosarcoma	Nasal cavity	70.4	4.4
9	Chordoma	Clivus	70.4	4.4
10	Chordoma	Clivus	70.4	4.4
11	Chordoma	Clivus	70.4	4.4
12	ACC	Maxillary sinus	68.8	4.3
13	Chordoma	Clivus	70.4	4.4
14	Chordoma	Clivus	70.4	4.4
15	Chondrosarcoma	Clivus	70.4	4.4
16	Chordoma	Skull base	70.4	4.4
17	ACC	Maxillary sinus	68.8	4.3
18	ACC	Nasopharynx	68,8	4,3
19	Chordoma	Clivus	70.4	4.4
20	Chondrosarcoma	Skull base	70.4	4.4
21	Chordoma	Clivus	70.4	4.4
22	ACC	Maxillary sinus	68.8	4.3
23	ACC	Skull base	68.8	4.3
24	Chordoma	Clivus	70.4	4.4
25	Pleomorphic sarcoma	Clivus	76.8	4.8
26	ACC	Paranasal sinuses	68.8	4.3
27	Chordoma	Clivus	70.4	4.4
28	Acinar cell carcinoma	Ethmoid/nasal cavity	68.8	4.3
29	ACC	Maxillary sinus	68.8	4.3
30	Chordoma	Clivus	70.4	4.4

MPNST: Malignant peripheral nerve sheath tumor; ACC: Adenoid cystic carcinoma.

Applying the NTCP model derived by Shirai et al. suggested the probability of developing an asymptomatic brainstem reaction to be close to 0% for 29 of the patients, and 2% for 1 patient.

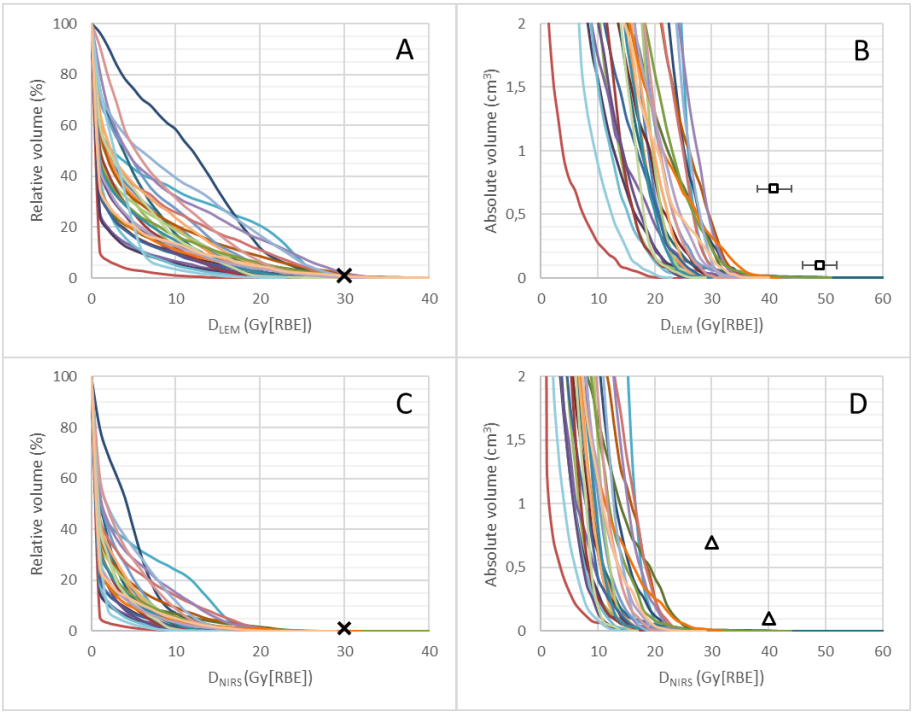

Figure 32: *Brainstem DVHs in relative (A, C) and absolute volume (≤2 cm³) (B, D) of 30 patients treated at CNAO, presented in $D_{LEM\ I}$ (A, B) and D_{MKM} (=D_{NIRS}) (C, D). Crosses represents the former CNAO and NIRS dose constraint of $D_{1\%} \leq 30$ Gy(RBE). Triangles represent the new D_{NIRS} constraints $V_{40\ Gy(RBE)} < 0.1\ cm^3$ and $V_{30\ Gy(RBE)} < 0.7\ cm^3$ as defined by Shirai et al. (14). Squares in panel B represent the possible new $D_{LEM\ I}$ constraints (error bars = 95% CI) resulting from the dose translation model presented in this work, see Figure 33.*

For the dose metrics $D_{0.7cm3}$ and $D_{0.1cm3}$, the D_{NIRS} value was plotted as function of the corresponding value in $D_{LEM\ I}$, represented as the black squares in **Figure 33**. Although a linear function would describe the relationship well, our experience from Paper II clearly suggested that a quadratic function would be a better fit to describe the relationship also at higher dose levels. Therefore, a quadratic function was fitted, showing high coefficients of determination (R^2). This dose translation model revealed

that the D_{NIRS} constraints corresponded to $D_{LEM\ I|0.7cm3}$ <41 Gy (RBE) (95% CI: 38-44 Gy [RBE]) and $D_{LEM\ I|0.1cm3}$ <49 Gy (RBE) (95% CI: 46-52 Gy [RBE]). However, these values were derived from extrapolation from the data (black squares), using a function that not necessarily would be correct at higher dose levels. Therefore, we reoptimized five of the treatment plans using new tentative brainstem constraints within the lower half of the 95%CI of the dose translation estimates, i.e. $D_{LEMI|0.7cm3}$ = 38-41 Gy (RBE) and $D_{LEM\ I|0.1cm3}$ = 46-49 Gy (RBE). Subsequently, these plans were recalculated to D_{NIRS}. The relationship of D_{NIRS} /$D_{LEM\ I}$ for the dose metrics are plotted at open circles in **Figure 33b**, showing that the quadratic function correctly predicted the relationship at these dose levels.

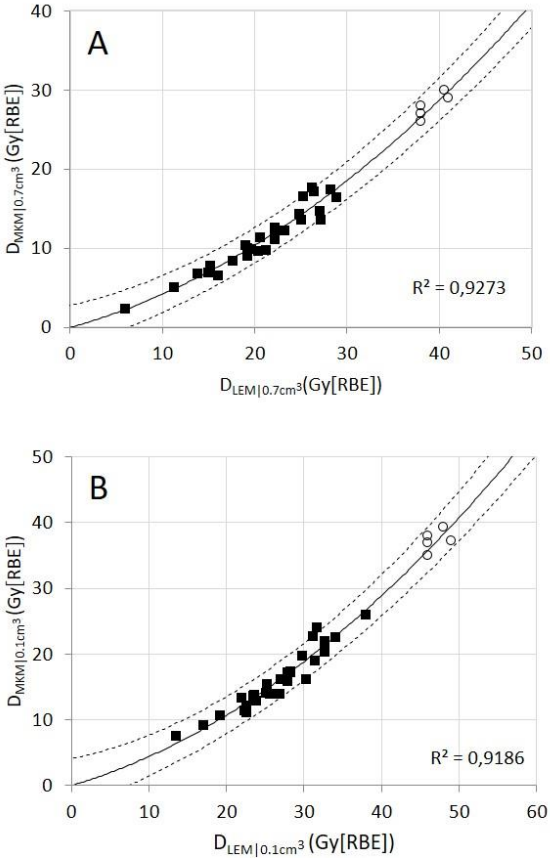

Figure 33: *Squares represent the relationship of D_{LEM} and D_{MKM} (=D_{NIRS}) for dose metrics $D_{0.7\ cm3}$ (A) and $D_{0.1\ cm3}$ (B) for each individual brainstem. The solid line represents the best fit with 95%CI (dashed lines). The open circles represent the data collected from the reoptimized plans, which were not used for the curve fitting procedure.*

10. Discussion

10.1 Methodological considerations

10.1.1 Paper I

Patient selection

The entire cohort retreated with particle therapy to the head and neck region at CNAO formed the basis of this study. Although not directly relevant for the overall topic of this thesis, also the minor subgroup retreated with protons were included in the analysis, since also the outcome of these patients is important. Under the assumption that the cumulative dose to the carotid artery is the major factor governing the risk of carotid blowout, we deliberately excluded patients in whom there was no overlap of dose in the carotid artery in the prior and last radiotherapy at CNAO. 27 of 128 potential cases where therefore excluded. However, if the cumulative dose to the carotid artery is of lesser importance, we may have unintentionally excluded relevant patients in regards to detecting other possible risk factors from the analysis. As a comment, we can state that none of these excluded patients were registered with carotid blowout events in the CNAO database. However, for the sake of transparency also these cases should have been analyzed as an overall presentation of the retreatment cohort at CNAO.

Follow-up time

The follow-up time in this paper was median 13.4 months (range 0.8 – 49.2). Although median time to event is reported to be around 6 months, some cases of carotid blowout develop several years after treatment. As can be seen in **Figure 27,** only 15 patients remain in follow-up at 24 months, while 19 patients were dead. As many as 62 patients (65%) were lost to follow-up at this time point. The high proportion of patients being lost to follow-up is most likely an effect of CNAO being a standalone particle therapy center, recruiting patients from all over Italy and even from foreign countries. Obviously, many patients, having side effects after being

heavily treated with radiotherapy, or even having a new relapse of the disease, may not prioritize to spend time and money on travelling far distances to meet for follow-up. Certainly, some of the patients lost to follow-up may have developed carotid blowout events which have not been registered in the CNAO database. As it follows, this may imply a greater risk for carotid blowout following particle therapy at CNAO than our work suggests.

10.1.2 Paper II

Detection of endpoint event

The follow-up program at CNAO did not include routine examination by an ophthalmologist. Rather, simpler clinical test were performed, e.g. finger counting test and visual field test ad modum Donders', in addition to the recording of the patients' subjective experience of visual decline. When potential visual defects were detected, patients were referred to an ophthalmologist for further investigations and diagnosis. Hence, one cannot expect that this routine will detect the less severe grades of optic neuropathy. However, the more severe forms (≥grade 3), which are most important in regards to quality of life, would most certainly be detected.

Follow-up time

In the study design we excluded patients with less than 2 years of follow-up, which we regarded as an adequate balance between obtaining a reasonably sized cohort against risking to include patients in which the endpoint still had yet to develop. However, this may even have been too short. In the paper by Hasegawa et al., on optic nerve toxicity following CIRT at NIRS, the *onset* of visual loss started later than 2 years following therapy in 4/11 damaged nerves (Hasegawa et al. 2006). Furthermore, in 6/11 optic nerves, the progression to complete blindness occurred from 25 – 41 months following the therapy.

However, among the 8 optic nerves receiving high dose in our cohort, i.e. $D_{LEM\ I|1\%}$ >50 Gy (RBE) and/or $D_{LEM\ I|20\%}$ >40 Gy (RBE), all but one had follow-up of more than 3 years, see **Figure 34.** Consequently, most patients at risk had been observed for an adequate time period.

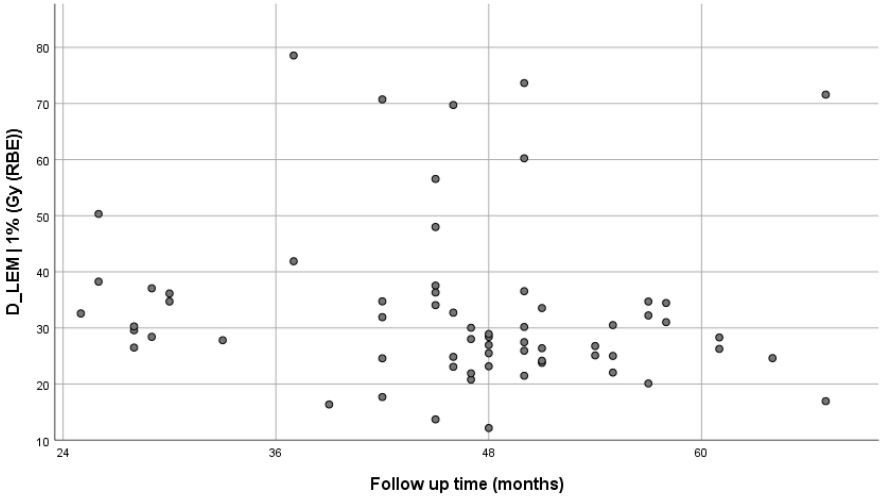

Figure 34: *Scatterplot of follow-up time vs. $D_{LEM|1\%}$ for the 65 optic nerves analyzed in Paper I.*

The dose translation model

The major weakness in the dose translation model is that many factors may modulate the RBE at different centres (Vogin et al. 2019). Most importantly, transferring dose constraints defined by a center with passive scattering beam delivery (PS) to a center with pencil beam scanning (PBS) may be considered controversial. The beam delivery techniques will inevitably cause differences in the radiation quality of the beams, and the distribution and weighting of Bragg peaks may be very dissimilar. However, two studies have confirmed that the biological effect of the carbon ion beams of NIRS, HIT and CNAO is identical (Uzawa et al. 2009; Facoetti et al. 2015).

Furthermore, the absorbed dose underlying the RBE-weighted dose is calculated by different beam models, dependent on which TPS the institution uses. Therefore, as soon as the beam penetrates into a patient's body, each TPS will generate unique dose

calculation uncertainties. As an example, Molinelli et al. simulated patient treatments given at the passive scattering beamline at NIRS in the FLUKA Monte Carlo code (Molinelli et al. 2016). When comparing the absolute dose as originally calculated by the NIRS TPS to the dose calculated by the far more sophisticated beam model of the FLUKA Monte Carlo code, they found a mean absolute dose difference of 2.4% along the SOPB for head and neck cases. Differences related to beam modelling in the *out-of-target* areas have not been investigated. More profound differences in absorbed dose as they are calculated by different TPS's may be expected within the lateral penumbra dose fall-off. This region is certainly sensitive to how the lateral spread of the beam is modelled, and the sharp lateral penumbra of the carbon ion beam is typically utilized to avoid high doses to the brainstem and optic nerve when these are located close to the tumor. These issues infer that the D_{NIRS} distributions that we have calculated in this work, based on the absorbed dose distribution originating from LEM I optimized treatment plans at CNAO, definitely are not exact replicas of D_{NIRS} treatment plans used for patient treatments in Japanese centers.

A better way to translate the Japanese dose constraints to $D_{LEM\ I}$, would therefore be to simulate NIRS patient treatments as described in the previous section (Molinelli et al. 2016). However, this method is not practically applicable for larger sets of patient data as the simulation-process requires tremendous resources, both in regard to computational capacity and man-power, including the effort of programming the exact geometries of every patient's specific hardware (e.g. collimators and compensators) for *each* beam in each treatment plan.

10.1.3 Paper III

An underlying premise for Paper III was that even asymptomatic brainstem lesions were yet to be seen at CNAO following LEM I-optimized CIRT. Thus, an overall outcome analysis for this endpoint would be of doubtful scientific value. We therefore made use of patient treatment plans already recalculated to D_{NIRS} for Paper II, as they this would provide an adequate sample of typical brainstem dose distributions at CNAO. As can be seen in **Figure 33**, the values for $D_{LEM\ I}$ were nicely dispersed and thus adequate to fulfil the aim of the study. Methodologically, Paper III

shares the limitations and uncertainties of the dose translation model, as discussed for Paper II, see section 10.1.2. Moreover, in the lack of relevant toxic events at CNAO, the results and conclusions of Paper III are therefore principally based on the translation of the Japanese dose constraints proposed by Shirai et al. and thus share the limitations of their study (Shirai et al. 2017). Most importantly the Shirai et al. study was also rather small, having 4 events within a total of 85 patients. However, since the endpoint relating to these constraints was asymptomatic (grade 1) brainstem damage, as detected on routine MRI, we are confident that there is a buffer towards the more meaningful clinical endpoint (brainstem necrosis grade ≥ 2), thus mitigating the both the limitations of the Shirai study and the uncertainties of the dose translation model of Paper III. Isolated contrast enhancement on MRI is regarded as evidence of increased permeability of the blood brain barrier (BBB), which results from radiation-induced alterations in endothelial and glial cell function (Yuan et al. 2006). However, increased permeability does not necessarily lead to parenchymal damage as demonstrated for the spinal cord in a rat model (Siegal and Pfeffer 1995). The phenomenon of reversible or asymptomatic lesions has also been documented for radiation-induced injury of the brain following CIRT, and it is hypothesized that since smaller volumes of CNS tissue is irradiated by particle therapy in comparison to photon RT, the probability of recovery will be higher (Kishimoto et al. 2005). The observation that the lesions reported by Shirai et al. were reversible or stable in the absence of therapeutic intervention further supports the argument that no real necrosis had occurred.

10.2 General discussion of results

10.2.1 Paper I

Paper I was the first paper to analyze the risk of carotid blowout following re-RT with particle therapy. In addition, it is the first paper, regardless of radiation modality, to reproduce the cumulative doses to the carotid artery in a detailed manner.

Early reports on photon SBRT suggested higher rates of carotid blowout (8-17%) (Cengiz et al. 2011; Yamazaki et al. 2013; Kodani et al. 2011) than with conventionally fractionated photon RT, which was one of the motivations for Paper I; exploring the risk of moderately hypofractionation with particle therapy at CNAO. However, a recent large multi-institutional study, comparing SBRT (n=197) vs. IMRT (n=217) showed both to be equally safe, with only 2 cases of carotid blowout in each group (Vargo et al. 2018). SBRT fractions were given on non-consecutive days, an approach also described by smaller SBRT series as safer in regards to carotid blowout (Gebhardt et al. 2018; Yazici et al. 2013).

As presented in Paper I, we found one confirmed and one potential case of carotid blowout. Contrary to the expectations, both were in the subgroup of 17 patients re-irradiated with protons. This seems as a high rate, when comparing to recent reports on re-RT with protons. Neither McDonald et al. (McDonald et al. 2016) or Phan et al. (Phan et al. 2016) found cases of carotid blowout in their retrospective studies comprising of 61 and 60 patients re-irradiated with protons. Romesser et al. described 2 hemorrhagic events that could be attributed to carotid rupture among 69 patients with assessable follow-up data in a retrospective study based on a multi-institutional prospectively managed proton RT database (Romesser et al. 2016). An important distinction is that these were general outcome studies, and not specific for the carotid blowout event. In contrast, in our study we excluded 1/5th of the entire retreated cohort at CNAO because there was no overlap of dose to the carotid artery, thus potentially enriching it with patients with higher risk of carotid blowout. Additionally, the proton cohort in our paper was small, and therefore random coincidences may dramatically affect the observed carotid blowout rate as demonstrated by the 95% CI of the 1 year actuarial rate which ranged from 0.11% – 19.0%.

Looking at the carbon ion cohort, results were encouraging, since no carotid blowout events were found among the 79 patients in this group. One possible explanation, which we did not report in the paper, is that the choice of radiation quality can affect the time interval between primary radiotherapy and re-RT in a favorable way for the

carbon ion group: In general, risk of severe toxicities increase when there is shorter time interval between the primary and the reirradiation course (Lee et al. 2016). At CNAO, as Paper I shows, cancer types that typically recur early (i.e. squamous cell carcinomas) were more likely retreated with protons, while more slow-growing tumors, (i.e. adenoid cystic carcinomas and chordomas) were retreated with carbon ions. Consequently, the carbon ion group consisted of patients with longer time intervals from primary to re-RT, reducing the risk of carotid blowout in this group compared to the proton group as shown by this post hoc analysis: Median time interval was 1.8 (range 0.75-6.1) years for proton radiotherapy group and 3.6 (range 0.3 – 49.9) years for the CIRT group, $p<0.02$ according to Mann-Whitney U-test.

Regardless of this, our findings are favorable compared to other reports mentioning carotid blowout in the setting of re-RT with carbon ions. Jensen et al. found 2 cases of grade IV carotid hemorrhage, within a cohort of 52 patients retreated at HIT for recurrent adenoid cystic carcinoma (Jensen et al. 2015). In a more recent publication from HIT concerning carbon ion re-RT for recurrent head and neck cancer (Held et al. 2019), only one case of carotid hemorrhage among 229 patients was reported, although the defined time period of the study (2010-2017) would seem to overlap with the time period for the Jensen et al. report (4/2010 – 5/2013) in which to two cases were reported. Anyhow, in these reports the cumulative lifetime EQD2 received by the patients were high, i.e. 149 and 182 Gy (RBE), and > 160 Gy (RBE), respectively. As there were no dose constraints on the carotid arteries, they might have received a substantial proportion of this dose, while only 3 of the 49 patients in the CNAO cohort received cumulative EQD2 doses to the carotid artery of this magnitude. A clear distinction in treatment planning, is that CNAO has had a proactive approach to reduce the risk of carotid blowout by applying a dose constraint in the re-RT setting, restricting the cumulative EQD2 received by the carotid artery to < 120 Gy (RBE) for most patients.

Hu et al. recently published initial results on 75 patients receiving re-RT with CIRT due to recurrent nasopharyngeal carcinoma (Hu et al. 2018). The patients were treated at the SPHIC in China, the only Asian center using the LEM I for optimization of

CIRT. Doses applied were comparable to the practice at GSI/HIT; 50-66 Gy (RBE) were given in daily fractions of 2 -3 Gy (RBE). The median follow-up time was 15.4 months (range, 2.6-29.7 months). Seven patients developed nasopharyngeal necrosis ≥ grade 3 in the tumor bed, in which one patient (1.3% of the cohort) died of a related massive hemorrhage 7 months after completion of the re-RT. Cumulative dose to the bleeding site was not reported.

Finally, Hayashi et al. reported 1 case of carotid artery rupture within 48 patients re-irradiated with carbon ions at NIRS. An important distinction in regard to the before mentioned studies, was that these patients also had been treated with CIRT in the primary setting. Doses were generally high, the most common being 57.6 Gy (RBE) in 16 fractions in the initial irradiation, and 52.8 Gy (RBE) in 12 fractions in the re-RT course.

In summary, these studies report on generally low crude rates of carotid blowout following re-RT with carbon ions, ranging from 0.8 – 2%, which is comparable to results following photon or proton radiotherapy. However, since CIRT is still confined to a limited number of centres worldwide, patients will have to travel farther for follow-up. Thus, potentially a larger proportion of patients may be lost to follow-up, especially compared to patients which have been treated with photons (which is a widespread technology). This may result in that more carotid blowout events remain undetected in CIRT cohorts.

Albeit our efforts to provide detailed and exact data on cumulative dose to the carotid artery for most patients, a definitive conclusion on a relation of carotid artery dose and carotid blowout could not be drawn, due to the small number of events. Of note, the only confirmed carotid blowout case in our study had a cumulative dose to the carotid artery of 129 Gy (RBE). The review of Dionisi et al. (Dionisi et al. 2019) was neither able to conclude on this matter. However, based on the individual cases of carotid blowout reported within the reviewed papers, it seems as though carotid blowout occurs more frequently when cumulative doses exceed 120 Gy. The current strategy of CNAO of defining the carotid artery as an OAR in the re-RT setting, and

preferential restricting cumulative EQD2 to <120 Gy (RBE) seems to be reasonable, especially when it does not compromise dose coverage of the tumor.

Another interesting observation by Dionisi et al. was that 107 of the 156 bleeding events occurred after re-RT to the nasopharynx (Dionisi et al. 2019). This is in line with our discussion in Paper I, were we hypothesized that patients with nasopharyngeal site may be at higher risk. It may also be that carotid blowout is a secondary event following necrosis of the surrounding soft tissues, as described for the 2 cases in the Jensen et al. report. This development is indeed also described in the setting of normofractionated chemoradiation using photons in the *primary* radiotherapy setting (Esteller et al. 2012). Thus, an alternative hypothesis may be that the relevant "organ at risk" for the development of carotid blowout is not the carotid artery itself, but rather the adjacent supportive tissues. Following this thought, the maximum dose to the carotid artery may not be a sufficient surrogate to represent the dose-volume effects governing the development of necrosis in these tissues.

Finally, other studies assessing the risk of carotid blowout have dominantly reported the cumulative lifetime dose, i.e. the summation of prescribed doses from a patients radiotherapy courses. In our study, we clearly show that there is poor correlation between the lifetime dose, and the cumulative dose received by the carotid artery as can be seen by **Figure 35** and demonstrated by a Spearman's rho correlation coefficient of 0.363. Recollecting that we in addition excluded 1/5th of the retreated population at CNAO, because there was no overlap of dose to the carotid artery, it is obvious that the cumulative lifetime dose does not reflect the cumulative dose received by the carotid artery or its adjacent tissues. Subsequently, one cannot expect to find a relation between the event of carotid blowout and the cumulative lifetime dose.

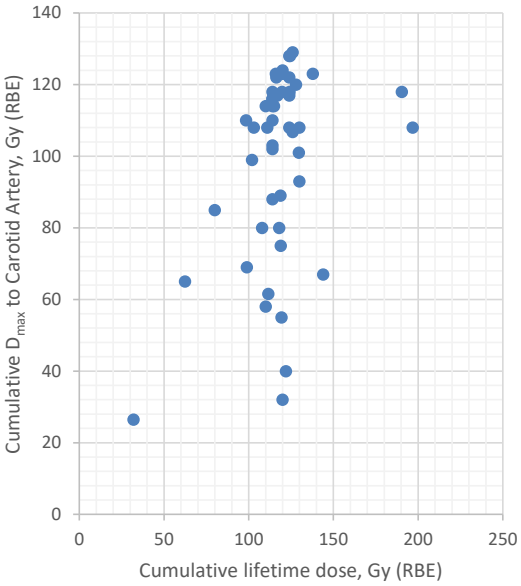

Figure 35: *Cumulative maximum dose to the carotid artery as a function of Cumulative prescribed lifetime dose. As can be seen, typically prescribed doses of 120 Gy (RBE) has been given, in which the dose to the carotid artery ranges from 32 to 126 Gy (RBE).*

10.2.2 Paper II

As shown in the chapter 6 there was almost a complete lack of published data concerning the risk of optic neuropathy following LEM I optimized CIRT at the time of publication of Paper II. With the exception of Paper II, this is still the case. However, during 2019 Akbaba and various co-authors from HIT published four papers which are worth mentioning: In a cohort of 227 patients treated with combined modality radiotherapy (IMRT + carbon ion boost) for sinonasal adenoid cystic carcinoma, they found only one case (0.8%) of late CTCAE grade 1 optic nerve affection (Akbaba, Ahmed, Mock, et al. 2019). Unfortunately, details regarding the dose received by this nerve were not mentioned. When dealing with sinonasal tumors, it is not unusual to transgress optic nerve dose constraints unilaterally to ensure adequate tumor dose coverage, so this may have been an expected toxicity. Within three additional papers they reported outcome of collectively 109 patients treated for other tumor sites (nasopharyngeal and lacrimal gland tumors) in which the optic pathways is a relevant organ at risk, in which no relevant toxicity occurred (Akbaba,

Ahmed, Lang, et al. 2019; Akbaba, Held, et al. 2019; Akbaba, Lang, et al. 2019). SPHIC in Shanghai is the only Asian center applying LEM I for CIRT. Guan et al. recently reported preliminary results of 91 patients treated at SPHIC for chordoma or chondrosarcomas of the skull base or cervical spine. The majority of patients (n=69) were treated in the primary setting with either carbon ions alone (n=47) or protons + carbon ion boost (n=22). Interestingly, they applied $D_{LEM\ I|20\%} < 30$ Gy (RBE) as optic nerve dose constraint, nominally the same as the former CNAO constraint, although becoming more conservative since the carbon ion treatments were given within 20-23 fraction. Not surprisingly, they did not experience optic nerve toxicity. Furthermore, considering the diversity in dose constraints applied for LEM I-based centres worldwide, there is obviously a need for an analysis as Paper II represents. These publications, together with the relevant papers already mentioned in the chapter 6 are summarized in **Table 8.**

As a result Paper II is the first, and remains the only publication providing detailed information on dose-volume metrics in regard to optic nerve toxicity for CIRT optimized with the LEM I. The three cases of radiation induced optic neuropathy appeared at doses $D_{20\%} > 62$ Gy (RBE) and $D_{1\%} > 70$ Gy (RBE)/16 fractions, the latter being considerable higher than the former constraints at CNAO (<40 Gy (RBE)). Furthermore the events occurred at doses far from the currently applied constraint used at HIT (EQD2 <54 Gy (RBE)), which according to the LQ model converts into 45 Gy (RBE) for a 16 fraction treatment (assuming an α/β of 2 Gy).

According to the QUANTEC review, the incidence of radiation induced optic neuropathy increased between 55 and 60 Gy (3–7%) and was substantial (>7–20%) for $D_{max} > 60$ Gy, although was noted that in some studies even at these high doses no clinically significant neuropathy occurred. Assuming an α/β of 2 Gy for the optic nerve most patients (30/38 nerves) in our cohort $D_{LEM\ I\ |1\%} < 43$ Gy (RBE) (= EQD2 < 50 Gy), which is considered harmless in regards to optic nerve toxicity for photon RT, see **Figure 34**. Furthermore, all 3 toxic events occurred within the 9 optic nerves (33%) receiving EQD2 > 60 Gy (i.e. > 48 Gy (RBE) nominally). Thus, our findings are not in conflict with data from photon radiotherapy.

TABLE 8: overview of relevant clinical studies on LEM-optimized carbon ion radiotherapy for tumor sites in which the optic nerve and brainstem are relevant organs at risk

Publication	Site and histology	n	Median FU (range) months	Modality	Optic nerve toxicity	Brainstem toxicity
Schulz-Ertner et al. 2007	Skull base chordoma	96	Not specified	Carbon ion	4 (4.2%)*	0 (0%)
Uhl et al. 2014	Skull base chondrosarcoma	79	91 (3-175)	Carbon ion	No mention	No mention
Uhl et al. 2014	Skull base chordoma	155	72 (12-165)	Carbon ion	3 (2%) potential cases**	0 (0%)
Mattke et al. 2018	Skull base chondrosarcoma	101	40 (1-78)	Carbon ion (79) Proton (22)	No mention	1 potential case ***
Akbaba et al. 2019	Sinonasal ACC	227	50 (3-109)	IMRT + carbon ion boost	1 (0.8%)	0 (0%)
Akbaba et al. 2019	Nasopharyneal ACC	59	32 (7-106)	IMRT + carbon ion boost	0 (0%)	0 (0%)
Akbaba et al. 2019	Nasopharyngal carcinoma	26	40 (10-97)	IMRT + carbon ion boost	0 (0%)	0 (0%)
Akbaba et al. 2019	Lacrimal gland tumors	24	30 (6-102)	IMRT + carbon ion boost	0 (0%)	N/A
Guan et al. 2019	Chordoma or chondrosarcoma	69	28 (8-59)	Proton + Carbon ion boost (22) Carbon ion (47)	0 (%)	0 (%)

*3 of 4 cases due to prior tumor involvement.
**exact patophysiology of visual impairment not stated
***walking disability due to radiation necrosis in uspecified location. Not specified if this patient received proton or carbon ion RT

When evaluating the optic nerve DVHs in the D_{NIRS}, toxicity occurred at $D_{NIRS|1\%}$ ≥68 Gy (RBE) and $D_{NIRS|20\%} \geq 62$ Gy (RBE), which is comparable to the findings of Hasegawa et al. for patients treated at NIRS, see **Figure 36**. According to our dose translation model, the $D_{1\%}$ and $D_{20\%}$ constraints applied at NIRS was equal to 50 Gy (RBE) and 40 Gy (RBE) in $D_{LEM\ I}$, respectively. Unfortunately, due to the conservative approach at CNAO, only seven optic nerves in total (including the three cases) exceeded these limits, leaving our clinical data set unable to substantially support the safety of these translated constraints. The same issue, i.e. low number of events and patients, and a scarcity of optic nerves receiving mid-high doses reduces the validity of the NTCP-models presented in Paper I. Therefore, the estimates for

$D_{LEM\ I}$ constraints derived from translation of the Japanese dose constraints were a valuable asset in order to point to an approximate level for new $D_{LEM\ I}$ constraints.

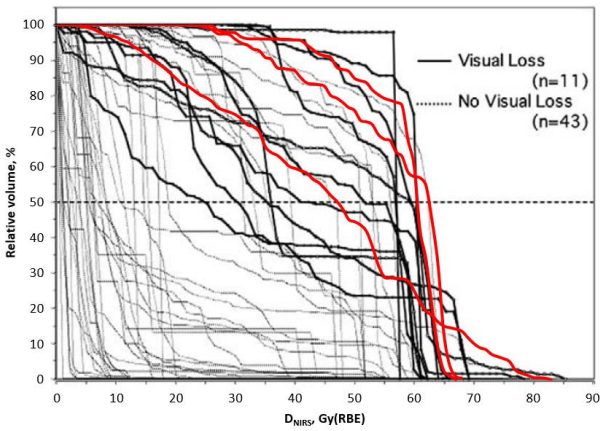

Figure 36: *Reprint of Fig. 4a from Hasegawa et al. (2006) showing the DVHs from the NIRS cohort, where black DVHs represent optic nerves that developed neuropathy, and gray DVHs represent optic nerves that did not develop neuropathy. Superimposed on the figure are the D_{NIRS} DVHs (red) of the three optic nerves from the CNAO cohort that developed neuropathy.*

A dose constraint of $D_{1\%} < 50$ Gy (RBE) given in 16 fractions, would according to the LQ model convert to an EQD2 of approximately 64 Gy (RBE). This would be slightly above the dose received by the patient developing bilateral blindness (EQD2 63 Gy (RBE)), as reported by Schulz-Ertner et al. (Schulz-Ertner, Nikoghosyan, et al. 2007). Therefore, as a consequence of the inherent uncertainties of the dose translation method and event number in the CNAO cohort, the clinical decision at CNAO was to implement slightly less relaxed constraints; $D_{LEM\ I|20\%} < 37$ Gy (RBE) and $D_{LEM\ I|1\%} < 45$ Gy (RBE). Thus, the new constraints are in line with the current practice at HIT (assuming the correctness of the LQ model), and are still conservative when compared to the TD5 estimates of the NTCP modelling of own institutional toxicity data or when compared to the translation of Japanese dose constraints, as seen in **Figure 37.** However, they represent an improvement compared to the formerly used constraints of $D_{LEM\ I|20\%} < 28$ Gy (RBE) and $D_{LEM\ I|1\%} < 40$ Gy (RBE).

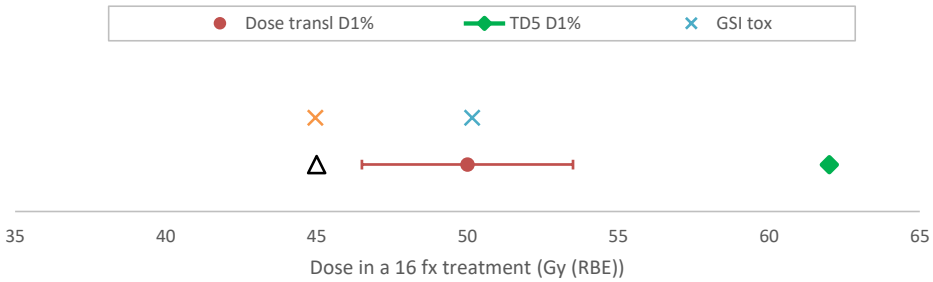

Figure 37: *Presents the an overview of results of NTCP modelling (TD5, green diamond) and dose translation for the D1% constraint (red circle w/95%CI), in relation to the toxic event reported by Schulz-Ertner et al. (blue cross), the current HIT constraint (yellow cross), the latter 2 dose values have been converted to a 16 fraction treatment by the LQ model. The black triangle represents the new D1% constraint at CNAO.*

A strength of Paper II is that we have used all available published clinical data for optic neuropathy following CIRT to propose new constraints to be used in a 16 fraction regime:

1) CNAO institutional toxicity data
2) Toxicity data from Japanese centers (by dose translation)
3) Traditions and experience from GSI/HIT (through the LQ model)

We believe that defining the new constraints at a level comparable to the most conservative of these estimates ensures the safety of patient treatments, while adequate dose to the target will become easier to achieve. However, patients should be included in closely monitored prospective protocols.

10.2.3 Paper III

An underlying premise for Paper III was that even asymptomatic brainstem lesions were yet to be seen at CNAO following LEM I-optimized CIRT. Furthermore,

regarding published data on tolerance doses for the brainstem following CIRT, there is even less information available than for the optic nerve. With the exception of the paper on lacrimal gland tumors (Akbaba, Lang, et al. 2019), the publications summarized in **Table 8** consist of tumor sites in which the vicinity to the brainstem very often will limit target dose coverage. In the two publications on skull base chordomas, both Schulz-Ertner et al. and Uhl et al. explicitly describe an absence of brainstem toxicity (Schulz-Ertner, Karger, et al. 2007; Uhl, Mattke, Welzel, Roeder, et al. 2014). Furthermore, there are no cases reported within the three relevant papers published by Akbaba et al. consisting of 312 patients collectively (Akbaba, Ahmed, Mock, et al. 2019; Akbaba, Ahmed, Lang, et al. 2019; Akbaba, Held, et al. 2019). Ultimately, within relevant patient cohorts consisting of 336 patients treated with carbon ions and 312 patients treated with IMRT + carbon ion boost, there was only one case potentially linked to brainstem necrosis (Mattke et al. 2018). However, the report did not to specify dosimetric parameters or whether or not this patient received proton or CIRT. Finally, Guan et al. reported preliminary results for 47 patients with chordoma or chondrosarcoma of the skull base or cervical spine, treated with CIRT at SPHIC (Guan et al. 2019), in which they applied a brainstem dose constraint of < 45 Gy (RBE) given in 20-23 fractions. This constraints was thus more conservative than GSI/HIT, though somewhat higher than the former constraint used at CNAO. However, there were no events of brainstem damage in this cohort either. Consequently, there is a more or less complete lack of data on tolerance doses for the brainstem following LEM I optimized CIRT. Thus, relying on the translation of Japanese dose constraints remains the only option to help guide the proposal of new $D_{LEM\ I}$ constraints.

The result of Paper III clearly showed that there was a considerable potential to increase the dose to the brainstem, while still adhering to the constraints currently applied in centres using the NIRS clinical dose, see **Figure 32d.** Moreover, applying the LKB model parameters described by Shirai et al. to the D_{NIRS} recalculated CNAO dose distributions suggested the probability of developing an asymptomatic brainstem reaction to be low, i.e. NTCP →0% for 29 of the patients and NTCP = 2% for 1 patient.

Applying the dose translation model suggested that the D_{NIRS} constraints corresponded to $D_{LEM\ I|0.7cm3}$ <41 Gy (RBE) (95% CI: 38-44 Gy [RBE]) and $D_{LEM\ I|0.1cm3}$ <49 Gy (RBE) (95% CI: 46-52 Gy [RBE]). Interestingly, these values were more closely related to the constraints used at GSI/HIT, than the former CNAO constraint, see **Figure 38**. To mitigate the uncertainties discussed under *Methodological considerations*, the values according to the lower bound of the 95% CI, i.e. $D_{LEM\ I|0.7\ cm3}$ < 38 Gy (RBE) and $D_{LEM\ I|0.1\ cm3}$ < 46 Gy (RBE), were suggested as new brainstem dose constraints to be used in a 16 fraction CIRT treatment applying the LEM I as the RBE model.

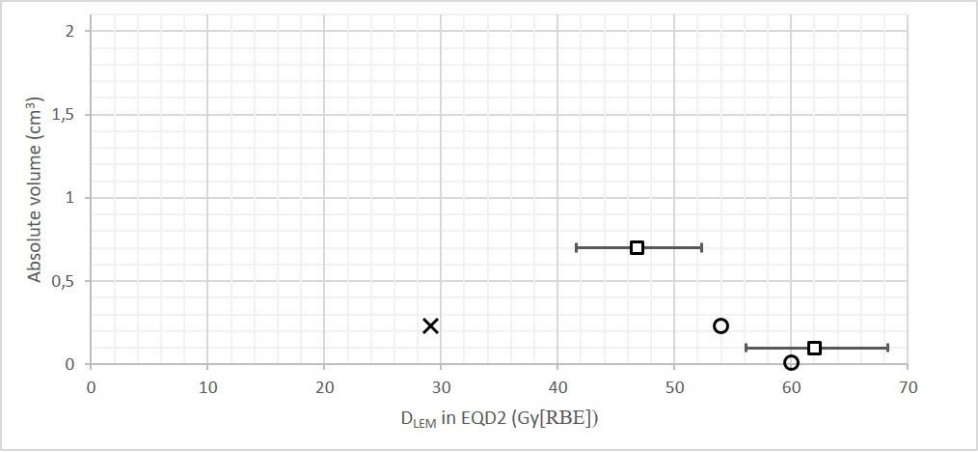

Figure 38: *Absolute volume DVH showing old CNAO $D_{LEM\ I|1\%}$ <30 Gy (RBE) constraint (cross) and the translated Shirai constraints $D_{LEM\ I|0.7cm3}$ <41 Gy (RBE) and $D_{LEM\ I|0.1cm3}$ <49 Gy (RBE) (squares, error bars=95%CI), converted into EQD2 (assuming α/β ratio = 2 Gy) in comparison to the EQD2 constraints applied at HIT: $D_{LEM\ I|1\%}$ <54 Gy (RBE) and $D_{LEM\ I|max}$ <60 Gy (RBE) (circles). As an approximation to the absolute volume relating to the $D_{1\%}$ constraints, the median brainstem volume in our data set (26 cm^3) was used. The translated constraints are more closely related to the constraints used at HIT than the old CNAO constraint.*

10.2.4 Implications of suboptimal dose constraints for the optic nerve and brainstem

The results of Paper II and III clearly demonstrated that the dose constraints originally applied at CNAO for the brainstem and optic nerve imposed an obvious restriction in achieving optimal carbon ion treatment plans. An analysis of relapse patterns in patients with adenoid cystic carcinomas (ACC) treated at CNAO suggest the possible clinical impact of this approach: approximately 70% of the local relapses occurred at sites where the target volume was underdosed in order to adhere to brainstem or optic pathways dose constraints (Molinelli, Bonora, et al. 2019). Moreover, a recent publication on skull base chordomas treated at CNAO, Iannalfi et al. found that 92% of the local recurrences were attributable to suboptimal target dose in regions close to the brainstem or optic pathways (Iannalfi et al. 2020). The estimated 5-year local control (LC) rate was 71%. This is inferior to the results reported by Japanese centers, where 5-year LC rates within the range 76-92% have been reported (Takagi et al. 2018; Koto et al. 2020). Certainly, no firm conclusions should be drawn by direct comparison of the outcome of these studies. However, in the context of the findings presented in this thesis, it does not come as a surprise that the outcome at CNAO may seem inferior to that of the Japanese centers. These observations clearly emphasize the necessity and urgency of Papers II and III.

11. Conclusion

11.1 Paper I

The current practice at of re-RT with particles at CNAO seems to result in acceptable rates of carotid blowout, although the total number of patients and events prevents any definitive conclusions. We found no indication that the use of moderately hypofractionated CIRT could be potentially more harmful than conventionally fractionated photon or proton RT.

The low number of events made it impossible to conclude on a potential dose threshold for at which risk increases. The paper was the first to address the risk of carotid blowout following particle therapy, and the first within any radiation modality presenting detailed data on cumulative dose to the carotid artery as an OAR.

11.2 Papers II and III

The papers show that the direct adoption of NIRS dose constraints for the optic nerve and brainstem has had an overly restrictive effect in regard to achieving optimal treatment plans at CNAO. As a result, the current scarcity of toxic events at CNAO prevents the definition of new dose constraints based on own institutional data.

Thus, the development of a pragmatic method to make use of dose constraints/toxicity data stemming from CIRT centres applying the NIRS clinical dose has been of crucial importance to guide the definition of updated, less restrictive dose constraints.

Moreover, the recalculation of institutional dose-response data to the alternative model is a valuable process to better understand the relationship of the models, and thus makes it easier to exchange information and experience across the CIRT community.

These studies have led to that more optimal dose constraints for the optic nerve and brainstem for LEM I based CIRT have been introduced at both CNAO and MedAustron (Vienna, Austria). The constraints would also be applicable for other LEM I based centres such as HIT, MIT and SPHIC if they in the future should introduce 16 fraction treatment schedules.

12. Future perspectives

CIRT is still a relatively new treatment modality in regard to clinical experience. Although a powerful tool, the utilization of its full potential is still hampered by an incomplete understanding of the radiobiological effects of this radiation. More studies on dose constraints and NTCP models for OARs, especially for the LEM I are needed. Within German CIRT centres there would be a rich amount of outcome data which could and should be used for detailed analyses of the relation of dose and toxicity for important OARs, either to challenge or support the findings in this thesis.

Following the implementation of updated dose constraints, close monitoring of adverse events must be upheld. Within some years, similar analysis of patient data from CNAO and other centres implementing new constraints should be performed to ensure the continued safety of the treatments, and to derive even more optimal dose constraints and NTCP models. Moreover, the clinical impact of more relaxed constraints in regard to probability of tumor control should be explored.

Commercial TPSs with the ability to optimize carbon ion treatment plans applying both the LEM I and the NIRS clinical dose is currently used in patient treatments at MedAustron, and is under commissioning at other centres. This technological improvement makes the comparison of different RBE-weighted dose distributions readily available and substantially less cumbersome and time-consuming than was the case for this project. Hence, the approach of dose translation presented in this thesis can be extended and validated within larger patient cohorts for a variety of OARs, and also for target volumes.

Furthermore, this approach can pave the way for future multicenter trials involving CIRT centres applying different RBE models, as it will be possible to harmonize patient treatments worldwide.

Reference list

Akbaba, S., D. Ahmed, K. Lang, T. Held, M. Mattke, J. Hoerner-Rieber, K. Herfarth, S. Rieken, P. Plinkert, J. Debus, and S. Adeberg. 2019. 'Results of a combination treatment with intensity modulated radiotherapy and active raster-scanning carbon ion boost for adenoid cystic carcinoma of the minor salivary glands of the nasopharynx', *Oral Oncol*, 91: 39-46.

Akbaba, S., D. Ahmed, A. Mock, T. Held, S. Bahadir, K. Lang, M. Syed, J. Hoerner-Rieber, T. Forster, P. Federspil, K. Herfarth, P. Plinkert, J. Debus, and S. Adeberg. 2019. 'Treatment Outcome of 227 Patients with Sinonasal Adenoid Cystic Carcinoma (ACC) after Intensity Modulated Radiotherapy and Active Raster-Scanning Carbon Ion Boost: A 10-Year Single-Center Experience', *Cancers (Basel)*, 11.

Akbaba, S., T. Held, K. Lang, T. Forster, P. Federspil, K. Herfarth, M. Hafner, P. Plinkert, S. Rieken, J. Debus, and S. Adeberg. 2019. 'Bimodal Radiotherapy with Active Raster-Scanning Carbon Ion Radiotherapy and Intensity-Modulated Radiotherapy in High-Risk Nasopharyngeal Carcinoma Results in Excellent Local Control', *Cancers (Basel)*, 11.

Akbaba, S., K. Lang, T. Held, K. Herfarth, J. Rieber, P. Plinkert, G. U. Auffarth, S. Rieken, J. Debus, and S. Adeberg. 2019. 'Carbon-ion radiotherapy in accelerated hypofractionated active raster-scanning technique for malignant lacrimal gland tumors: feasibility and safety', *Cancer Manag Res*, 11: 1155-66.

Ando, K., and Y. Kase. 2009. 'Biological characteristics of carbon-ion therapy', *Int J Radiat Biol*, 85: 715-28.

Ando, Koichi, and Dudley T. Goodhead. 2016. 'Dependence and independence of survival parameters on linear energy transfer in cells and tissues', *J Radiat Res*, 57: 596-606.

Asli, L. M., S. O. Kvaloy, V. Jetne, T. A. Myklebust, S. G. Levernes, K. M. Tveit, T. O. Green, and T. B. Johannesen. 2014. 'Utilization of radiation therapy in Norway after the implementation of the national cancer plan--a national, population-based study', *Int J Radiat Oncol Biol Phys*, 90: 707-14.

Barendsen, G. W. 1982. 'Dose fractionation, dose rate and iso-effect relationships for normal tissue responses', *Int J Radiat Oncol Biol Phys*, 8: 1981-97.

Barton, M. B., S. Jacob, J. Shafiq, K. Wong, S. R. Thompson, T. P. Hanna, and G. P. Delaney. 2014. 'Estimating the demand for radiotherapy from the evidence: a review of changes from 2003 to 2012', *Radiother Oncol*, 112: 140-4.

Belli, M., D. Bettega, P. Calzolari, R. Cherubini, G. Cuttone, M. Durante, G. Esposito, Y. Furusawa, S. Gerardi, G. Gialanella, G. Grossi, L. Manti, R. Marchesini, M. Pugliese, P. Scampoli, G. Simone, E. Sorrentino, M. A. Tabocchini, and L. Tallone. 2008. 'Effectiveness of monoenergetic and spread-out bragg peak carbon-ions for inactivation of various normal and tumour human cell lines', *J Radiat Res*, 49: 597-607.

Benton, E. V., and E. Tochilin. 1966. 'Heavy ion tracks in nuclear emulsions: applications to charged particle dosimetry', *Health Phys*, 12: 49-52.

Bert, C., and M. Durante. 2011. 'Motion in radiotherapy: particle therapy', *Phys Med Biol*, 56: R113-44.

Blakely, E. A., and P. Y. Chang. 2009. 'Biology of charged particles', *Cancer J*, 15: 271-84.

Blakely, Eleanor A. 1983. 'HEAVY-ION RADIOBIOLOGY: CELLULAR STUDIES'.

Bragg, W. H., and R. Kleeman. 1904. 'LXXIV. On the ionization curves of radium', *The London, Edinburgh, and Dublin Philosophical Magazine and Journal of Science*, 8: 726-38.

Burman, C., G. J. Kutcher, B. Emami, and M. Goitein. 1991. 'Fitting of normal tissue tolerance data to an analytic function', *Int J Radiat Oncol Biol Phys*, 21: 123-35.

Cengiz, M., G. Ozyigit, G. Yazici, A. Dogan, F. Yildiz, F. Zorlu, M. Gurkaynak, I. H. Gullu, S. Hosal, and F. Akyol. 2011. 'Salvage reirradiaton with stereotactic body radiotherapy for locally recurrent head-and-neck tumors', *Int J Radiat Oncol Biol Phys*, 81: 104-9.

Chen, G. T., J. R. Castro, and J. M. Quivey. 1981. 'Heavy charged particle radiotherapy', *Annu Rev Biophys Bioeng*, 10: 499-529.

Chen, K. C., T. T. Yen, Y. L. Hsieh, H. C. Chen, R. S. Jiang, W. H. Chen, and K. L. Liang. 2015. 'Postirradiated carotid blowout syndrome in patients with nasopharyngeal carcinoma: a case-control study', *Head Neck*, 37: 794-9.

Chen, Y. J., C. P. Wang, C. C. Wang, R. S. Jiang, J. C. Lin, and S. A. Liu. 2015. 'Carotid blowout in patients with head and neck cancer: associated factors and treatment outcomes', *Head Neck*, 37: 265-72.

Choi, Kyungdon, Silvia Molinelli, Stefania Russo, Alfredo Mirandola, Maria Fiore, Barbara Vischioni, Piero Fossati, Rachele Petrucci, Irene Turturici, Jon Dale, Francesca Valvo, Mario Ciocca, and Andrea Mairani. 2019. 'Rectum Dose Constraints for Carbon Ion Therapy: Relative Biological Effectiveness Model Dependence in Relation to Clinical Outcomes', *Cancers (Basel)*, 12: 46.

Chu, W. T., B. A. Ludewigt, and T. R. Renner. 1993. 'Instrumentation for treatment of cancer using proton and light-ion beams', *Review of Scientific Instrumuments*, 64: 2055-122.

Cisternas, E., A. Mairani, P. Ziegenhein, O. Jäkel, and M. Bangert. 2015. 'matRad - a multi-modality open source 3D treatment planning toolkit.' in David A. Jaffray (ed.), *World Congress on Medical Physics and Biomedical Engineering, June 7-12, 2015, Toronto, Canada* (Springer International Publishing: Cham).

Conte, V., P. Colautti, B. Grosswendt, D. Moro, and L. De Nardo. 2012. 'Track structure of light ions: experiments and simulations', *New Journal of Physics*, 14.

Danesh-Meyer, Helen V. 2008. 'Radiation-induced optic neuropathy', *Journal of Clinical Neuroscience*, 15: 95-100.

Debus, J., M. Scholz, T. Haberer, P. Peschke, O. Jäkel, C. P. Karger, and M. Wannenmacher. 2003. 'Radiation tolerance of the rat spinal cord after single and split doses of photons and carbon ions', *Radiat Res*, 160: 536-42.

Dionisi, F., F. Fiorica, E. D'Angelo, M. Maddalo, I. Giacomelli, E. Tornari, A. Rosca, F. Vigo, D. Romanello, M. Cianchetti, F. Tommasino, M. Massaccesi, and E. Orlandi. 2019. 'Organs at risk's tolerance and dose limits for head and neck cancer re-irradiation: A literature review', *Oral Oncol*, 98: 35-47.

Douglas, B. G., and J. F. Fowler. 1976. 'The Effect of Multiple Small Doses of X Rays on Skin Reactions in the Mouse and a Basic Interpretation', *Radiat Res*, 66: 401-26.

Durante, M., R. Orecchia, and J. S. Loeffler. 2017. 'Charged-particle therapy in cancer: clinical uses and future perspectives', *Nat Rev Clin Oncol*, 14: 483-95.

Elsässer, T., M. Krämer, and M. Scholz. 2008. 'Accuracy of the local effect model for the prediction of biologic effects of carbon ion beams in vitro and in vivo', *Int J Radiat Oncol Biol Phys*, 71: 866-72.

Emami, B., J. Lyman, A. Brown, L. Coia, M. Goitein, J. E. Munzenrider, B. Shank, L. J. Solin, and M. Wesson. 1991. 'Tolerance of normal tissue to therapeutic irradiation', *Int J Radiat Oncol Biol Phys*, 21: 109-22.

Esteller, E., X. Leon, M. de Juan, and M. Quer. 2012. 'Delayed carotid blow-out syndrome: a new complication of chemoradiotherapy treatment in pharyngolaryngeal carcinoma', *J Laryngol Otol*, 126: 1189-91.

Evans, J. D., D. R. Gomez, A. Amini, N. Rebueno, P. K. Allen, M. K. Martel, J. M. Rineer, K. K. Ang, S. McAvoy, J. D. Cox, R. Komaki, and J. W. Welsh. 2013. 'Aortic dose constraints when reirradiating thoracic tumors', *Radiother Oncol*, 106: 327-32.

Facoetti, A., B. Vischioni, M. Ciocca, M. Ferrarini, Y. Furusawa, A. Mairani, Y. Matsumoto, A. Mirandola, S. Molinelli, A. Uzawa, F. G. Vilches, and R. Orecchia. 2015. 'In vivo radiobiological assessment of the new clinical carbon ion beams at CNAO', *Radiat Prot Dosimetry*, 166: 379-82.

Filipak, M. 2012. 'Comparison of dose profiles for proton v. x-ray radiotherapy', Wikimedia Commons. https://commons.wikimedia.org/w/index.php?curid=27983203.

Fossati, P., S. Molinelli, N. Matsufuji, M. Ciocca, A. Mirandola, A. Mairani, J. Mizoe, A. Hasegawa, R. Imai, T. Kamada, R. Orecchia, and H. Tsujii. 2012. 'Dose prescription in carbon ion radiotherapy: a planning study to compare NIRS and LEM approaches with a clinically-oriented strategy', *Phys Med Biol*, 57: 7543-54.

Fowler, John F. 1989. 'The linear-quadratic formula and progress in fractionated radiotherapy', 62: 679-94.

Friedrich, T., M. Durante, and M. Scholz. 2013. 'The Local Effect Model - Principals and Applications ', The Health Risks of Extraterrestial Environments, Accessed 09.10.2019. https://three.jsc.nasa.gov/articles/LEM_20130426.pdf.

Friedrich, Thomas, Uwe Scholz, Thilo ElsäSser, Marco Durante, and Michael Scholz. 2012. 'Systematic analysis of RBE and related quantities using a database of cell survival experiments with ion beam irradiation', *J Radiat Res*, 54: 494-514.

Fukahori, Mai, Naruhiro Matsufuji, Takeshi Himukai, Nobuyuki Kanematsu, Hideyuki Mizuno, Akifumi Fukumura, Hiroshi Tsuji, and Tadashi Kamada. 2016. 'Estimation of late rectal normal tissue complication probability

parameters in carbon ion therapy for prostate cancer', *Radiotherapy and Oncology*, 118: 136-40.

Gebhardt, B. J., J. A. Vargo, D. Ling, B. Jones, M. Mohney, D. A. Clump, J. P. Ohr, R. L. Ferris, and D. E. Heron. 2018. 'Carotid Dosimetry and the Risk of Carotid Blowout Syndrome After Reirradiation With Head and Neck Stereotactic Body Radiation Therapy', *Int J Radiat Oncol Biol Phys*, 101: 195-200.

Gray, L. H., A. D. Conger, M. Ebert, S. Hornsey, and O. C. Scott. 1953. 'The concentration of oxygen dissolved in tissues at the time of irradiation as a factor in radiotherapy', *Br J Radiol*, 26: 638-48.

Guan, X., J. Gao, J. Hu, W. Hu, J. Yang, X. Qiu, C. Hu, L. Kong, and J. J. Lu. 2019. 'The preliminary results of proton and carbon ion therapy for chordoma and chondrosarcoma of the skull base and cervical spine', *Radiat Oncol*, 14: 206.

Guimas, V., J. Thariat, P. Graff-Cailleau, P. Boisselier, Y. Pointreau, P. Pommier, X. Montbarbon, C. Laude, and S. Racadot. 2016. 'Radiothérapie conformationnelle avec modulation d'intensité des cancers des voies aérodigestives supérieures, dose de tolérance des tissus sains : appareil cochléovestibulaire et tronc cérébral', *Cancer/Radiothérapie*, 20: 475-83.

Hall, E. J., and A. Giacci (ed.)^(eds.). 2006. *Radiobiology for the radiologist* (Lippincott Williams and Wilkins: Philadelphia PA).

Hall, E. J., and C. S. Wuu. 2003. 'Radiation-induced second cancers: the impact of 3D-CRT and IMRT', *Int J Radiat Oncol Biol Phys*, 56: 83-8.

Hasegawa, A., J. E. Mizoe, A. Mizota, and H. Tsujii. 2006. 'Outcomes of visual acuity in carbon ion radiotherapy: analysis of dose-volume histograms and prognostic factors', *Int J Radiat Oncol Biol Phys*, 64: 396-401.

Hawkins, R. B. 1994. 'A statistical theory of cell killing by radiation of varying linear energy transfer', *Radiat Res*, 140: 366-74.

Hayashi, Kazuhiko, Naoyoshi Yamamoto, Masataka Karube, Mio Nakajima, Naruhiro Matsufuji, Hiroshi Tsuji, Kazuhiko Ogawa, and Tadashi Kamada. 2017. 'Prognostic analysis of radiation pneumonitis: carbon-ion radiotherapy in patients with locally advanced lung cancer', *Radiation Oncology*, 12: 91.

Held, T., P. Windisch, S. Akbaba, K. Lang, R. El Shafie, D. Bernhardt, P. Plinkert, S. Kargus, S. Rieken, K. Herfarth, J. Debus, and S. Adeberg. 2019. 'Carbon Ion Reirradiation for Recurrent Head and Neck Cancer: A Single-Institutional Experience', *Int J Radiat Oncol Biol Phys*, 105: 803-11.

Hu, J., C. Bao, J. Gao, X. Guan, W. Hu, J. Yang, C. Hu, L. Kong, and J. J. Lu. 2018. 'Salvage treatment using carbon ion radiation in patients with locoregionally recurrent nasopharyngeal carcinoma: Initial results', *Cancer*, 124: 2427-37.

Iannalfi, A., E. D'Ippolito, G. Riva, S. Molinelli, S. Gandini, G. Viselner, M. R. Fiore, B. Vischioni, V. Vitolo, M. Bonora, S. Ronchi, R. Petrucci, A. Barcellini, A. Mirandola, S. Russo, A. Vai, E. Mastella, G. Magro, D. Maestri, M. Ciocca, L. Preda, F. Valvo, and R. Orecchia. 2020. 'Proton and carbon ions radiotherapy in skull base chordomas: a prospective study based on a dual particle and a patient-customized treatment strategy', *Neuro Oncol*.

ICRU, Report 78. 2007. 'PRESCRIBING, RECORDING, AND REPORTING PROTON-BEAM THERAPY', *Journal of the International Commission on Radiation Units and Measurements*, 7.

ICRU, Report 85a. 2011. 'Fundamental quantities and units for ionizing radiation (Revised)', *Journal of the International Commission on Radiation Units and Measurements*, 11.

ICRU, Report 93. 2019. "Prescribing, Recording and Reporting Light Ion Beam Therapy." In *Journal of the International Commission on Radiation Units and Measurements*. Journal of the ICRU: International Commissions on Radiation Units and Measurements.

Inaniwa, T., T. Furukawa, Y. Kase, N. Matsufuji, T. Toshito, Y. Matsumoto, Y. Furusawa, and K. Noda. 2010. 'Treatment planning for a scanned carbon beam with a modified microdosimetric kinetic model', *Phys Med Biol*, 55: 6721-37.

Inaniwa, T., N. Kanematsu, N. Matsufuji, T. Kanai, T. Shirai, K. Noda, H. Tsuji, T. Kamada, and H. Tsujii. 2015. 'Reformulation of a clinical-dose system for carbon-ion radiotherapy treatment planning at the National Institute of Radiological Sciences, Japan', *Phys Med Biol*, 60: 3271-86.

Inaniwa, T., N. Kanematsu, K. Noda, and T. Kamada. 2017. 'Treatment planning of intensity modulated composite particle therapy with dose and linear energy transfer optimization', *Phys Med Biol*.

Jakel, O., D. Schulz-Ertner, and J. Debus. 2007. 'Specifying carbon ion doses for radiotherapy: the heidelberg approach', *J Radiat Res*, 48 Suppl A: A87-95.

Jensen, A. D., M. Poulakis, A. V. Nikoghosyan, N. Chaudhri, M. Uhl, M. W. Munter, K. K. Herfarth, and J. Debus. 2015. 'Re-irradiation of adenoid cystic carcinoma: analysis and evaluation of outcome in 52 consecutive patients treated with raster-scanned carbon ion therapy', *Radiother Oncol*, 114: 182-8.

Joiner, Michael C., and A. J. van der Kogel (ed.)^(eds.). 2009. *Basic Clinical Radiobiology* (Hodder Arnold, an Hachette UK Company: London, Great Britain).

Kanai, T., M. Endo, S. Minohara, N. Miyahara, H. Koyama-ito, H. Tomura, N. Matsufuji, Y. Futami, A. Fukumura, T. Hiraoka, Y. Furusawa, K. Ando, M. Suzuki, F. Soga, and K. Kawachi. 1999. 'Biophysical characteristics of HIMAC clinical irradiation system for heavy-ion radiation therapy', *Int J Radiat Oncol Biol Phys*, 44: 201-10.

Kanai, T., Y. Furusawa, K. Fukutsu, H. Itsukaichi, K. Eguchi-Kasai, and H. Ohara. 1997. 'Irradiation of mixed beam and design of spread-out Bragg peak for heavy-ion radiotherapy', *Radiat Res*, 147: 78-85.

Kanai, T., K. Kawachi, Y. Kumamoto, H. Ogawa, T. Yamada, H. Matsuzawa, and T. Inada. 1980. 'Spot scanning system for proton radiotherapy', *Med Phys*, 7: 365-9.

Kanai, T., N. Matsufuji, T. Miyamoto, J. Mizoe, T. Kamada, H. Tsuji, H. Kato, M. Baba, and H. Tsujii. 2006. 'Examination of GyE system for HIMAC carbon therapy', *Int J Radiat Oncol Biol Phys*, 64: 650-6.

Karger, C. P., and P. Peschke. 2017. 'RBE and related modeling in carbon-ion therapy', *Phys Med Biol*, 63: 01tr02.

Karger, C. P., P. Peschke, R. Sanchez-Brandelik, M. Scholz, and J. Debus. 2006. 'Radiation tolerance of the rat spinal cord after 6 and 18 fractions of photons and carbon ions: experimental results and clinical implications', *Int J Radiat Oncol Biol Phys*, 66: 1488-97.

Kase, Y., T. Kanai, Y. Matsumoto, Y. Furusawa, H. Okamoto, T. Asaba, M. Sakama, and H. Shinoda. 2006. 'Microdosimetric measurements and estimation of human cell survival for heavy-ion beams', *Radiat Res*, 166: 629-38.

Khan, F, and J. P. Gibbons (ed.)^(eds.). 2014. *The physics of radiation therapy* (Lippincott Williams and Wilkins, PA, USA).

Kishimoto, R., J. E. Mizoe, S. Komatsu, S. Kandatsu, T. Obata, and H. Tsujii. 2005. 'MR imaging of brain injury induced by carbon ion radiotherapy for head and neck tumors', *Magn Reson Med Sci*, 4: 159-64.

Kodani, N., H. Yamazaki, T. Tsubokura, H. Shiomi, K. Kobayashi, T. Nishimura, N. Aibe, H. Ikeno, and T. Nishimura. 2011. 'Stereotactic body radiation therapy for head and neck tumor: disease control and morbidity outcomes', *J Radiat Res*, 52: 24-31.

Koehler, A. M., R. J. Schneider, and J. M. Sisterson. 1977. 'Flattening of proton dose distributions for large-field radiotherapy', *Med Phys*, 4: 297-301.

Koike, S., K. Ando, C. Oohira, T. Fukawa, R. Lee, N. Takai, M. Monobe, Y. Furusawa, M. Aoki, S. Yamada, W. Shimizu, K. Nojima, and H. Majima. 2002. 'Relative biological effectiveness of 290 MeV/u carbon ions for the growth delay of a radioresistant murine fibrosarcoma', *J Radiat Res*, 43: 247-55.

Kong, F. M., C. Pan, A. Eisbruch, and R. K. Ten Haken. 2007. 'Physical models and simpler dosimetric descriptors of radiation late toxicity', *Semin Radiat Oncol*, 17: 108-20.

Koto, M., A. Hasegawa, R. Takagi, G. Sasahara, H. Ikawa, J. E. Mizoe, K. Jingu, H. Tsujii, T. Kamada, and Y. Okamoto. 2014. 'Feasibility of carbon ion radiotherapy for locally advanced sinonasal adenocarcinoma', *Radiother Oncol*, 113: 60-5.

Koto, M., H. Ikawa, T. Kaneko, Y. Hagiwara, K. Hayashi, and H. Tsuji. 2020. 'Long-term outcomes of skull base chordoma treated with high-dose carbon-ion radiotherapy', *Head Neck*.

Kramer, M., and M. Scholz. 2000. 'Treatment planning for heavy-ion radiotherapy: calculation and optimization of biologically effective dose', *Phys Med Biol*, 45: 3319-30.

Kutcher, G. J., and C. Burman. 1989. 'Calculation of complication probability factors for non-uniform normal tissue irradiation: the effective volume method', *Int J Radiat Oncol Biol Phys*, 16: 1623-30.

Lambrecht, M., D. B. P. Eekers, C. Alapetite, N. G. Burnet, V. Calugaru, I. E. M. Coremans, P. Fossati, M. Hoyer, J. A. Langendijk, A. M. Romero, F. Paulsen, A. Perpar, L. Renard, D. de Ruysscher, B. Timmermann, P. Vitek, D. C. Weber, H. L. van der Weide, G. A. Whitfield, R. Wiggenraad, E. Roelofs, P. W. Nystrom, and E. G. C. Troost. 2018. 'Radiation dose constraints for organs at risk in neuro-oncology; the European Particle Therapy Network consensus', *Radiother Oncol*, 128: 26-36.

Langendijk, Johannes A., Philippe Lambin, Dirk De Ruysscher, Joachim Widder, Mike Bos, and Marcel Verheij. 2013. 'Selection of patients for radiotherapy with protons aiming at reduction of side effects: The model-based approach', *Radiotherapy and Oncology*, 107: 267-73.

Lea, D. E., and D. G. Catcheside. 1942. 'The mechanism of the induction by radiation of chromosome aberrations inTradescantia', *Journal of Genetics*, 44: 216-45.

Lee, A. W., S. H. Ng, J. H. Ho, V. K. Tse, Y. F. Poon, C. C. Tse, G. K. Au, S. K. O, W. H. Lau, and W. W. Foo. 1988. 'Clinical diagnosis of late temporal lobe necrosis following radiation therapy for nasopharyngeal carcinoma', *Cancer*, 61: 1535-42.

Lee, Jae Y., Krithika Suresh, Rebecca Nguyen, Eli Sapir, Janell S. Dow, George S. Arnould, Francis P. Worden, Matthew E. Spector, Mark E. Prince, Scott A. McLean, Andrew G. Shuman, Kelly M. Malloy, Keith Casper, Carol R. Bradford, Matthew J. Schipper, and Avraham Eisbruch. 2016. 'Predictors of severe long-term toxicity after re-irradiation for head and neck cancer', *Oral Oncol*, 60: 32-40.

Liang, N. L., B. D. Guedes, U. Duvvuri, M. J. Singh, R. A. Chaer, M. S. Makaroun, and U. Sachdev. 2016. 'Outcomes of interventions for carotid blowout syndrome in patients with head and neck cancer', *J Vasc Surg*, 63: 1525-30.

Lindborg, L., M. Hultqvist, Å Carlsson Tedgren, and H. Nikjoo. 2013. 'Lineal energy and radiation quality in radiation therapy: model calculations and comparison with experiment', *Phys Med Biol*, 58: 3089-105.

Loeffler, J. S., and M. Durante. 2013. 'Charged particle therapy--optimization, challenges and future directions', *Nat Rev Clin Oncol*, 10: 411-24.

Lomax, A. J., E. Pedroni, H. Rutz, and G. Goitein. 2004. 'The clinical potential of intensity modulated proton therapy', *Z Med Phys*, 14: 147-52.

Luxton, G., P. J. Keall, and C. R. King. 2008. 'A new formula for normal tissue complication probability (NTCP) as a function of equivalent uniform dose (EUD)', *Phys Med Biol*, 53: 23-36.

Lyman, J. T. 1985. 'Complication probability as assessed from dose-volume histograms', *Radiat Res Suppl*, 8: S13-9.

Magro, G., T. Dahle, S. Molinelli, M. Ciocca, P. Fossati, A. Ferrari, T. Inaniwa, N. Matsufuji, K. Ytre-Hauge, and A. Mairani. 2017. 'The FLUKA Monte Carlo code coupled with the NIRS approach for clinical dose calculations in carbon ion therapy', *Phys Med Biol*.

Mairani, A., S. Brons, F. Cerutti, A. Fasso, A. Ferrari, M. Kramer, K. Parodi, M. Scholz, and F. Sommerer. 2010. 'The FLUKA Monte Carlo code coupled with the local effect model for biological calculations in carbon ion therapy', *Phys Med Biol*, 55: 4273-89.

Malouff, T. D., A. Mahajan, S. Krishnan, C. Beltran, D. S. Seneviratne, and D. M. Trifiletti. 2020. 'Carbon Ion Therapy: A Modern Review of an Emerging Technology', *Front Oncol*, 10: 82.

Marks, L. B., E. D. Yorke, A. Jackson, R. K. Ten Haken, L. S. Constine, A. Eisbruch, S. M. Bentzen, J. Nam, and J. O. Deasy. 2010. 'Use of normal tissue complication probability models in the clinic', *Int J Radiat Oncol Biol Phys*, 76: S10-9.

Mattke, M., K. Vogt, N. Bougatf, T. Welzel, J. Oelmann-Avendano, H. Hauswald, A. Jensen, M. Ellerbrock, O. Jakel, T. Haberer, K. Herfarth, J. Debus, and M. Uhl. 2018. 'High control rates of proton- and carbon-ion-beam treatment with intensity-modulated active raster scanning in 101 patients with skull base chondrosarcoma at the Heidelberg Ion Beam Therapy Center', *Cancer*, 124: 2036-44.

Mayo, C., M. K. Martel, L. B. Marks, J. Flickinger, J. Nam, and J. Kirkpatrick. 2010. 'Radiation dose-volume effects of optic nerves and chiasm', *Int J Radiat Oncol Biol Phys*, 76: S28-35.

Mayo, C., E. Yorke, and T. E. Merchant. 2010. 'Radiation associated brainstem injury', *Int J Radiat Oncol Biol Phys*, 76: S36-41.

McDonald, M. W., M. G. Moore, and P. A. Johnstone. 2012. 'Risk of carotid blowout after reirradiation of the head and neck: a systematic review', *Int J Radiat Oncol Biol Phys*, 82: 1083-9.

McDonald, M. W., O. Zolali-Meybodi, S. J. Lehnert, N. C. Estabrook, Y. Liu, A. A. Cohen-Gadol, and M. G. Moore. 2016. 'Reirradiation of Recurrent and Second Primary Head and Neck Cancer With Proton Therapy', *Int J Radiat Oncol Biol Phys*, 96: 808-19.

McMahon, S. J. 2018. 'The linear quadratic model: usage, interpretation and challenges', *Phys Med Biol*, 64: 01tr01.

Mohamad, O., H. Makishima, and T. Kamada. 2018. 'Evolution of Carbon Ion Radiotherapy at the National Institute of Radiological Sciences in Japan', *Cancers (Basel)*, 10.

Molinelli, S., M. Bonora, G. Magro, S. Casale, J. E. Dale, P. Fossati, A. Hasegawa, A. Mirandola, S. Ronchi, S. Russo, L. Preda, F. Valvo, R. Orecchia, M. Ciocca, and B. Vischioni. 2019. 'RBE-weighted dose in carbon ion therapy for ACC patients: Impact of the RBE model translation on treatment outcomes', *Radiother Oncol*.

Molinelli, S., G. Magro, A. Mairani, N. Matsufuji, N. Kanematsu, T. Inaniwa, A. Mirandola, S. Russo, E. Mastella, A. Hasegawa, H. Tsuji, S. Yamada, B. Vischioni, V. Vitolo, A. Ferrari, M. Ciocca, T. Kamada, H. Tsujii, R. Orecchia, and P. Fossati. 2016. 'Dose prescription in carbon ion radiotherapy: How to compare two different RBE-weighted dose calculation systems', *Radiother Oncol*, 120: 307-12.

Molinelli, S., S. Russo, G. Magro, D. Maestri, A. Mairani, E. Mastella, A. Mirandola, A. Vai, B. Vischioni, F. Valvo, and M. Ciocca. 2019. 'Impact of TPS calculation algorithms on dose delivered to the patient in proton therapy treatments', *Phys Med Biol*, 64: 075016.

Musha, A., H. Shimada, K. Shirai, J. Saitoh, S. Yokoo, K. Chikamatsu, T. Ohno, and T. Nakano. 2015. 'Prediction of Acute Radiation Mucositis using an Oral Mucosal Dose Surface Model in Carbon Ion Radiotherapy for Head and Neck Tumors', *PLoS One*, 10: e0141734.

Niemierko, A. 1997. 'Reporting and analyzing dose distributions: a concept of equivalent uniform dose', *Med Phys*, 24: 103-10.

Nikoghosyan, A. V., I. Karapanagiotou-Schenkel, M. W. Munter, A. D. Jensen, S. E. Combs, and J. Debus. 2010. 'Randomised trial of proton vs. carbon ion

radiation therapy in patients with chordoma of the skull base, clinical phase III study HIT-1-Study', *BMC Cancer*, 10: 607.

Paganetti, H. 2014. 'Relative biological effectiveness (RBE) values for proton beam therapy. Variations as a function of biological endpoint, dose, and linear energy transfer', *Phys Med Biol*, 59: R419-72.

Pedroni, E., R. Bacher, H. Blattmann, T. Böhringer, A. Coray, A. Lomax, S. Lin, G. Munkel, S. Scheib, U. Schneider, and et al. 1995. 'The 200-MeV proton therapy project at the Paul Scherrer Institute: conceptual design and practical realization', *Med Phys*, 22: 37-53.

Phan, J., T. T. Sio, T. P. Nguyen, V. Takiar, G. B. Gunn, A. S. Garden, D. I. Rosenthal, C. D. Fuller, W. H. Morrison, B. Beadle, D. Ma, M. E. Zafereo, K. A. Hutcheson, M. E. Kupferman, W. N. William, Jr., and S. J. Frank. 2016. 'Reirradiation of Head and Neck Cancers With Proton Therapy: Outcomes and Analyses', *Int J Radiat Oncol Biol Phys*, 96: 30-41.

Powitzky, R., N. Vasan, G. Krempl, and J. Medina. 2010. 'Carotid blowout in patients with head and neck cancer', *Ann Otol Rhinol Laryngol*, 119: 476-84.

Puck, T. T., and P. I. Marcus. 1956. 'Action of x-rays on mammalian cells', *J Exp Med*, 103: 653-66.

Romesser, Paul B., Oren Cahlon, Eli D. Scher, Eugen B. Hug, Kevin Sine, Carl DeSelm, Jana L. Fox, Dennis Mah, Madhur K. Garg, John Han-Chih Chang, and Nancy Y. Lee. 2016. 'Proton Beam Reirradiation for Recurrent Head and Neck Cancer: Multi-institutional Report on Feasibility and Early Outcomes', *International Journal of Radiation Oncology*Biology*Physics*, 95: 386-95.

Safai, S., T. Bortfeld, and M. Engelsman. 2008. 'Comparison between the lateral penumbra of a collimated double-scattered beam and uncollimated scanning beam in proton radiotherapy', *Phys Med Biol*, 53: 1729-50.

Sasahara, Go, Masashi Koto, Hiroaki Ikawa, Azusa Hasegawa, Ryo Takagi, Yoshitaka Okamoto, and Tadashi Kamada. 2014. 'Effects of the dose-volume relationship on and risk factors for maxillary osteoradionecrosis after carbon ion radiotherapy', *Radiation Oncology*, 9: 92.

Schlampp, I., C. P. Karger, O. Jakel, M. Scholz, B. Didinger, A. Nikoghosyan, A. Hoess, M. Kramer, L. Edler, J. Debus, and D. Schulz-Ertner. 2011. 'Temporal lobe reactions after radiotherapy with carbon ions: incidence and estimation of the relative biological effectiveness by the local effect model', *Int J Radiat Oncol Biol Phys*, 80: 815-23.

Scholz, M. 1996. 'Calculation of RBE for normal tissue complications based on charged particle track structure', *Bulletin du Cancer/Radiothérapie*, 83, Supplement 1: 50s-54s.

Scholz, M., M. A. Kellerer, W. Kraft-Weyrather, and G. Kraft. 1997. 'Computation of cell survival in heavy ion beams for therapy', *Radiation and Environmental Biophysics*, 36: 59-66.

Schuemann, J., D. Giantsoudi, C. Grassberger, M. Moteabbed, C. H. Min, and H. Paganetti. 2015. 'Assessing the Clinical Impact of Approximations in Analytical Dose Calculations for Proton Therapy', *Int J Radiat Oncol Biol Phys*, 92: 1157-64.

Schulz-Ertner, D., C. P. Karger, A. Feuerhake, A. Nikoghosyan, S. E. Combs, O. Jakel, L. Edler, M. Scholz, and J. Debus. 2007. 'Effectiveness of carbon ion radiotherapy in the treatment of skull-base chordomas', *Int J Radiat Oncol Biol Phys*, 68: 449-57.

Schulz-Ertner, D., A. Nikoghosyan, H. Hof, B. Didinger, S. E. Combs, O. Jäkel, C. P. Karger, L. Edler, and J. Debus. 2007. 'Carbon ion radiotherapy of skull base chondrosarcomas', *Int J Radiat Oncol Biol Phys*, 67: 171-7.

Schulz-Ertner, D., and H. Tsujii. 2007. 'Particle radiation therapy using proton and heavier ion beams', *J Clin Oncol*, 25: 953-64.

Semenenko, V. A., and R. D. Stewart. 2006. 'Fast Monte Carlo simulation of DNA damage formed by electrons and light ions', *Phys Med Biol*, 51: 1693-706.

Shinoto, M., Y. Shioyama, A. Matsunobu, K. Okamoto, H. Suefuji, S. Toyama, H. Honda, and S. Kudo. 2016. 'Dosimetric analysis of upper gastrointestinal ulcer after carbon-ion radiotherapy for pancreatic cancer', *Radiother Oncol*, 120: 140-4.

Shirai, K., K. Fukata, A. Adachi, J. I. Saitoh, A. Musha, T. Abe, T. Kanai, D. Kobayashi, Y. Shigeta, S. Yokoo, K. Chikamatsu, T. Ohno, and T. Nakano. 2017. 'Dose-volume histogram analysis of brainstem necrosis in head and neck tumors treated using carbon-ion radiotherapy', *Radiother Oncol*, 125: 36-40.

Shirasuna, K., M. Sato, and T. Miyazaki. 1981. 'A neoplastic epithelial duct cell line established from an irradiated human salivary gland', *Cancer*, 48: 745-52.

Siegal, T., and M. R. Pfeffer. 1995. 'Radiation-induced changes in the profile of spinal cord serotonin, prostaglandin synthesis, and vascular permeability', *Int J Radiat Oncol Biol Phys*, 31: 57-64.

Staffurth, J. 2010. 'A review of the clinical evidence for intensity-modulated radiotherapy', *Clin Oncol (R Coll Radiol)*, 22: 643-57.

Steinstrater, O., R. Grun, U. Scholz, T. Friedrich, M. Durante, and M. Scholz. 2012. 'Mapping of RBE-weighted doses between HIMAC- and LEM-Based treatment planning systems for carbon ion therapy', *Int J Radiat Oncol Biol Phys*, 84: 854-60.

Sutherland, B. M., P. V. Bennett, H. Schenk, O. Sidorkina, J. Laval, J. Trunk, D. Monteleone, and J. Sutherland. 2001. 'Clustered DNA damages induced by high and low LET radiation, including heavy ions', *Phys Med*, 17 Suppl 1: 202-4.

Suzuki, M., Y. Kase, T. Kanai, and K. Ando. 2000. 'Change in radiosensitivity with fractionated-dose irradiation of carbon-ion beams in five different human cell lines', *Int J Radiat Oncol Biol Phys*, 48: 251-8.

Takagi, M., Y. Demizu, F. Nagano, K. Terashima, O. Fujii, D. Jin, M. Mima, Y. Niwa, K. Katsui, M. Suga, T. Yamashita, T. Akagi, K. I. Sakata, N. Fuwa, and T. Okimoto. 2018. 'Treatment outcomes of proton or carbon ion therapy for skull base chordoma: a retrospective study', *Radiat Oncol*, 13: 232.

Takakusagi, Yosuke, Jun-ichi Saitoh, Hiroki Kiyohara, Takahiro Oike, Shin-ei Noda, Tatsuya Ohno, and Takashi Nakano. 2017. 'Predictive factors of acute skin reactions to carbon ion radiotherapy for the treatment of malignant bone and soft tissue tumors', *Radiation Oncology*, 12: 185.

Tejpal, G., A. Jaiprakash, B. Susovan, S. Ghosh-Laskar, V. Murthy, and A. Budrukkar. 2010. 'IMRT and IGRT in head and neck cancer: Have we delivered what we promised?', *Indian J Surg Oncol*, 1: 166-85.

Tenforde, T. S., S. D. Tenforde, K. E. Crabtree, D. L. Parks, W. A. Schilling, S. S. Parr, M. J. Flynn, J. Howard, J. T. Lyman, and S. B. Curtis. 1981. 'RBE values for radiation-induced growth delay in rat rhabdomyosarcoma tumors exposed to plateau and peak carbon, neon and argon ions', *Int J Radiat Oncol Biol Phys*, 7: 217-22.

Tommasino, F., E. Scifoni, and M. Durante. 2016. 'New Ions for Therapy', *Int J Part Ther*, 2: 428-38.

Tommasino, Francesco, Alan Nahum, and Laura %J Translational Cancer Research Cella. 2017. 'Increasing the power of tumour control and normal tissue complication probability modelling in radiotherapy: recent trends and current issues', *Translational Cancer Research*, 6: S807-S21.

Tsujii, H., T. Kamada, T. Shirai, K. Noda, H. Tsuji, and K. Karasawa (ed.)^(eds.). 2014. *Carbon-Ion Radiotherapy* (Springer: Japan).

Tsujii, H., J. E. Mizoe, T. Kamada, M. Baba, S. Kato, H. Kato, H. Tsuji, S. Yamada, S. Yasuda, T. Ohno, T. Yanagi, A. Hasegawa, T. Sugawara, H. Ezawa, S. Kandatsu, K. Yoshikawa, R. Kishimoto, and T. Miyamoto. 2004. 'Overview of clinical experiences on carbon ion radiotherapy at NIRS', *Radiother Oncol*, 73 Suppl 2: S41-9.

Uhl, M., M. Mattke, T. Welzel, J. Oelmann, G. Habl, A. D. Jensen, M. Ellerbrock, T. Haberer, K. K. Herfarth, and J. Debus. 2014. 'High control rate in patients with chondrosarcoma of the skull base after carbon ion therapy: first report of long-term results', *Cancer*, 120: 1579-85.

Uhl, M., M. Mattke, T. Welzel, F. Roeder, J. Oelmann, G. Habl, A. Jensen, M. Ellerbrock, O. Jakel, T. Haberer, K. Herfarth, and J. Debus. 2014. 'Highly effective treatment of skull base chordoma with carbon ion irradiation using a raster scan technique in 155 patients: first long-term results', *Cancer*, 120: 3410-7.

Uzawa, A., K. Ando, S. Koike, Y. Furusawa, Y. Matsumoto, N. Takai, R. Hirayama, M. Watanabe, M. Scholz, T. Elsasser, and P. Peschke. 2009. 'Comparison of biological effectiveness of carbon-ion beams in Japan and Germany', *Int J Radiat Oncol Biol Phys*, 73: 1545-51.

Vargo, J. A., M. C. Ward, J. J. Caudell, N. Riaz, N. E. Dunlap, D. Isrow, S. J. Zakem, J. Dault, M. J. Awan, K. A. Higgins, C. Hassanadeh, J. J. Beitler, C. A. Reddy, S. Marcrom, D. H. Boggs, J. A. Bonner, M. Yao, M. Machtay, F. Siddiqui, A. M. Trotti, N. Y. Lee, S. A. Koyfman, R. L. Ferris, and D. E. Heron. 2018. 'A Multi-institutional Comparison of SBRT and IMRT for Definitive Reirradiation of Recurrent or Second Primary Head and Neck Cancer', *Int J Radiat Oncol Biol Phys*, 100: 595-605.

Vogin, G., A. Wambersie, M. Koto, T. Ohno, M. Uhl, P. Fossati, J. Balosso, Richard Pötter, Michael Beuve, Stephanie E. Combs, Giulio Magrin, Ramona Mayer, Ulrike Mock, David Sarrut, Thomas Schreiner, and Ulice W. P. working group on behalf of. 2019. 'A step towards international prospective trials in carbon ion radiotherapy: investigation of factors influencing dose distribution in the

facilities in operation based on a case of skull base chordoma', *Radiation Oncology*, 14: 24.

Wang, W., Z. Huang, Y. Sheng, J. Zhao, K. Shahnazi, Q. Zhang, and G. Jiang. 2019. 'RBE-weighted dose conversions for carbon ionradiotherapy between microdosimetric kinetic model and local effect model for the targets and organs at risk in prostate carcinoma', *Radiother Oncol*, 144: 30-36.

Weyrather, W. K., S. Ritter, M. Scholz, and G. Kraft. 1999. 'RBE for carbon track-segment irradiation in cell lines of differing repair capacity', *Int J Radiat Biol*, 75: 1357-64.

Wieser, Hans-Peter, Eduardo Cisternas, Niklas Wahl, Silke Ulrich, Alexander Stadler, Henning Mescher, Lucas-Raphael Müller, Thomas Klinge, Hubert Gabrys, Lucas Burigo, Andrea Mairani, Swantje Ecker, Benjamin Ackermann, Malte Ellerbrock, Katia Parodi, Oliver Jäkel, and Mark Bangert. 2017. 'Development of the open-source dose calculation and optimization toolkit matRad', *Med Phys*, 44: 2556-68.

Yamazaki, H., M. Ogita, K. Himei, S. Nakamura, T. Kotsuma, K. Yoshida, and Y. Yoshioka. 2015. 'Carotid blowout syndrome in pharyngeal cancer patients treated by hypofractionated stereotactic re-irradiation using CyberKnife: A multi-institutional matched-cohort analysis', *Radiother Oncol*, 115: 67-71.

Yamazaki, H., M. Ogita, N. Kodani, S. Nakamura, H. Inoue, K. Himei, T. Kotsuma, K. Yoshida, Y. Yoshioka, K. Yamashita, and H. Udono. 2013. 'Frequency, outcome and prognostic factors of carotid blowout syndrome after hypofractionated re-irradiation of head and neck cancer using CyberKnife: a multi-institutional study', *Radiother Oncol*, 107: 305-9.

Yanagi, T., T. Kamada, H. Tsuji, R. Imai, I. Serizawa, and H. Tsujii. 2010. 'Dose-volume histogram and dose-surface histogram analysis for skin reactions to carbon ion radiotherapy for bone and soft tissue sarcoma', *Radiother Oncol*, 95: 60-5.

Yang, J., J. Gao, X. Wu, J. Hu, W. Hu, L. Kong, and J. J. Lu. 2018. 'Salvage Carbon Ion Radiation Therapy for Locally Recurrent or Radiation-Induced Second Primary Sarcoma of the Head and Neck', *J Cancer*, 9: 2215-23.

Yazici, G., T. Y. Sanli, M. Cengiz, D. Yuce, M. Gultekin, P. Hurmuz, F. Yildiz, F. Zorlu, F. Akyol, M. Gurkaynak, and G. Ozyigit. 2013. 'A simple strategy to decrease fatal carotid blowout syndrome after stereotactic body reirradiaton for recurrent head and neck cancers', *Radiat Oncol*, 8: 242.

Yuan, H., M. W. Gaber, K. Boyd, C. M. Wilson, M. F. Kiani, and T. E. Merchant. 2006. 'Effects of fractionated radiation on the brain vasculature in a murine model: blood-brain barrier permeability, astrocyte proliferation, and ultrastructural changes', *Int J Radiat Oncol Biol Phys*, 66: 860-6.

I

Advances in Radiation Oncology (2017) **2**, 465-474

advances
in radiation oncology

www.advancesradonc.org

Scientific Article

Risk of carotid blowout after reirradiation with particle therapy

Jon Espen Dale MD [a,*], Silvia Molinelli MSc [b], Elisa Ciurlia MD [b], Mario Ciocca MSc [b], Maria Bonora MD [b], Viviana Vitolo MD [b], Alfredo Mirandola MSc [b], Stefania Russo MSc [b], Roberto Orecchia MD [b,c], Olav Dahl PhD, MD [a,d], Piero Fossati MD [b,c]

[a] *Department of Oncology and Medical Physics, Haukeland University Hospital, Bergen, Norway*
[b] *National Centre of Hadrontherapy (CNAO), Pavia, Italy*
[c] *European Institute of Oncology (IEO), Milan, Italy*
[d] *Department of Clinical Science, Faculty of Medicine, University of Bergen, Bergen, Norway*

Received 16 March 2017; received in revised form 23 May 2017; accepted 29 May 2017

Abstract

Purpose: Carotid blowout (CB) is a serious complication in retreatment of neoplasms in the head and neck (H&N) region. Rates seem to increase in hypofractionated or accelerated hyperfractionated regimens. In this study, we investigate the CB rate and the cumulative doses received by the carotid artery (CA) in a cohort of patients who were reirradiated at CNAO with particle therapy in the H&N region.

Methods and materials: The dosimetric information, medical records, and tumor characteristics of 96 patients were analyzed. For 49 of these patients, the quality of dosimetric information was sufficient to calculate the cumulative doses to the CA. The corresponding biological equivalent dose in 2 Gy fractions (EQD2) was calculated with an α/β-ratio of 3.

Results: In the final reirradiation at CNAO, 17 patients (18%) had been treated with protons and 79 (82%) with carbon ions. Two patients experienced profuse oronasal bleeding, of which one case was confirmed to be caused by CB. If attributing both cases to CB, we found an actuarial CB rate of 2.7%. Interestingly, there were no CB cases in the carbon ion group even though this was the large majority of patients and they generally were treated more aggressively in terms of larger fraction doses and higher cumulative EQD2.

Conclusions: The current practice of particle reirradiation at CNAO for recurrent neoplasms in the H&N region results in acceptable rates of CB.

Sources of support: This study was supported by grants from the Bergen Research Foundation in Bergen, Norway (Org.nr. 988 029 327).
Conflicts of interest: None.

* Corresponding author. Piazzetta Regisole 8, 27100 Pavia PV, Italy.
E-mail address: jonespendale@gmail.com (J.E. Dale)

http://dx.doi.org/10.1016/j.adro.2017.05.007

Introduction

Carotid blowout (CB), defined as a sudden rupture of the carotid artery (CA) or one of its main branches, is a feared complication in the treatment of neoplasms in the head and neck (H&N) region. CB results from pathologic alterations in or loss of the soft tissues surrounding the CA and from alterations in the vessel wall itself. Risk factors include ulceration, radiation to lymph nodes, dose to the neck >70 Gy, reirradiation, radical neck surgery, nutritional status (body mass index <22.5 kg/m^2), osteonecrosis, and the degree to which the CA is involved in the tumor.[1-4]

The properties of radiation therapy (RT) also seem to affect the risk of CB because rates as high as 8.4% to 15% are observed in reirradiation with hypofractionated stereotactic body RT (SBRT)[4-6] in contrast to >4% with more conventional fractionated photon regimens.[2,7]

Particle therapy, because of its physical advantages in dose distribution, is a suitable treatment modality for recurrent neoplasms in the H&N region. For carbon ion RT (CIRT) in particular, there are even biological advantages that could be harnessed through the use of hypofractionated schedules.[8,9] In a report on CIRT reirradiation of 52 patients with recurrent adenoid cystic carcinoma, 2 patients (3.8%) developed CB after nasopharyngeal necrosis.[10] The patients received reirradiation doses of 36 Gy (relative biological effectiveness [RBE]) to 74 Gy (RBE) in a moderately hypofractionated regimen of 3 Gy (RBE) per fraction.

At the National Center of Oncological Hadrontherapy (CNAO) in Pavia, Italy, patients with recurrent neoplasms in the H&N region are treated under protocols for reirradiation using protons or carbon ions with fraction doses ranging from 2 Gy (RBE) to 5 Gy (RBE). This prompted us to investigate the outcome of these patients with regard to CB with a special focus on the cumulative doses received by the CA.

Methods and materials

Reirradiation at CNAO

All patients were treated under prospective protocols that were approved by the regional ethics committee. A signed consent was required for participation. Proton RT was used as a first option, with conventional fractionation of 2 Gy (RBE) per fraction. A fixed RBE value of 1.1 was employed. CIRT was used for histologies with a poor response to low linear energy transfer (LET) radiation (eg, sarcoma, melanoma, and salivary gland tumors), in cases of early in-field recurrence after photon RT (assuming selection of a radio-resistant clone), or in cases in which the sharper lateral penumbra of CIRT resulted in significantly better sparing of organs at risk (OARs). Dose per fraction ranged from 2 Gy (RBE) to 5 Gy (RBE). RBE was calculated with the local effect model version 1[11] using the *syngo* RT Planning (Siemens Healthcare, Erlangen, Germany) treatment planning system (TPS).

To avoid long-term toxicity to OARs that were previously irradiated, an estimate of the cumulative biological equivalent dose (EQD2) from the prior and planned reirradiation was performed using a conservative α/β-ratio of 2 Gy for all OARs. When using an active scanning technique, it is feasible to selectively restrain the dose to the CA while retaining a high dose to most of the target (Fig 1b). The current practice at CNAO is to avoid cumulative EQD2 to the CA that exceeds 120 Gy (RBE) by using this method.

Patient population

A total of 128 patients were reirradiated at CNAO with either protons or carbon ions from September 2012 to March 2016. Four patients were excluded from the study because there were no records on the doses given in the previous RT, and 27 patients were excluded because they did not receive doses to their CA in the primary RT or the reirradiation or because these doses did not overlap in their CA. One patient, a foreign citizen, never appeared for follow-up and was also excluded.

A total of 96 patients were available for analysis with regard to the rate of CB (Fig 2; pink boxes). General details on past and present RT, patient and disease characteristics, and prior surgery were collected. In addition, the following information was also gathered:

1) tumor involvement grade: *(a)* no involvement, *(b)* <1/3 of CA circumference, *(c)* 1/3 to 2/3 of CA circumference, or *(d)* >2/3 of CA circumference
2) segment of CA that received the highest dose: *(a)* neck, *(b)* skull base, *(c)* sinus cavernosus, or *(d)* intracranial
3) whether surgery had been performed in the immediate vicinity of the high-dose segment of the CA, thus potentially making the CA more vulnerable.

Because tumor involvement grade and surgery near the CA have been suggested as factors that decrease the integrity of the CA wall and thereby increase the risk of CB,[1,2,7] we defined 2 potential high-risk features to assess their impact on CB rate in our material:

1) tumor involvement grade that is >2/3 of the CA circumference
2) prior surgery in the immediate vicinity of the segment of the CA that received the highest cumulative dose

Calculation of cumulative dose statistics to carotid arteries

For 49 of the 96 patients, there was sufficient documentation on prior RT to calculate cumulative doses to

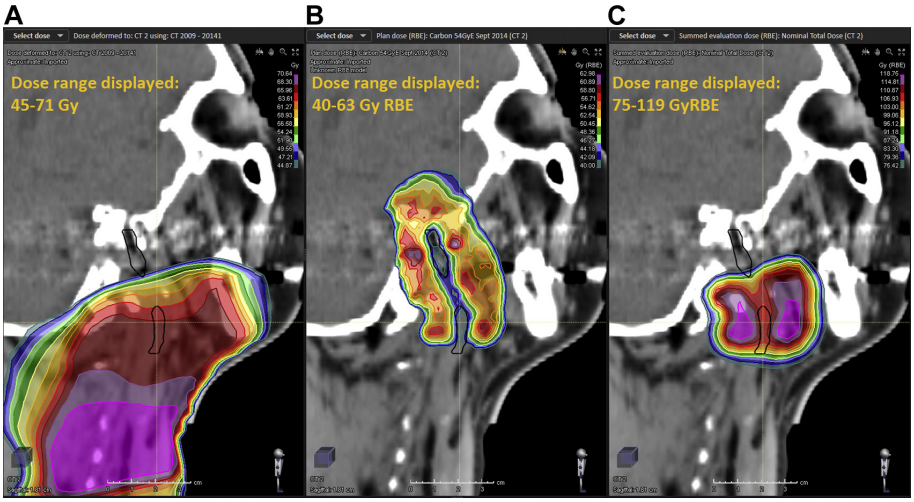

Figure 1 Dose distribution from (A) first photon treatment (70 Gy), (B) reirradiation at CNAO with carbon ions (54 Gy [RBE]) and (C) cumulative nominal dose. The carotid artery is outlined in black and demonstrates the selective sparing of the carotid artery in (B).

the CA. In 25 patients, both CAs had been reirradiated, giving a total of 74 CAs to be analyzed. For 32 of these patients (49 CAs), Digital Imaging and Communications in Medicine (DICOM) files of their previous RT was available. For the remaining 17 patients (25 CAs), dose data of previous RT could be extracted from printed computed tomography (CT) images with isodose curves (Fig 2; blue boxes).

For the group of patients with DICOM files, the CT images, structure set files, and dose files from both the primary and subsequent RT courses were imported to a workstation with the RayStation version 5.0 TPS (RaySearch Laboratories AB, Stockholm, Sweden). For the treatment course at CNAO, magnetic resonance imaging (MRI) scans in the treatment position were also imported and co-registered with the planning CT and used to

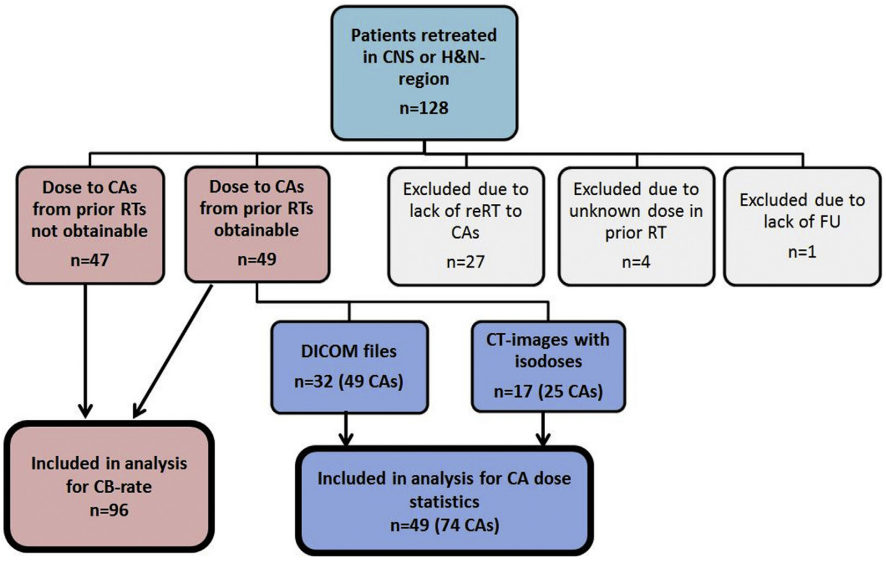

Figure 2 Patient selection.

support the contouring of the CAs on the CNAO planning CT. For the purpose of this study, the CA was defined as the common CA and internal CA, with a distal limit at the origin of the medial cerebral artery. Thus, we excluded smaller branches and the external CA because these arteries would be impossible to contour in many of the patients and because the current practice at CNAO is to delineate only the common CA and internal CA. All contouring was done by the same radiation oncologist, and only the segment of the CAs that was reirradiated was contoured.

To obtain the cumulative dose to the CA, the doses from patients' previous RT courses were deformed to the planning CT of the final RT course (CNAO CT) as follows: A rigid registration was made between the patients' different planning CTs, with a focus on achieving the best possible match in the area of the reirradiated CAs. We then performed a deformable registration between the planning CTs with the CNAO CT defined as the reference CT.

A cumulative nominal dose distribution was then created with the RayStation TPS by summing the deformed doses with the dose from the final RT on the CNAO CT (Fig 1). Cumulative nominal maximum dose ($\mathrm{CumDmax_{nom}}$) to the CA and nominal dose to 1% of the CA volume ($\mathrm{CumD1_{nom}}$) then were collected from the TPS. To provide an indication of the concentration of the highest dose, we calculated the volume of the CAs that received $\geq$90% of the $\mathrm{CumD1_{nom}}$ ($\mathrm{V90\%_{CumD1nom}}$).

Because many of the treatments were given with fraction doses well above 2 Gy/Gy (RBE), we also calculated a cumulative maximal EQD2 to the CA ($CumDmax_{EQD2}$) with the following equation:

$$CumDmax_{EQD2} = \frac{D_{1st}\left(\frac{D_{1st}}{Fx_{1st}} + \frac{\alpha}{\beta}\right)}{\left(2 + \frac{\alpha}{\beta}\right)} + \frac{D_{2nd}\left(\frac{D_{2nd}}{Fx_{2nd}} + \frac{\alpha}{\beta}\right)}{\left(2 + \frac{\alpha}{\beta}\right)} + \frac{D_{3}\left(\frac{D_{3rd}}{Fx_{3rd}} + \frac{\alpha}{\beta}\right)}{\left(2 + \frac{\alpha}{\beta}\right)}$$

where D_{1st} was the dose from the first RT course contributing to the $CumDmax_{nom}$ and Fx_{1st} was the fraction number of the same course. The second term of the equation was used for patients who had more than one previous RT, and the third term represented the final reirradiation at CNAO. Due to the lack of published data on the α/β-ratio of the CA, an α/β-ratio of 3 Gy was chosen, acknowledging that the α/β-ratio of 2 Gy, which has been employed at CNAO, probably is too conservative compared with what would be used at most other institutions. This is also in agreement with other publications on the toxicity to arteries induced by radiation.[12,13]

For the 17 patients for whom the dose distribution was obtainable from printed CT slices, the dose statistics were collected as follows: We identified the segment of the CA in which the highest $CumDmax_{nom}$ would be located by visually comparing the dose plan from the particle therapy course at CNAO with the printed CT slices from the previous RT courses. The doses (D_{1st}, D_{2nd},…) that contributed to the $CumDmax_{nom}$ were then collected from the prints for the respective segment of the CA. If, for example, the CA in the first RT course was situated between the 50 Gy and 60 Gy isodose curves, an approximation of the D_{1st} was set to 55 Gy. Thereafter, the dose given to the same segment in the particle therapy course at CNAO (D_{3rd}) was derived directly from the *syngo* TPS that is installed at CNAO. In this way, an approximation of the $CumDmax_{nom}$ was collected for these 17 patients. A $CumDmax_{EQD2}$ was also calculated using the previously mentioned equation.

Follow-up

Patients were followed at CNAO with a clinical examination and an MRI scan every 3 months after completion of the reirradiation.

Statistics

The data were analyzed with the IBM SPSS Statistics for Windows, Version 23.0 (IBM Corp., Armonk, NY). Differences in frequencies between groups were compared using the χ^2 or Fischer's exact test. Nonparametrical distributions were compared with the Mann-Whitney U-test, and normally distributed data were compared with the independent samples *t* test. Bivariate correlations between skewed data were analyzed with Spearman's rho. All *P*-values were obtained from two-sided tests. Survival estimates were generated with the Kaplan-Meier method.

Results

The median follow-up was 13.4 months (range, 0.8-49.2 months), and the median time from the first RT to the final reirradiation was 3.4 years (range, 0.3-50 years). Eleven patients (11.5%) had previously undergone 2 courses of RT. Two of these patients had been treated with photons primarily, followed by a second and third course of CIRT at CNAO due to 2 consecutive relapses. One patient had been treated at CNAO with CIRT for all

Table 1 Patient and disease characteristics

	Quality of Final Re-RT			*P* value
	All (n = 96)	Proton RT (n = 17)	CIRT (n = 79)	
Median age (range), y	61 (24-88)	55 (24-75)	63 (24-88)	
Sex, male:female	56:40	8:9	48:31	NS
Comorbidity, n (%)				
Hypertension	26 (27.0)	2 (11.8)	24 (30.4)	NS
Diabetes mellitus	6 (6.3)	2 (11.8)	4 (5.1)	NS
Cardiovascular disease	5 (5.2)	3 (17.6)	2 (2.5)	.037
Histology, n (%)				
Adenoid cystic carcinoma	28 (29.2)	0 (0.0)	28 (35.4)	.003
Squamous cell carcinoma	27 (28.1)	13 (76.5)	14 (17.7)	
Sarcoma	11 (11.5)	0 (0.0)	11 (13.9)	
Mucoepidermoid carcinoma	5 (5.2)	0 (0.0)	5 (6.3)	
Undifferentiated carcinoma	5 (5.2)	1 (5.9)	4 (5.1)	
Pleomorphic adenoma	5 (5.2)	0 (0.0)	5 (6.3)	
Adenocarcinoma	3 (3.1)	0 (0.0)	3 (3.8)	
Myoepithelial carcinoma	3 (3.1)	0 (0.0)	3 (3.8)	
Meningioma	3 (3.1)	1 (5.9)	2 (2.5)	
High grade glioma	2 (2.1)	2 (11.8)	0 (0.0)	
Other[a]	4 (4.2)	0 (0.0)	6 (7.8)	
Site of Primary Tumor, n (%)				
Parotid gland	18 (18.8)	0 (0.0)	18 (22.8)	.003
Paranasal sinuses	17 (17.7)	0 (0.0)	17 (21.5)	
Rhinopharynx	15 (15.6)	6 (35.3)	9 (11.4)	
Oropharynx	10 (10.4)	3 (17.6)	7 (8.9)	
Oral cavity	7 (7.3)	2 (11.8)	5 (6.3)	
Brain/meninges	5 (5.2)	3 (17.6)	2 (2,5)	
Nasal cavity	5 (5.2)	1 (5.9)	4 (5.1)	
Skull base	5 (5.2)	0 (0.0)	5 (6.3)	
Skin of scalp or face	4 (4.2)	1 (5.9)	3 (3.8)	
Submandibular gland	3 (3.1)	0 (0.0)	3 (3.8)	
Larynx	2 (2.1)	1 (5.9)	1 (1.3)	
Lacrimal gland	2 (2.1)	0 (0.0)	2 (2.5)	
Other[b]	3 (3.1)	0 (0.0)	3 (3.8)	
Site of Highest Dose to CA, n (%)				
Neck	50 (52.1)	9 (52.9)	41 (51.9)	NS
Skull base	34 (35.4)	4 (23.5)	30 (38.0)	
Sinus cavernosus	10 (10.4)	3 (17.6)	7 (8.9)	
Intracranial	2 (2.1)	1 (5.9)	1 (1.3)	
Tumor Involvement Grade, n (%)				
No involvement	24 (25.0)	6 (35.3)	18 (22.8)	NS
<1/3 of CA circumference	14 (14.6)	2 (11.8)	12 (15.2)	
≥1/3 < 2/3 of CA circumference	9 (9.4)	2 (11.8)	7 (8.9)	
≥2/3 of CA circumference	49 (51.1)	7 (41.2)	42 (53.2)	
Surgery, n (%)				
Any surgery	80 (83.3)	10 (58.8)	70 (88.6)	.007
Neck dissection	26 (27.1)	6 (35.3)	20 (25.3)	NS
In vicinity of highest dose to CA	46 (47.9)	5 (29.4)	41 (51.9)	NS
High-Risk Features[c], n (%)				
0 risk factors	28 (29.2)	8 (47.1)	20 (25.3)	NS
1 risk factor	41 (42.7)	6 (35.3)	35 (44.3)	
2 risk factors	27 (28.1)	3 (17.6)	24 (30.4)	

CA, carotid artery; CIRT, carbon ion radiation therapy; NS, not significant; RT, radiation therapy.

[a] Esthesioneuroblastoma, sinonasal carcinoma, carcinoma ex pleomorphic adenoma, oncocytoma.

[b] Mandible, hyoid bone, lymph node metastasis neck.

[c] Risk factors: Tumor involvement grade ≥2/3 and surgery in high-dose areas.

Table 2 Radiation therapy and dose statistics

	Quality of Final Re-RT			*P* value
	All (n = 96)	Proton (n = 17)	CIRT (n = 79)	
Previous RT Courses	107 courses	17 courses	90 courses	
Nom. prescribed dose, median (range)				
Gy/Gy (RBE)	60 (8-79.2)	66 (32-70)	60 (8-79.2)	.036
Fraction dose, median (range)				
Gy/Gy (RBE)	2 (1-6)	2 (1.8-4)	2 (1-6)	NS
Fraction dose, n (%)				
≤2 Gy/Gy (RBE)	75 (70.1)	11 (64.7)	65 (72.2)	NS
>2 to ≤3 Gy/Gy (RBE)	19 (17.8)	5 (29.4)	14 (15.6)	
>3 Gy/Gy (RBE)	10 (9.3)	1 (5.9)	9 (1.0)	
Unknown	3 (2.8)		2 (2.2)	
Radiation quality, n (%)				
Cobalt-60	4 (3.7)		4 (4.4)	NS
Photon	96 (89.7)	17 (100)	79 (87.8)	
Photon+Proton boost	1 (1.0)		1 (1.1)	
Photon+Carbon boost	1 (1.0)		1 (1.1)	
Proton	1 (1.0)		1 (1.1)	
Carbon	4 (3.7)		4 (4.4)	
Radiation technique, n (%)				
Conventional	83 (77.6)	17 (100)	66 (73.3)	NS
SBRT/SRS	10 (9.3)		10 (11.1)	
Conv.+particle boost	2 (1.9)		2 (2.2)	
Particle scanning technique	4 (3.7)		4 (4.4)	
Particle passive technique	1 (1.0)		1 (1.1)	
unknown	7 (6.5)		7 (7.8)	
Chemotherapy, n (%)				
Yes	31 (29.0)	10 (58.8)	21 (26.6)	.007
No	76 (71.0)	7 (41.2)	69 (73.4)	
Final Re-RT Course				
Nom. prescribed dose, median (range)				
Gy (RBE)	56 (12-76.8)	54 (30-70)	60 (12-76.8)	NS
Fraction dose, median (range)				
Gy (RBE)	3 (2-5)	2 (2-3)	3 (2-5)	<.005
Fraction dose, n (%)				
2 Gy (RBE)	17 (17.7)	15 (88.2)	2 (2.5)	
≥3 to <4 Gy (RBE)	59 (61.5)	2 (11.8)	57 (72.2)	
≥4 Gy (RBE)	20 (20.8)		20 (25.3)	
Prescribed Cumulative Lifetime Doses				
Nominal, median (range)				
Gy (RBE)	120 (32-197)	120 (62-138)	119 (32-197)	NS
EQD2, $\alpha/\beta = 3$ Gy, median (range)				
Gy (RBE)	132 (46-296)[a]	122 (67-140)[a]	132 (46-296)[a]	<.005
median (range)				
CumDmax, median (range)				
nominal, Gy (RBE)	103 (27-129)[b]	107 (40-129)[b]	101 (27-128)[b]	NS
EQD2 ($\alpha/\beta = 3$), Gy (RBE)	109 (25-167)[b]	107 (33-131)[b]	109 (25-167)[b]	NS
CumD1, median (range)				
nominal, Gy (RBE)	107 (35-128)[c]	107 (40-128)[c]	107 (35-127)[c]	NS
V90%CumD1, median (range)				
cm^3	0.18 (0.01-3.44)[c]	0.18 (0.01-3.44)[c]	0.18 (0.01-1.19)[c]	NS

CA, carotid artery; CIRT, carbon ion radiation therapy; CumD1, dose to 1% of the CA volume; CumDmax, cumulative maximum dose; NS, not significant; RBE, relative biological effectiveness; RT, radiation therapy; SBRT, stereotactic body radiation therapy; SRS, stereotactic radiosurgery; V90%CumD1, volume of the CAs that received ≥90% of the CumD1.

[a] Based on 94 patients because data on fraction size were missing for 2 patients.

[b] Based on 74 CAs of the 49 patients with dose data available.

[c] Based on the 49 CAs of the 32 patients with Digital Imaging and Communications in Medicine files.

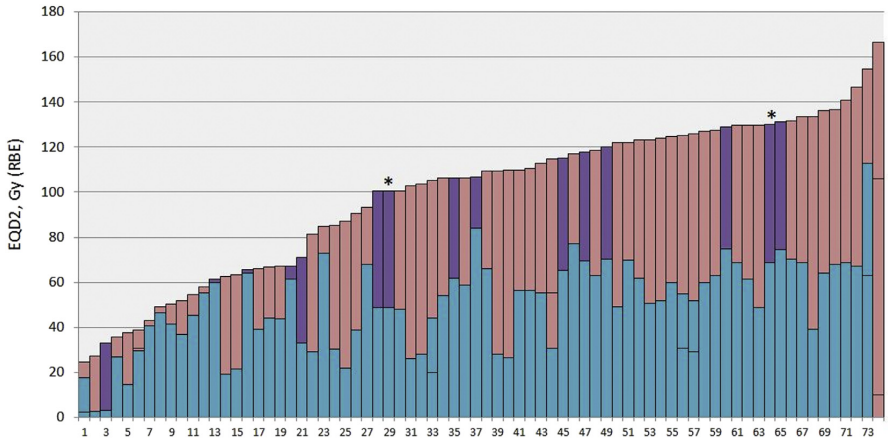

Figure 3 $CumDmax_{EQD2}$ for all 74 carotid arteries, displaying the contribution from photon radiation therapy (RT) (blue), carbon RT (pink), and proton RT (purple). * Carotid arteries of the 2 patients who developed oronasal hemorrhage.

3 courses, and another had undergone 2 Cobalt-60 treatments 50 years before reirradiation at CNAO. The remaining 7 patients had a first and second course of photon RT before the final reirradiation at CNAO. In the final reirradiation at CNAO, 17 patients (18%) were treated with protons versus 79 (82%) with carbon ions. Tables 1 and 2 present details on patient and disease characteristics, prior surgery, and previous and final RT courses for all patients and their distribution among the patients who received either proton RT or CIRT in the final reirradiation at CNAO.

A significantly larger proportion of patients had received chemotherapy in the proton group compared with the carbon group (55.6% vs 27.8%; $P = .026$), and the prescribed cumulative lifetime EQD2 was significantly higher in the carbon ion group, which was a result of higher fraction doses because the prescribed cumulative nominal lifetime doses were similar. There was a significant difference ($P < .005$) in the distribution of histologic entities between the two groups, with a dominans of salivary gland tumors and sarcomas in the CIRT group (69.5% total) while the proton RT group was dominated by squamous cell carcinomas (SCCs) (76.5%).

Dose statistics to carotid arteries

For the group of 49 patients with detailed dosimetric data, a total of 74 CAs had been reirradiated. When only analyzing the CA that received the highest cumulative dose in each patient, the difference between the prescribed cumulative nominal lifetime dose and the $CumDmax_{nom}$ ranged from −12 Gy (RBE) to 89 Gy (RBE) with a median of 6 Gy (RBE). In addition, the correlation between these 2 parameters was poor, with a Spearman's rho correlation coefficient of 0.363 ($P = .010$).

Median $CumDmax_{EQD2}$ for all 74 CAs was 109 Gy (RBE) (range, 25-167 Gy [RBE]). The contributions from each RT course to each individual CA are presented in Figure 3. The median $CumD1_{nom}$ was 107 Gy (RBE) (range, 35-128 Gy [RBE]). In most cases only small volumes of the CA recieved the highest dose, demonstrated by the median $V90\%_{CumD1nom}$ of 0.18 cm^3 (range, 0.01-3.44 cm^3), which corresponds to the volume of a cylinder 0.92 cm long with a diameter of 5 mm.

Cases of carotid blowout

Two of the 96 patients experienced an acute oronasal hemorrhage. The first patient had been treated for an SCC of the nasopharynx with chemotherapy and photon RT (66 Gy/33 fractions) in the primary setting. Eighteen months later, the patient was reirradiated with protons (60 Gy [RBE]/30 fractions) because of a recurrent tumor that completely surrounded his CAs at the skull base. Both CAs received a $CumDmax_{nom}$ of 107 Gy (RBE), which corresponds to a $CumDmax_{EQD2}$ of 100 Gy (RBE). Before the acute hemorrhage, which occurred 6 months after the reirradiation, the patient had a second relapse in the reirradiated site of the nasopharynx. The hemorrhage was fatal and an autopsy was refused, so whether the bleeding was caused by the recurrent tumor or by a rupture of one of the CAs is uncertain.

The second patient, also with an SCC of the nasopharynx, was initially treated with chemoradiation with photons (70 Gy/35 fractions). Twenty months later, the patient underwent total parotidectomy due to metastases. Because of a recurrent tumor in the cranial part of the surgical bed, which completely encased the CA, the patient received reirradiation with protons (56 Gy [RBE]/28 fractions) 72 months after the primary RT. This CA

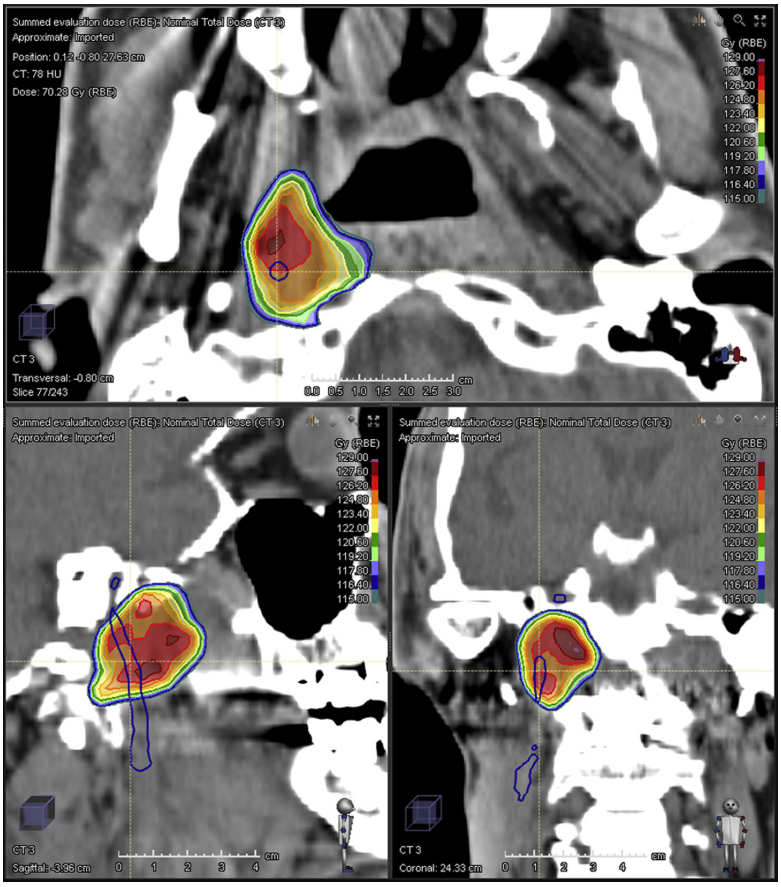

Figure 4 Dose corresponding to ≥90% of CumD1nom (115-129 Gy [RBE]). $V90\%_{CumD1}$ for this patient was 0.28 cm^3.

received a $CumDmax_{nom}$ of 129 Gy (RBE), which corresponds to a $CumDmax_{EQD2}$ of 130 Gy (RBE). The cumulative dose distribution is presented in Fig 4. Eight months later, the patient was admitted to his local hospital with profuse oronasal bleeding that required intubation. A CT angiography revealed a pseudoaneurysm on the CA in the high-dose area. No intervention was performed. The next night, the patient experienced another profuse bleed and died.

When attributing both cases to CB, we found a gross CB rate of 2.1% (95% confidence interval, 0.01-7.3%) in our series. The actuarial 1-year CB rate and overall survival probability were 2.7% and 81.5%, respectively. Figure 5 presents the Kaplan-Meier plot for the CB rate.

Discussion

In this study, we examined the rate of CB in a cohort of patients who underwent particle reirradiation for recurrent neoplasms of the head and neck. The patient population was diverse with regard to histology and site, in contrast to most other publications on CB, due to the current indications and referral practices for particle therapy.

Interestingly, both cases of probable CB were reirradiated with protons in 2 Gy (RBE) fractions, although we initially were more concerned about the high-LET, hypofractionated carbon ion reirradiation. This apparent difference in CB rate likely is caused by chance or by other confounding factors. For example, reirradiation for mucosal carcinomas of the upper pharynx may be more susceptible to CB than other combinations of histology and site because these tumors will always receive high doses to the tissues separating the CA from the pharynx lumen. Indeed, the highest CB rates published were in patient populations that were dominated by SCC and oro-/nasopharyngeal locations reirradiated by SBRT.[4,5] On the other hand, if this were true, we should have encountered CB in the CIRT group as well; the CIRT group had at least as many patients in terms of absolute numbers who

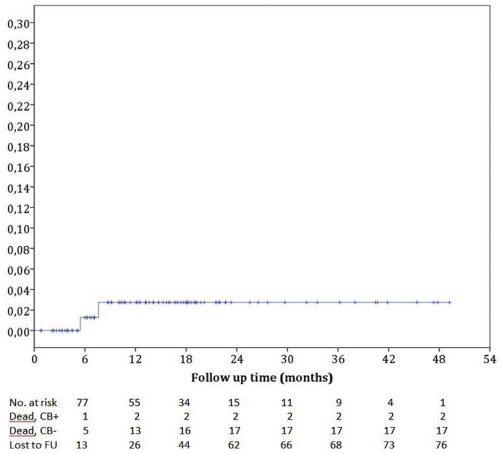

Figure 5 Cumulative carotid blowout (CB) rate. The table displays the absolute number of patients who were at risk of CB, death due to CB, death due to cause other than CB, and loss to follow-up at the end of each 6-month interval.

had similar site and histology and in whom treatments generally were more aggressive in dose and fractionation.

Another possible explanation for this apparent higher risk of proton RT versus CIRT could be that hypofractionation using high-LET radiation theoretically widens the therapeutic window between normal tissue complications and tumor control so that an equivalent CIRT dose generally would lead to fewer complications.[8,9]

In a report by Jensen et al[10] on outcome and toxicity after reirradiation with CIRT for recurrent adenoid cystic carcinoma, CB occurred in 2 of 52 patients (3.8%). In our study, there was no CB among the 77 patients who received CIRT, even though the prescribed total dose and fractionation at CNAO were more aggressive and the cumulative biological equivalent lifetime doses were comparable between the series. The apparent difference may be explained by the small study populations, differences in histology and site, or the possible benefit of more aggressive hypofractionation when using high-LET radiation. Most likely, the difference can be explained by CNAO's current practice of selectively sparing the CAs, thus resulting in the cumulative doses to the CAs probably being lower in our study. If this is the case, this strategy would be reasonable to pursue in the future as long as it does not affect tumor control probability. This will be a topic for upcoming publications.

To the best of our knowledge, there are no other studies on the CA as an OAR in which the cumulative doses to CAs have been reproduced in this detailed manner. Among the 74 CAs analyzed, our confirmed CB case had received among the highest nominal cumulative doses to the CA, and only a few patients had received significantly higher $CumDmax_{EQD2}$ (Fig 3). These few patients were all in the CIRT group, and it is questionable whether the conversion of nominal dose to EQD2 is valid for CIRT.

From the experience of our analysis, in which we found a substantial difference and poor correlation between the prescribed cumulative lifetime dose and the *CumDmax* to the CA, we conclude that a simple summation of a patient's prescribed doses is an unsuitable surrogate for this organ, especially with highly conformal RT techniques. We propose considering the CA to be an OAR, especially in the reirradiation setting, and use CA sparing when using proton or carbon ion RT. Other authors also suggest this in the setting of SBRT reirradiation.[14] More publications on cumulative doses to this organ are needed. Only by pooling data from different institutions can we hopefully shed more light on the impact of dose, volume, and fractionation with regard to the life threatening complication of CB.

Conclusions

The current practice of particle reirradiation at CNAO for recurrent neoplasms in the H&N region results in acceptable rates of CB that are better than the published results of photon SBRT and comparable to rates achieved with non-hypofractionated photon reirradiation. Applying specific dose constraints to the CA in re-RT with CIRT using the carotid sparing technique may explain the apparent favorable rate of CB compared with those from other institutions.

References

1. Yamazaki H, Ogita M, Himei K, et al. Carotid blowout syndrome in pharyngeal cancer patients treated by hypofractionated stereotactic re-irradiation using CyberKnife: A multi-institutional matched-cohort analysis. *Radiother Oncol*. 2015;115:67-71.
2. Chen YJ, Wang CP, Wang CC, Jiang RS, Lin JC, Liu SA. Carotid blowout in patients with head and neck cancer: Associated factors and treatment outcomes. *Head Neck*. 2015;37:265-272.
3. Chen KC, Yen TT, Hsieh YL, et al. Postirradiated carotid blowout syndrome in patients with nasopharyngeal carcinoma: A case-control study. *Head Neck*. 2015;37:794-799.
4. Cengiz M, Ozyigit G, Yazici G, et al. Salvage reirradiaton with stereotactic body radiotherapy for locally recurrent head-and-neck tumors. *Int J Radiat Oncol Biol Phys*. 2011;81:104-109.
5. Yamazaki H, Ogita M, Kodani N, et al. Frequency, outcome and prognostic factors of carotid blowout syndrome after hypofractionated re-irradiation of head and neck cancer using CyberKnife: A multi-institutional study. *Radiother Oncol*. 2013;107:305-309.
6. Kodani N, Yamazaki H, Tsubokura T, et al. Stereotactic body radiation therapy for head and neck tumor: disease control and morbidity outcomes. *J Radiat Res*. 2011;52:24-31.
7. McDonald MW, Moore MG, Johnstone PA. Risk of carotid blowout after reirradiation of the head and neck: A systematic review. *Int J Radiat Oncol Biol Phys*. 2012;82:1083-1089.

8. Ando K, Koike S, Uzawa A, et al. Biological gain of carbon-ion radiotherapy for the early response of tumor growth delay and against early response of skin reaction in mice. *J Radiat Res*. 2005; 46:51-57.
9. Denekamp J, Waites T, Fowler JF. Predicting realistic RBE values for clinically relevant radiotherapy schedules. *Int J Radiat Biol*. 1997;71:681-694.
10. Jensen AD, Poulakis M, Nikoghosyan AV, et al. Re-irradiation of adenoid cystic carcinoma: Analysis and evaluation of outcome in 52 consecutive patients treated with raster-scanned carbon ion therapy. *Radiother Oncol*. 2015;114:182-188.
11. Kramer M, Scholz M. Treatment planning for heavy-ion radiotherapy: Calculation and optimization of biologically effective dose. *Phys Med Biol*. 2000;45:3319-3330.
12. Yazici G, Sanli TY, Cengiz M, et al. A simple strategy to decrease fatal carotid blowout syndrome after stereotactic body reirradiaton for recurrent head and neck cancers. *Radiat Oncol*. 2013;8:242.
13. Evans JD, Gomez DR, Amini A, et al. Aortic dose constraints when reirradiating thoracic tumors. *Radiother Oncol*. 2013;106:327-332.
14. Thariat J, Marcy PY, Lacout A. Benefit of optimizing the dose to the carotid in hypofractionated stereotactic body reirradiation? *Int J Radiat Oncol Biol Phys*. 2011;81:1593-1594.

II

Radiotherapy and Oncology 140 (2019) 175–181

Contents lists available at ScienceDirect

Radiotherapy and Oncology

journal homepage: www.thegreenjournal.com

Original Article

Optic nerve constraints for carbon ion RT at CNAO – Reporting and relating outcome to European and Japanese RBE

Jon Espen Dale [a,b,*], Silvia Molinelli [c], Viviana Vitolo [c], Barbara Vischioni [c], Maria Bonora [c], Giuseppe Magro [c], Helge Egil Seime Pettersen [a], Andrea Mairani [c,d], Azusa Hasegawa [c,e], Olav Dahl [a,b], Francesca Valvo [c], Piero Fossati [c,f]

[a] Department of Oncology and Medical Physics, Haukeland University Hospital, Bergen; [b] Department of Clinical Science, Faculty of Medicine, University of Bergen, Norway; [c] National Center of Oncological Hadrontherapy, Pavia, Italy; [d] Heidelberg Ion-Beam Therapy Center, Heidelberg, Germany; [e] Osaka Heavy Ion Therapy Center, Osaka, Japan; [f] MedAustron Ion Therapy Center, Wiener Neustadt, Austria

ARTICLE INFO

Article history:
Received 11 March 2019
Received in revised form 18 June 2019
Accepted 18 June 2019
Available online 13 July 2019

Keywords:
Carbon ion radiotherapy
Optic nerve
Relative biological effectiveness
Organs at risk
Vision disorders
Long term adverse effects

ABSTRACT

Background and purpose: Until now, carbon ion RT (CIRT) dose constraints for the optic nerve (ON) have only been validated and reported in the NIRS RBE-weighted dose (D_{NIRS}). The aim of this work is to improve CNAO's RBE-weighted dose (D_{LEM}) constraints by analyzing institutional toxicity data and by relating it to D_{NIRS}.

Material and methods: A total of 65 ONs from 38 patients treated with CIRT to the head and neck region in the period 2013–14 were analyzed. The absorbed dose (D_{Abs}) of the treatment plans was reproduced and subsequently both D_{LEM} and D_{NIRS} were applied, thus relating CNAO clinical toxicity to D_{NIRS}.

Results: Median FU was 47 (26–67) months. Visual acuity was preserved for the 56 ONs in which the old constraints were respected. Three ONs developed visual decline at $D_{LEM|1\%} \geq 71$ Gy(RBE)/$D_{LEM|20\%} \geq 68$ Gy (RBE), corresponding to $D_{NIRS|1\%} \geq 68$ Gy(RBE)/$D_{NIRS|20\%} \geq 62$ Gy(RBE). Dose recalculation revealed that NIRS constraints of $D_{NIRS|1\%} \leq 40$ Gy(RBE)/$D_{NIRS|20\%} \leq 28$ Gy(RBE) corresponded to $D_{LEM|1\%} \leq 50$ Gy(RBE)/$D_{LEM|20\%} \leq 40$ Gy(RBE). Reoptimization of treatment plans with these new D_{LEM} constraints showed that the dose distribution still complied with NIRS constraints when evaluated in D_{NIRS}. However, due to uncertainties in the method, and to comply with the EQD2-based constraints used at GSI/HIT, a more moderate constraint relaxation to $D_{LEM|1\%} \leq 45$ Gy(RBE)/$D_{LEM|20\%} \leq 37$ Gy(RBE) has been implemented in CNAO clinical routine since October 2018.

Conclusion: New D_{LEM} constraints for the ON were derived by analyzing CNAO toxicity data and by linking our results to the experience of NIRS and GSI/HIT. This work demonstrates the value of recalculating and reporting results in both D_{LEM} and D_{NIRS}.

 Radiotherapy and Oncology 140 (2019) 175–181

In order to optimize carbon ion radiotherapy (CIRT) there is a need to validate dose constraints for important organs at risk (OARs). For the optic nerve (ON), constraints have been validated by the *National Institute of Radiobiological Sciences* (NIRS, Japan) [1], in which the *relative biological effectiveness* (RBE) for CIRT has been predicted by the *mixed beam model* (RBE_{NIRS}) [2,3], and have been reported as the *NIRS RBE-weighted dose* (D_{NIRS}). The NIRS constraints are not immediately useful for European centers where the *Local effect model I* (RBE_{LEM})[4,5] is used, because comparative studies show that RBE_{LEM} can predict a 60% higher RBE in the entrance region of the beam [6], and 5–15% higher RBE in the spread-out Bragg peak [7–9], relative to RBE_{NIRS}. At the *National Center of Oncological Hadrontherapy* (CNAO, Italy) [10,11], dose constraints for ONs complied nominally with the NIRS constraints: $D_{1\%} \leq 40$ Gy(RBE) and $D_{20\%} \leq 28$ Gy(RBE), although RBE_{LEM} is used in treatment plan optimization. This was a conservative approach, adopted at the beginning of clinical activity to minimize the risk of unexpected visual impairment due to lack of clinically validated RBE_{LEM}-weighted dose (D_{LEM}) constraints. The aim of this work was to improve CNAO's ON dose constraints by analyzing institutional toxicity and by relating the results to the constraints validated by NIRS.

* Corresponding author at: Department of Oncology and Medical Physics, Haukeland University Hospital, PB 1400, 5021 Bergen, Norway.
E-mail address: jon.espen.dale@helse-bergen.no (J.E. Dale).

https://doi.org/10.1016/j.radonc.2019.06.028
0167-8140/

Material and methods

Patient selection

We identified a total of 38 patients (65 ONs) who had been treated at CNAO in the period 2013–14 with CIRT to the head and neck region and who had:

- at least 2 years of follow-up.
- maximum dose ($D_{LEM|1\%}$) >20 Gy(RBE) to optic nerve.
- available records of visual acuity before and after CIRT.

and did not have:

- radiotherapy before or after CIRT at CNAO.
- higher dose to the chiasm than to the optic nerve.
- preexisting visual impairment.
- development of visual impairment in the follow-up period due to other causes than radiation induced optic pathway neuropathy (e.g. recurrent tumor, etc.).

Carbon ion radiotherapy at CNAO

All patients were treated to a prescribed D_{LEM} of 68.8 or 70.4 Gy (RBE) in 16 fractions (4 fractions/week) using the *syngo*® RT Planning (Siemens Healthcare, Erlangen, Germany) treatment planning system (TPS). The patients were included in prospective protocols (CNAO S9/2012/C, CNAO S12/2012/C and CNAO S15/2012/C) approved by the regional ethics committee, and signed consent was required for participation. Dose constraints for the ONs and chiasm were $D_{LEM|1\%} \leq 40$ Gy(RBE) and $D_{LEM|20\%} \leq 28$ Gy(RBE). A 2 mm margin was applied to the planning organ at risk volume (PRV) in which the dose constraints, for plan optimization purposes, were $D_{LEM|1\%} \leq 60$ Gy(RBE) and $D_{LEM|20\%} \leq 40$ Gy(RBE). Following the patient's consent, the constraints could be exceeded if they prevented adequate dose coverage to the target volume, provided that the function of the contralateral ON was adequate and would be preserved.

Follow-up

Patients were followed at CNAO every 3rd month with a clinical examination and magnetic resonance imaging (MRI). If symptoms of visual defects were reported by the patient or detected on clinical examination, the patient was referred to an ophthalmologist for further investigations and diagnosis. *Radiation induced optic neuropathy* (RION) was scored according to the *Optic Nerve Disorder* term of the *Common Terminology Criteria for Adverse Events version 4.03* (CTCAE) [12].

Recalculation to RBE_{NIRS}-weighted dose distributions

The patients' computer tomography (CT) image files, structure set files, dose files and plan files (DICOM files) were exported from *syngo*® TPS and imported to the *matRad* open source multimodality radiation TPS (https://e0404.github.io/matRad/) in which the absorbed dose (D_{Abs}) and D_{LEM} were reproduced. Dose–volume histograms (DVHs) of targets and OARs were compared with the corresponding DVHs of the dose distribution from the *syngo*® TPS to ensure correct reproduction of both D_{Abs} and D_{LEM} (results not reported). Secondly, the RBE_{NIRS} was implemented in the matRad TPS code and D_{NIRS} was derived from the exact same absorbed dose. This enabled a direct comparison of each patient's D_{LEM} and D_{NIRS} based exclusively on the differences in the RBE modeling.

Statistics and normal tissue complication probability (NTCP) modeling

Differences in frequencies between cohorts were compared using Chi-Square test or Fischer's exact test. Non-parametrical distributions were compared with the Mann–Whitney *U*-test, while normally distributed data were compared with the independent samples *T*-test. NTCP was calculated for cumulative DVH variables $D_{1\%}$, $D_{10\%}$, $D_{20\%}$ through $D_{50\%}$ and were used to derive the dose that would result in 5% (TD5) and 50% (TD50) probability of RION according to the equation:

$$\mathrm{NTCP}(Dx\%) = 1 - \frac{1}{1 + e^{a+b*d}}$$

where d is the RBE-weighted dose to x% of the ON volume and a and b are constants estimated to provide the best fit to the data set, using binary logistic regression. All statistical procedures were performed with the software IBM SPSS Statistics for Windows, Version 24.0 (IBM Corp., Armonk, NY, U.S.A.). All *p*-values were obtained from two-sided tests. *P*-values <0.05 were considered significant.

Reoptimization of treatment plans with new set of constraints

Finally, a subset of patients, in which the original constraints had caused inadequate dose coverage to the clinical target volume (CTV) in their original D_{LEM} plan, was reoptimized with the RayStation® 7.0 TPS (RaySearch Laboratories AB, Stockholm, Sweden) (currently under commissioning at CNAO) applying RBE_{LEM} as RBE model and optimizing the plan with a new set of D_{LEM} constraints, as proposed by this work (see *Results*). Subsequently, also these plans were recalculated to D_{NIRS}, to validate that the reoptimized ON DVHs still complied with the original NIRS constraints.

A flow chart of the steps involved in our method is presented in Appendix A, Fig. A1.

Results

Patient and disease characteristics are presented in Table 1. Median follow-up time was 47 (range 26–67) months. Among the 38 patients and 65 ONs analyzed, toxicity did not occur in the 52 ONs in which the current constraints were respected. Three patients developed unilateral RION (all CTCAE grade 4) at doses $D_{LEM|1\%} \geq 71$ Gy(RBE)/$D_{NIRS|1\%} \geq 68$ Gy(RBE) and $D_{LEM|20\%} \geq 68$ Gy (RBE)/$D_{NIRS|20\%} \geq 62$ Gy (RBE). In all these cases, the ON constraints were intentionally violated in order to achieve adequate dose coverage to the nearby tumor. RION was detected at 11, 29 and 42 months after completed CIRT. In addition to the 3 ONs that developed toxicity, the applied constraints were breached for 10 ONs with a median follow-up of 45 (range 26–50) months. When evaluating the DVHs with D_{NIRS}, only 6 of these ONs still exceeded NIRS constraints. All individual ONs in both D_{LEM} and D_{NIRS} are presented in Fig. 1, demonstrating that RBE_{NIRS} generally predicts lower RBE than RBE_{LEM}, resulting in the DVHs being shifted toward lower doses. Key dosimetric data are presented in Table 2.

The relationship of D_{NIRS} and D_{LEM} for $D_{1\%}$ and $D_{20\%}$ is presented in Fig. 2, showing that a $D_{NIRS|1\%}$ of ≤ 40 Gy(RBE) and a $D_{NIRS|20\%}$ of ≤ 28 Gy(RBE) could approximately be translated into new CNAO constraints of $D_{LEM|1\%} \leq 50$ Gy(RBE) and $D_{LEM|20\%} \leq 40$ Gy(RBE). These new constraints for D_{LEM} are plotted as open red squares in Fig. 1. As can be observed, the ONs that comply with the original NIRS constraints when their DVHs are evaluated in D_{NIRS}, remain compliant with the new CNAO constraints when their DVHs are evaluated in D_{LEM}. Likewise, the ONs that exceed the NIRS constraints when evaluated in D_{NIRS} still exceed the new CNAO constraints when evaluated in D_{LEM}.

The estimates of TD5 and TD50 for parameters D1%–D50%, and their relation to the same parameters from the dose constraint val-

Table 1
Patient and disease characteristics for all patients and grouped by patients that developed (*RION = yes*) or did not develop (*RION = no*) radiation induced optic neuropathy.

		All (n = 38)	RION = yes (n = 3)	RION = no (n = 35)
Sex, female:male		18:20	2:1	16:19
Median age (range), y		59 (16–81)	62 (54–68)	54 (16–81)
Comorbidity, n (%)				
	Hypertension	9 (23.7%)	1 (33.3%)	8 (22.9%)
	Diabetes mellitus	8 (21.1%)	1 (33.3%)	7 (20.0%)
	Cardiovascular disease	4 (10.5%)	1 (33.3%)	3 (8.6%)
Histology, n (%)				
	Adenoid cystic carcinoma	14 (36.8%)	2 (66.7%)	12 (34.3%)
	Chordoma	14 (36.8%)	0 (0.0%)	14 (40.0%)
	Chondrosarcoma	3 (7.9%)	0 (0.0%)	3 (8.6%)
	Other sarcoma	5 (13.2%)	1 (33.3%)	4 (11.4%)
	Acinar cell carcinoma	1 (2.6%)	0 (0.0%)	1 (2.9%)
	Mucosal malignant melanoma	1 (2.6%)	0 (0.0%)	1 (2.9%)
Site, n (%)				
	Clivus	12 (31.6%)	1 (33.3%)	11 (31.4%)
	Paranasal sinus	9 (23.7%)	2 (66.7%)	7 (20.0%)
	Skull base	9 (23.7%)	0 (0.0%)	9 (25.7%)
	Nasal cavity	4 (10.5%)	0 (0.0%)	4 (11.4%)
	Nasopharynx	2 (5.2%)	0 (0.0%)	2 (5.7%)
	Other	2 (5.2%)	0 (0.0%)	2 (5.7%)

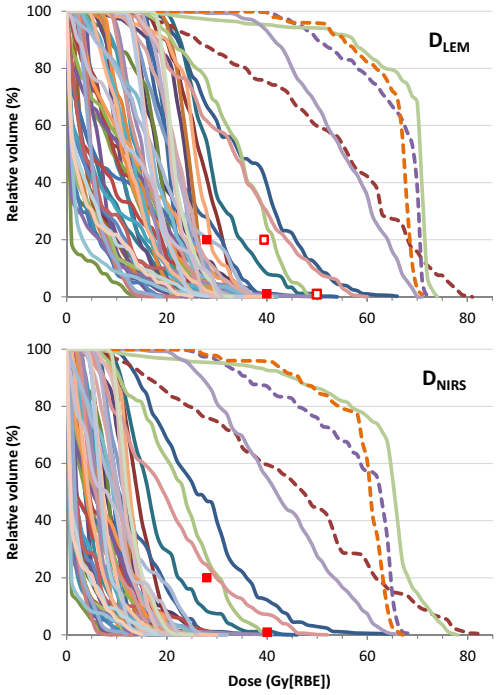

Fig. 1. Cumulative DVH of all 65 ONs in D_{LEM} (upper panel) and D_{NIRS} (lower panel). Dashed DVH-lines represent optic nerves that developed RION. Red, filled squares indicate the current dose constraints of $D_{1\%}$ ≤40 Gy(RBE) and $D_{20\%}$ ≤28 Gy(RBE). Red, open squares in upper panel represent possible new D_{LEM} constraints for CNAO based on RBE-weighted dose translation.

idation at NIRS [1] are presented in Table 3, showing a remarkable agreement of TD50 between NIRS and CNAO data in D_{NIRS}, while estimates of TD5 are substantially higher when based on the CNAO data.

The NIRS validation cohort consisted of 30 patients (54 ONs), in which visual impairment occurred in 9 patients (11 ONs). All ON DVHs from this cohort are displayed in Fig. 3 (black DVHs). The DVHs of the ONs developing toxicity in the CNAO cohort (in D_{NIRS}) are superimposed in red, showing good agreement to the NIRS cohort in respect to the dose levels at which toxicity seems to develop. The figure also displays the TD50 and TD5 estimates from Table 3, demonstrating the coherency of TD50 values and the discrepancy in TD5 values between the cohorts.

A subset of patients in which the current constraints hindered adequate dose coverage to the clinical target volume (CTV) was reoptimized applying the proposed new set of D_{LEM} constraints, i.e. $D_{LEM|1\%}$ ≤50 Gy(RBE) and $D_{LEM|20\%}$ ≤40 Gy(RBE). After recalculation of the new plan to D_{NIRS}, the ON DVHs consistently remained compliant to the original NIRS constraints. The dose distributions of a representative patient, in which the right ON needed to be spared in order to avoid bilateral blindness, are shown in Fig. 4. The conservative constraints applied in the original plan inevitably resulted in inadequate dose coverage to the part of the CTV adjacent to the right ON (Fig. 4A). Post hoc recalculation of the plan to D_{NIRS} (Fig. 4B) suggests that the right ON was excessively spared relative to the NIRS validated constraints. Reoptimizing the plan with the new D_{LEM} constraints significantly improves CTV coverage (Fig. 4C-D vs. A-B) while maintaining compliance with the NIRS validated constraints in respect to D_{NIRS} (Fig. 4D). In this patient, the reoptimized plan achieved a dose coverage in which 99% of the prescribed dose covered 92% of the CTV and 95% of the prescribed dose covered 97.7% of the CTV. The respective dose coverage to the CTV of the original plan was only 82% and 93.2%.

Discussion

Due to the many uncertainties involved in the prediction of the RBE of CIRT, there will inevitably be substantial uncertainties related to the extrapolation of OAR constraints from the experience of photon RT. Therefore, the strategy of CNAO has been to define OAR constraints for CIRT based on CIRT clinical data. To date, there is a general lack of validated constraints for most OARs. The few publications addressing this topic have all reported the dose statistics and NTCPs solely in the respective institutional RBE-weighted dose [1,13–18], thus making them incomprehensible to institutions applying a different RBE model.

Table 2
Dose statistics for all ONs and/or grouped by ONs that developed (*RION = yes*) or did not develop (*RION = no*) radiation induced optic neuropathy. *P* values represent the significance level for the observed difference in variable distribution between *RION = yes* and *RION = no* groups.

	All ($n = 65$)	RION = yes ($n = 3$)	RION = no ($n = 62$)	*P* value
Median ON volume (range), cm^3	0.92 (0.45–1.52)	0.74 (0.46–1.34)	0.94 (0.45–1.52)	0.485
D1%, median (range)				
D_{LEM}, Gy (RBE)		71.6 (70.7–78.6)	28.4 (12.2–73.6)	<0.001
D_{NIRS}, Gy (RBE)		67.2 (66.3–79.3)	18.1 (6.1–76.2)	<0.001
D10%, median (range)				
D_{LEM}, Gy (RBE)		70.8 (69.1–72.5)	22.9 (6.5–71.8)	<0.001
D_{NIRS}, Gy (RBE)		65.2 (63.8–70.0)	12.8 (3.0–71.8)	<0.001
D20%, median (range)				
D_{LEM}, Gy (RBE))		68.5 (68.1–70.5)	19.5 (0.7–71.4)	<0.001
D_{NIRS}, Gy (RBE)		63.0 (61.8–64.7)	10.2 (0.2–68.2)	<0.001
D30%, median (range)				
D_{LEM}, Gy (RBE)		68.1 (62.6–70.1)	17.1 (0.2–71.1)	<0.001
D_{NIRS}, Gy (RBE)		62.2 (54.6–64.2)	8.4 (0.0–66.7)	<0.001
D50%, median (range)				
D_{LEM}, Gy (RBE)		67.4 (56.1–69.3)	12.6 (0.1–70.7)	<0.001
D_{NIRS}, Gy (RBE)		60.4 (47.3–62.6)	5.6 (0.0–65.4)	<0.001

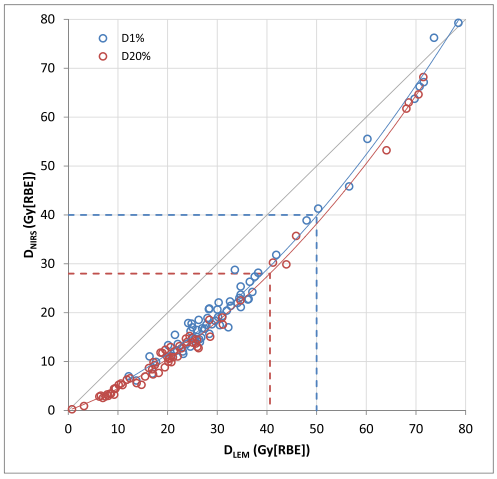

Fig. 2. Relationship of D_{NIRS} and D_{LEM} for $D_{1\%}$ (blue circles) and $D_{20\%}$ (red circles) with corresponding trend lines. Dashed lines represent translation from D_{NIRS} to D_{LEM} for constraint $D_{1\%}$ (blue) and $D_{20\%}$ (red).

Table 3
TD5 and TD50 values for optic nerve DVH parameters as derived from the present study (CNAO), presented in D_{LEM} and D_{NIRS}, compared to corresponding values reported by Hasegawa et al. [1] (NIRS).

		CNAO		NIRS	*CNAO/NIRS-1 (D_{NIRS})*
		D_{LEM}	D_{NIRS}	D_{NIRS}[a]	
TD5, Gy(RBE)	D1%	62	49	n.s.	
	D10%	61	45	30*	50.0%
	D20%	55	42	28*	50.0%
	D30%	47	37	24*	54.2%
	D50%	41	30	12*	150.0%
TD50, Gy(RBE)	D1%	71	68	n.s.	
	D10%	69	63	63	0.0%
	D20%	66	60	60*	0.0%
	D30%	64	57	59	−3.4%
	D50%	61	53	51	3.9%

n.s. = not specified.
[a] Doses as reported in Hasegawa et al. [1].
* Approximated from Fig. 7 in Hasegawa et al. [1].

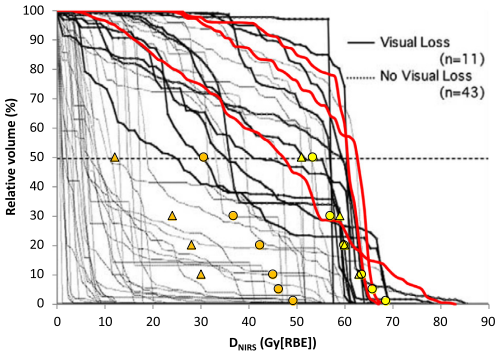

Fig. 3. Reprint of Fig. 4a from Hasegawa et al. [1] showing the DVHs from the NIRS validation cohort, where black DVHs represent ONs that developed RION, and gray DVHs represent ONs that did not develop RION. Superimposed on the figure are the D_{NIRS} DVHs (red) of the three ONs from the CNAO cohort that developed RION, TD5 (orange) and TD50 (yellow) of NIRS cohort (triangles) and CNAO cohort (circles).

The aim of this work was first and foremost to establish less conservative constraints for the ON which could be used at CNAO for a 16 fraction CIRT treatment in which RBE_{LEM} is applied. Our data show that the original constraints have been conservative, resulting in no unanticipated toxic events and with a seemingly large buffer zone separating these constraints and the dose levels where toxicity was observed. In NTCP modeling, we found TD50 to agree well with the published TD50 estimates at NIRS, while there was a discrepancy in TD5 estimates. This discrepancy is probably a result of a scarcity of observations in the CNAO cohort in the middle to high doses, relative to the NIRS cohort, which is evident when comparing the neatly scattered DVHs of Fig. 3 (NIRS DVHs) to the DVHs of Fig. 1 (CNAO DVHs) which are clustered at lower doses. As a consequence the TD5 estimates of the CNAO data may be unreliable. However, by recalculating our data to D_{NIRS}, it was possible to translate the constraints validated at NIRS into D_{LEM} and thereby propose new CNAO constraints to be evaluated for feasibility. As shown in *Results*, new CNAO constraints of $D_{LEM|1\%} \leq 50$ Gy(RBE) and $D_{LEM|20\%} \leq 40$ Gy(RBE) seem to correspond well with the NIRS validated constraints.

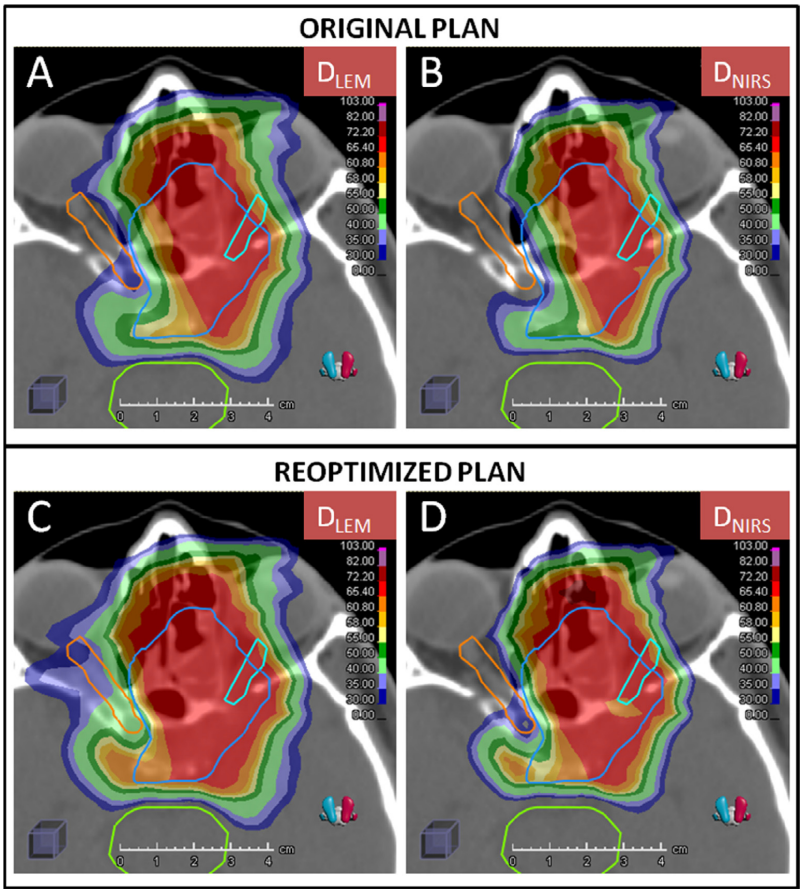

Fig. 4. Original and reoptimized plan in D_{LEM} and D_{NIRS}, demonstrating improved CTV (*blue contour*) dose coverage when applying the new D_{LEM} constraints (Fig. 4c) to the right ON (*orange contour*) and maintained compliance to original NIRS constraints after recalculation to D_{NIRS} (Fig. 4d). Legend for dose distribution in Gy(RBE): *dark blue* = 30–35; *light blue* = 35–40; *light green* = 40–50; *dark green* = 50–55; *yellow* = 55–58; *light orange* = 58–61; *dark orange* = 61–65; *red* = 65–72.

It should be noted that this approach assumes a perfect agreement between the D_{NIRS} recalculated for our cohort, and the D_{NIRS} reported for the validation cohort at NIRS. This may not be correct, since the CIRT at NIRS is delivered by a passive scattering system and with a different beam model calculating the underlying absorbed dose. It has been shown that the absorbed dose of a given RBE-weighted dose could on average vary about 2.5% in the *target region* of head and neck treatments, depending on the beam model [8]. Differences in *out-of-target* areas have not been described in detail, but one might expect to find similar or even more profound deviations in absorbed dose especially within the lateral penumbra dose fall-off. This region is indeed very sensitive to how the lateral spread of the beam is modeled. This is of importance, since the sharp lateral penumbra of the carbon ion beam typically is utilized to avoid high doses to optic nerves located close to the tumor.

Therefore, it is also valuable to relate our proposed new constraints to the traditions of *GSI Helmholtzzentrum für Schwerionenforschung* (GSI), Darmstadt, Germany, later adapted at the *Heidelberg Ion-Beam Therapy center* (HIT), Heidelberg, Germany [19], which together are Europe's most experienced heavy ion therapy center. Their ON constraint has been a maximum dose ($D_{LEM|max}$) of $\leq$54 Gy(RBE), expressed as the *biologically equivalent dose in 2 Gy(RBE) fractions* (EQD2), applying $\alpha/\beta = 2$ Gy [20]. Although GSI/HIT, as CNAO, applies both active scanning beam delivery and the RBE_{LEM} as their RBE model, direct comparison to CNAO is hampered by a difference in fractionation scheme. Typically, HIT uses 20 fractions of 3 Gy(RBE) delivered within 3–3.5 weeks [20,21], while CNAO uses 16 fractions of 4.3–4.4 Gy (RBE) delivered within 4 weeks. Unfortunately, a validation of the GSI/HIT constraint has not yet been published. However, of interest is their published observation of a patient developing bilateral blindness after receiving a nominal $D_{LEM|max}$ of 54 Gy(RBE) to the optic pathways, corresponding to an EQD2 of 63 Gy(RBE) [20]. This raises concern that our proposed new CNAO constraint of $D_{LEM|1\%}$ $\leq$50 Gy(RBE) might be too high, since it converts into an EQD2 of as much as 64 Gy(RBE). Although the application of EQD2 and the use of $\alpha/\beta = 2$ Gy for optic pathways are supported by the European Particle Therapy Network (EPTN) also for proton RT [22], this method may not be sufficiently precise for CIRT, due to the greater uncertainties involved in RBE prediction. However, to our knowl-

edge this approach has been implemented without unanticipated toxicity at GSI/HIT, thus supporting the feasibility of using EQD2 conversion within an institution applying RBE_{LEM}. Accordingly, within the 16 fraction regimen at CNAO, an EQD2 constraint of $\leq$54 Gy(RBE) corresponds to a nominal $D_{LEM|1\%}$ to the ON of $\leq$45 Gy(RBE), and implies a 9% reduction relative to the initial proposal of $D_{LEM|1\%} \leq$50 Gy(RBE). A proportionately equal reduction in the proposed $D_{LEM|20\%}$ constraint results in $D_{LEM|20\%} \leq$37 Gy(RBE).

Regardless of the validity of EQD2 for CIRT, a reduction in the initially proposed new CNAO constraints mitigates the uncertainties involved in our D_{LEM} to D_{NIRS} translation, and is therefore a reasonable first step for dose constraint relaxation at CNAO. As a consequence of the results and deliberations presented in this paper, new ON constraints of $D_{LEM|1\%} \leq$45 Gy(RBE) and $D_{LEM|20\%} \leq$37 Gy(RBE) have been implemented at CNAO since October 2018.

This paper demonstrates the value of assessing and reporting data on CIRT clinical toxicity in both the institution's native RBE model and the alternative model which is widely used clinically. To date, dose recalculation has been a cumbersome affair, but we anticipate that the introduction of such functionality in commercial TPS' within the next years will facilitate this process. We therefore hope that future publications will report OAR dose statistics and NTCPs in both D_{NIRS} and D_{LEM}, and thus accelerate the much needed validation of OAR constraints for both RBE models.

We have derived new and safe dose constraints for the ON to be used at CNAO by analyzing the available institutional data and by mitigating the uncertainties caused by a rather small sample size linking our results to the experience and traditions of NIRS and GSI/HIT. This work also demonstrates how valuable and much needed dose–response data can be saved from being lost in translation between Japanese and European CIRT institutions by recalculating and reporting results in both clinically applied RBE models.

Declaration of Competing Interest

None of the authors have any disclosures or conflicts of interest.

Acknowledgement

Supported by grants from the Trond Mohn Foundation, *Ytre-bygdsvegen 215, Kokstad, Postboks 7150, 5020 BERGEN, Norway.*

Appendix A

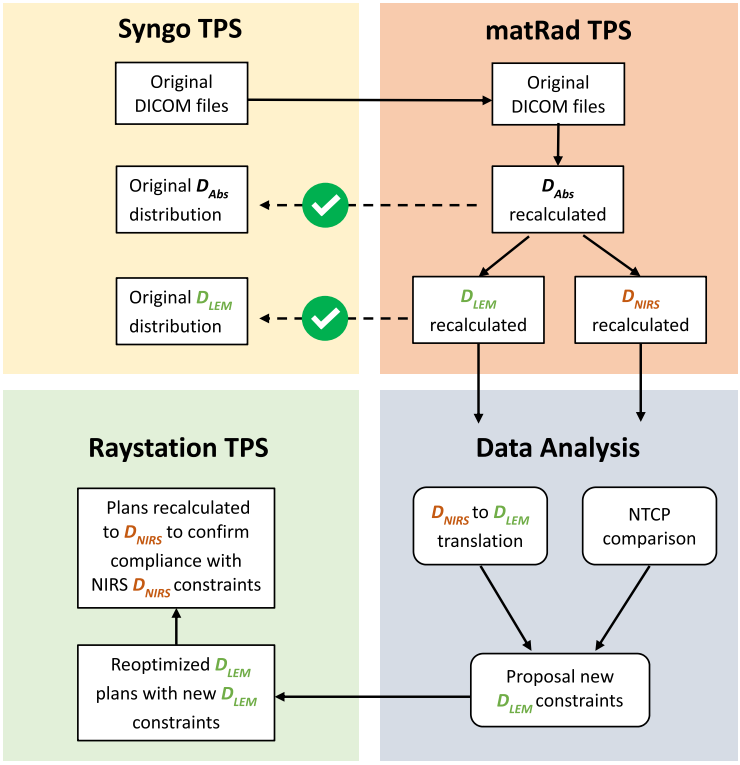

Fig. A1. Process of recalculation of RBE-weighted dose and proposal of new CNAO constraints. DICOM files from the original treatment plans were imported to the matRad TPS. The absorbed dose (D_{Abs}) and RBE-weighted dose distributions (D_{LEM} and D_{NIRS}) were recalculated. Correct reproduction of D_{Abs} and D_{LEM} compared to the original plans was confirmed. The recalculated D_{LEM} and D_{NIRS} were used for data analysis, in which new D_{LEM} constraints were proposed. Treatment plans were reoptimized with D_{LEM} in the RayStation TPS applying the new D_{LEM} constraints. Subsequently, these new plans were recalculated to D_{NIRS} to confirm that the plans still complied with the original NIRS constraints.

References

[1] Hasegawa A et al. Outcomes of visual acuity in carbon ion radiotherapy: analysis of dose-volume histograms and prognostic factors. Int J Radiat Oncol Biol Phys 2006;64:396–401.
[2] Kanai T et al. Biophysical characteristics of HIMAC clinical irradiation system for heavy-ion radiation therapy. Int J Radiat Oncol Biol Phys 1999;44:201–10.
[3] Kanai T et al. Irradiation of mixed beam and design of spread-out Bragg peak for heavy-ion radiotherapy. Radiat Res 1997;147:78–85.
[4] Kramer M, Scholz M. Treatment planning for heavy-ion radiotherapy: calculation and optimization of biologically effective dose. Phys Med Biol 2000;45:3319–30.
[5] Scholz M et al. Computation of cell survival in heavy ion beams for therapy. Radiat Environ Biophys 1997;36:59–66.
[6] Magro G et al. The FLUKA Monte Carlo code coupled with the NIRS approach for clinical dose calculations in carbon ion therapy. Phys Med Biol 2017.
[7] Fossati P et al. Dose prescription in carbon ion radiotherapy: a planning study to compare NIRS and LEM approaches with a clinically-oriented strategy. Phys Med Biol 2012;57:7543–54.
[8] Molinelli S et al. Dose prescription in carbon ion radiotherapy: how to compare two different RBE-weighted dose calculation systems. Radiother Oncol 2016;120:307–12.
[9] Steinstrater O et al. Mapping of RBE-weighted doses between HIMAC- and LEM-based treatment planning systems for carbon ion therapy. Int J Radiat Oncol Biol Phys 2012;84:854–60.
[10] Rossi S. The National Centre for Oncological Hadrontherapy (CNAO): status and perspectives. Phys Med 2015;31:333–51.
[11] Mirandola A et al. Dosimetric commissioning and quality assurance of scanned ion beams at the Italian National Center for Oncological Hadrontherapy. Med Phys 2015;42:5287–300.
[12] Common Terminology Criteria for Adverse Events v4.03. 2010, National Cancer Institute: NIH publication; no. 90-5410.
[13] Dale JE et al. Risk of carotid blowout after reirradiation with particle therapy. Adv Radiat Oncol 2017;2:465–74.
[14] Fukahori M et al. Estimation of late rectal normal tissue complication probability parameters in carbon ion therapy for prostate cancer. Radiother Oncol 2016;118:136–40.
[15] Shirai K et al. Dose-volume histogram analysis of brainstem necrosis in head and neck tumors treated using carbon-ion radiotherapy. Radiother Oncol 2017;125:36–40.
[16] Musha A et al. Prediction of acute radiation mucositis using an oral mucosal dose surface model in carbon ion radiotherapy for head and neck tumors. PLoS ONE 2015;10:e0141734.
[17] Shinoto M et al. Dosimetric analysis of upper gastrointestinal ulcer after carbon-ion radiotherapy for pancreatic cancer. Radiother Oncol 2016;120:140–4.
[18] Yanagi T et al. Dose-volume histogram and dose-surface histogram analysis for skin reactions to carbon ion radiotherapy for bone and soft tissue sarcoma. Radiother Oncol 2010;95:60–5.
[19] Jakel O et al. Treatment planning for carbon ion radiotherapy in Germany: review of clinical trials and treatment planning studies. Radiother Oncol 2004;73:S86–91.
[20] Schulz-Ertner D et al. Effectiveness of carbon ion radiotherapy in the treatment of skull-base chordomas. Int J Radiat Oncol Biol Phys 2007;68:449–57.
[21] Nikoghosyan AV et al. Randomised trial of proton vs. carbon ion radiation therapy in patients with low and intermediate grade chondrosarcoma of the skull base, clinical phase III study. BMC Cancer 2010;10:606.
[22] Lambrecht M et al. Radiation dose constraints for organs at risk in neuro-oncology; the European Particle Therapy Network consensus. Radiother Oncol 2018;128:26–36.

III

frontiers in Oncology

ORIGINAL RESEARCH
published: 24 November 2020
doi: 10.3389/fonc.2020.531344

Brainstem NTCP and Dose Constraints for Carbon Ion RT—Application and Translation From Japanese to European RBE-Weighted Dose

Jon Espen Dale[1,2], Silvia Molinelli[3], Barbara Vischioni[3], Viviana Vitolo[3], Maria Bonora[3], Giuseppe Magro[3], Andrea Mairani[3,4], Azusa Hasegawa[3,5], Tatsuya Ohno[6], Olav Dahl[1], Francesca Valvo[3] and Piero Fossati[3,7]*

[1] Department of Clinical Science, Faculty of Medicine, University of Bergen, Bergen, Norway, [2] Department of Oncology and Medical Physics, Haukeland University Hospital, Bergen, Norway, [3] National Center of Oncological Hadrontherapy, Pavia, Italy, [4] Heidelberg Ion-Beam Therapy Center, Heidelberg, Germany, [5] Osaka Heavy Ion Therapy Center, Osaka, Japan, [6] Department of Radiation Oncology, Gunma University Graduate School of Medicine, Gunma, Japan, [7] MedAustron Ion Therapy Center, Wiener Neustadt, Austria

OPEN ACCESS

Edited by:
Ester Orlandi,
Instituto Nazionale dei Tumori (IRCSS), Italy

Reviewed by:
Naruhiro Matsufuji,
National Institutes for Quantum and Radiological Science and Technology, Japan
Xuanfeng Ding,
William Beaumont Hospital, United States

***Correspondence:**
Barbara Vischioni
barbara.vischioni@cnao.it

Specialty section:
This article was submitted to Radiation Oncology, a section of the journal Frontiers in Oncology

Received: 31 January 2020
Accepted: 04 September 2020
Published: 24 November 2020

Citation:
Dale JE, Molinelli S, Vischioni B, Vitolo V, Bonora M, Magro G, Mairani A, Hasegawa A, Ohno T, Dahl O, Valvo F and Fossati P (2020) Brainstem NTCP and Dose Constraints for Carbon Ion RT—Application and Translation From Japanese to European RBE-Weighted Dose. Front. Oncol. 10:531344. doi: 10.3389/fonc.2020.531344

Background and Purpose: The Italian *National Center of Oncological Hadrontherapy* (CNAO) has applied dose constraints for carbon ion RT (CIRT) as defined by Japan's *National Institute of Radiological Sciences* (NIRS). However, these institutions use different models to predict the *relative biological effectiveness* (RBE). CNAO applies the *Local Effect Model I* (LEM I), which in most clinical situations predicts higher RBE than NIRS's *Microdosimetric Kinetic Model* (MKM). Equal constraints therefore become more restrictive at CNAO. Tolerance doses for the brainstem have not been validated for LEM I-weighted dose ($D_{\text{LEM I}}$). However, brainstem constraints and a *Normal Tissue Complication Probability* (NTCP) model were recently reported for MKM-weighted dose (D_{MKM}), showing that a constraint relaxation to $D_{\text{MKM}|0.7\ \text{cm}^3}$ <30 Gy (RBE) and $D_{\text{MKM}|0.1\ \text{cm}^3}$ <40 Gy (RBE) was feasible. The aim of this work was to evaluate the brainstem NTCP associated with CNAO's current clinical practice and to propose new brainstem constraints for LEM I-optimized CIRT at CNAO.

Material and Methods: We reproduced the absorbed dose of 30 representative patient treatment plans from CNAO. Subsequently, we calculated both $D_{\text{LEM I}}$ and D_{MKM}, and the relationship between D_{MKM} and $D_{\text{LEM I}}$ for various brainstem dose metrics was analyzed. Furthermore, the NTCP model developed for D_{MKM} was applied to estimate the NTCPs of the delivered plans.

Results: The translation of CNAO treatment plans to D_{MKM} confirmed that the former CNAO constraints were conservative compared with D_{MKM} constraints. Estimated NTCPs

were 0% for all but one case, in which the NTCP was 2%. The relationship $D_{MKM}/D_{LEM\ I}$ could be described by a quadratic regression model which revealed that the validated D_{MKM} constraints corresponded to $D_{LEM\ I|0.7\ cm^3}$ <41 Gy (RBE) (95% CI, 38–44 Gy (RBE)) and $D_{LEM\ I|0.1\ cm^3}$ <49 Gy (RBE) (95% CI, 46–52 Gy (RBE)).

Conclusion: Our study demonstrates that RBE-weighted dose translation is of crucial importance in order to exchange experience and thus harmonize CIRT treatments globally. To mitigate uncertainties involved, we propose to use the lower bound of the 95% CI of the translation estimates, *i.e.*, $D_{LEM\ I|0.7\ cm^3}$ <38 Gy (RBE) and $D_{LEM\ I|0.1\ cm^3}$ <46 Gy (RBE) as brainstem dose constraints for 16 fraction CIRT treatments optimized with LEM I.

Keywords: carbon ion radiotherapy, normal tissue complication probability, dose constraints, local effect model, microdosimetric kinetic model, relative biological effectiveness (RBE), brainstem tolerance

INTRODUCTION

There is an increasing interest in using carbon ion radiotherapy (CIRT) for the treatment of advanced, radioresistant tumors. The physical properties of CIRT allow for delivering a high dose to the tumor, while the finite distal depth dose and sharp lateral penumbra can be utilized to spare nearby organs at risk (OARs) from excessive dose. Furthermore, carbon ions exhibit high linear energy transfer (LET) properties, which lead to more efficient cell killing (higher relative biological effectiveness (RBE)), compared with photon and proton RT. However, there are substantial uncertainties regarding the clinical RBE of carbon ions. Therefore, prescription doses, tolerance doses to OARs, and normal tissue complication probability (NTCP) models based on experience with photon or proton RT may not be applicable to CIRT and should preferably be derived from CIRT data.

Two major approaches have been used for the clinical implementation of CIRT. Spearheaded by the National Institute of Radiological Sciences (NIRS), Chiba, Japan, the Japanese centers are using hypofractionated treatment schedules (16 fractions of 3.6–4.6 Gy (RBE)) in which prescription doses and OAR tolerance doses initially were defined through carefully conducted dose-escalation trials. Originally, the *mixed beam model* (1) was developed to predict the RBE of the passively scattered carbon ion beams with *tumor response* as the relevant endpoint. Later, with the implementation of scanned beam delivery, the *modified microdosimetric kinetic model* (MKM) (2–5) was introduced. Since these two models have been validated for consistency, they are hereby collectively abbreviated as MKM.

In contrast, CIRT at the Gesellschaft für Schwerionenforschung (GSI), Darmstadt, Germany, was initiated with moderately hypofractionated schedules (20–22 fractions of 3.0–3.5 Gy (RBE)) in which the *Local Effect Model Version I* (LEM I) (6, 7) was used to predict the RBE of CIRT for *late responding normal tissues* (*i.e.*, central nervous system tissue). Trusting the LEM I to be sufficiently accurate, dose constraints derived from photon RT could be applied for CIRT treatments. An additional assumption for this approach was that the linear quadratic (LQ) formalism was applicable also for CIRT.

When the *National Center of Oncological Hadrontherapy* (CNAO, Italy) (8) started treating patients with LEM I-optimized CIRT in 2012, the successful treatment approach developed at NIRS was adopted. However, comparative studies show that the LEM I predicts a 5–15% higher RBE in the spread out Bragg peak (SOBP) of a carbon ion beam, relative to the MKM (9, 10). In the entrance region, the RBE predicted by LEM I can be 60% higher (11). Consequently, dependent on the clinical indication, prescription doses at CNAO (reported in LEM I-weighted dose, $D_{LEM\ I}$) were increased 5–15% relative to the prescription doses at NIRS (reported in MKM-weighted dose (D_{MKM})) (9, 10). In contrast, dose constraints to OARs were not adjusted. This was a cautious approach mitigating various uncertainties related to the adaptation of NIRS prescription doses (*i.e.*, differences in RBE model, beam delivery method, dose optimization process, *etc.*).

For the brainstem, the dose constraint at CNAO was therefore set to be <30 Gy (RBE) to no more than 1% of the organ's volume ($D_{LEM\ I|1\%}$), following the tradition of NIRS (12). Since this constraint becomes more restrictive in LEM I-optimized CIRT, CNAO has so far treated more than 1,000 patients with advanced tumors in the head and neck region (for example, skull base, nasopharynx, and sinonasal sites) without experiencing any grade of radiation-induced brainstem injury. Thus, the constraint needs to be updated to provide optimal treatments in cases where the target volume is located close to the brainstem. However, it is challenging to propose new and reasonable constraints since no toxic events have been reported from any institution applying LEM I-weighted doses for CIRT.

Recently, a dose-response analysis of brainstem toxicity following D_{MKM}-optimized CIRT at *Gunma University Heavy Ion Medical Center* (GHMC) (13) was published by Shirai et al. (14). None of the 85 patients included in this analysis experienced symptomatic brainstem toxicity. However, four cases of focal brainstem contrast enhancement were detected on routine magnetic resonance imaging (MRI) during follow-up. This was defined as central nervous system (CNS) necrosis grade 1 events according to the *Common Terminology Criteria for Adverse Events version 4.0* (CTCAE). Even these asymptomatic

events did not occur before the maximum dose ($D_{MKM|max}$) exceeded 48 Gy (RBE), showing that current constraint may be conservative even when applied for D_{MKM}. The brainstem volume receiving more than 30 Gy (RBE) ($V_{30\ Gy\ (RBE)}$) and 40 Gy (RBE) ($V_{40\ Gy\ (RBE)}$) were independent risk factors for this endpoint. Brainstem toxicity of any grade did not occur before $V_{30\ Gy\ (RBE)}$ exceeded 0.7 cm^3 and $V_{40\ Gy\ (RBE)}$ exceeded 0.1 cm^3. Since these values relate to radiologically detectable, but asymptomatic alterations in the brainstem, they may serve as constraints to avoid symptomatic injury. Shirai et al. also fitted their data to the Lyman-Kutcher-Burman (LKB) NTCP model (15–17), resulting in the following model parameters: volume-effect parameter (n) = 0.08, biodiversity parameter (m) = 0.08, and the *equivalent uniform dose* (EUD) corresponding to 50% probability of toxicity (TD50) = 32.4 Gy (RBE).

The goal of this work is therefore to:

1. evaluate the brainstem NTCP associated with CNAOs current clinical practice by applying the NTCP model published by Shirai et al.
2. convert the D_{MKM} validated constraints into $D_{LEM\ I}$, providing guidance for the proposal of new dose constraints to be used at CNAO and other centers applying LEM I.

MATERIAL AND METHODS

Treatment Plan Selection and CIRT at CNAO

The dose distributions of 30 CIRT treatments with target volumes close to the brainstem were included in this study. Details on disease site, histology, and prescription dose are presented in **Table 1**. The treatments were given at CNAO in the period 2013–2014 as part of prospective protocols (CNAO S9/2012/C, CNAO S12/2012/C, and CNAO S15/2012/C) approved by the Regional Ethics Committee. Signed consent was required for participation. The plans were optimized for a prescribed $D_{LEM\ I}$ of 68.8–76.8 Gy (RBE) in 16 fractions (4 fractions/week) using the *syngo*® RT Planning (Siemens Healthcare, Erlangen, Germany) treatment planning system (TPS). Dose constraint for the brainstem was $D_{LEM\ I|1\%} \leq 30$ Gy (RBE). Additionally, a constraint of $D_{LEM\ I|1\%} \leq 35$ Gy (RBE) was applied to a 3-mm planning OAR volume (PRV) for plan optimization purposes.

In general, the strategy to obtain a robust treatment plan is similar at CNAO and GHMC: Multiple beam angles (3 to 4), dominantly originating from the horizontally fixed beam line, are achieved by couch rotation and/or by multiple immobilization positions where the patient's head is positioned either straight or

TABLE 1 | Disease and treatment characteristics.

Case nr.	Histology	Site	Total $D_{LEM\ I}$ (Gy (RBE))	Fraction $D_{LEM\ I}$ (Gy (RBE))
1	Chordoma	Skull base	70.4	4.4
2	Mesenchymal tumor	Frontal sinus	76.8	4.8
3	Chordoma	Skull base	70.4	4.4
4	Chordoma	Skull base	70.4	4.4
5	MPNST	Clivus	76.8	4.8
6	Chordoma	Skull base	70.4	4.4
7	ACC	Meckel's cave	68.8	4.3
8	Chondrosarcoma	Nasal cavity	70.4	4.4
9	Chordoma	Clivus	70.4	4.4
10	Chordoma	Clivus	70.4	4.4
11	Chordoma	Clivus	70.4	4.4
12	ACC	Maxillary sinus	68.8	4.3
13	Chordoma	Clivus	70.4	4.4
14	Chordoma	Clivus	70.4	4.4
15	Chondrosarcoma	Clivus	70.4	4.4
16	Chordoma	Skull base	70.4	4.4
17	ACC	Maxillary sinus	68.8	4.3
18	ACC	Nasopharynx	68,8	4,3
19	Chordoma	Clivus	70.4	4.4
20	Chondrosarcoma	Skull base	70.4	4.4
21	Cordoma	Clivus	70.4	4.4
22	ACC	Maxillary sinus	68.8	4.3
23	ACC	Skull base	68.8	4.3
24	Chordoma	Clivus	70.4	4.4
25	Pleomorphic sarcoma	Clivus	76.8	4.8
26	ACC	Paranasal sinuses	68.8	4.3
27	Chordoma	Clivus	70.4	4.4
28	Acinar cell carcinoma	Ethmoid/nasal cavity	68.8	4.3
29	ACC	Maxillary sinus	68.8	4.3
30	Chordoma	Clivus	70.4	4.4

MPNST, Malignant peripheral nerve sheath tumor; ACC, Adenoid cystic carcinoma.

rotated. Due to particle range uncertainty, beam angles are chosen so that most of the dose to the brainstem originates from the beam's sharp lateral penumbra, rather than the distal dose fall-off. Beams traversing through the brainstem are never used.

Recalculation of RBE-Weighted Dose Distributions

The patients' computed tomography (CT) image files, structure set files, dose files, and plan files were exported from the *syngo*® TPS and imported to the *matRad* open source multimodality radiation TPS (https://e0404.github.io/matRad/) (18) in which the absorbed dose (D_{Abs}) and $D_{\mathrm{LEM\ I}}$ were reproduced. The input parameters used clinically for LEM I were applied, *i.e.*, $\alpha_\gamma = 0.1\ \mathrm{Gy}^{-1}$, $\beta_\gamma = 0.05\ \mathrm{Gy}^{-2}$, $D_t = 30$ Gy, $s_{\max} = 3.1\ \mathrm{Gy}^{-1}$, $R_n = 5$ µm (7). The DVHs of targets and OARs were compared with the corresponding DVHs of the dose distribution from the *syngo*® TPS to ensure correct reproduction of both D_{Abs} and $D_{\mathrm{LEM\ I}}$ (results not reported). Secondly, MKM was implemented in the matRad TPS code using the input parameters used clinically ($R_d = 0.32$ µm, $R_n = 3.9$ µm, $\alpha_0 = 0.172\ \mathrm{Gy}^{-1}$, $\beta = 0.0615\ \mathrm{Gy}^{-2}$, $\alpha_r = 0.764\ \mathrm{Gy}^{-1}$, $F_{\mathrm{Clin}} = 2.39$) (2, 11) and D_{MKM} was derived from the exact same absorbed dose and LET spectra. This enabled a direct comparison of each patient's $D_{\mathrm{LEM\ I}}$ and D_{MKM} based exclusively on the differences in the RBE modeling.

Estimation of Brainstem NTCP

Using the D_{MKM} distributions, the brainstem NTCP for each treatment plan was calculated by the LKB method, using the model parameters suggested by Shirai et al. (14): $n = 0.08$, $m = 0.08$, and TD50 = 32.4 Gy (RBE).

RBE-Weighted Dose Translation

For each brainstem, the $D_{\mathrm{MKM|0.7\ cm^3}}$ and $D_{\mathrm{MKM|0.1\ cm^3}}$ were plotted as a function of $D_{\mathrm{LEM\ I|0.7\ cm^3}}$ and $D_{\mathrm{LEM\ I|0.1\ cm^3}}$, respectively. A curve fitting procedure was performed with the software IBM SPSS Statistics for Windows, version 24.0 (IBM Corp., Armonk, NY, U.S.A.) in order to produce a dose translation model.

Verification of Dose Translation Model

As a last step, we wanted to verify that the dose translation model correctly predicted the $D_{\mathrm{LEM\ I}}/D_{\mathrm{MKM}}$ relationship also for higher brainstem doses than our original data. Therefore, five treatment plans, in which the original $D_{\mathrm{LEM\ I}}$ constraint caused suboptimal dose coverage to the clinical target volume (CTV $D_{95\%}$ <95% of prescription dose), were reoptimized applying a new set of $D_{\mathrm{LEM\ I}}$ constraints as proposed by this work (see "**RESULTS**"). Subsequently, these new plans were recalculated to D_{MKM}. These procedures, which were conducted exclusively to confirm the relationship of the RBE models, were performed with the RayStation® 6.99 TPS (RaySearch Laboratories AB, Stockholm, Sweden), where both the LEM I and MKM were implemented with the respective model input parameters as mentioned earlier.

RESULTS

Brainstem DVHs in relative and absolute volumes are presented in both $D_{\mathrm{LEM\ I}}$ and D_{MKM} in **Figure 1**, showing the substantial decrease in RBE-weighted doses when the MKM is applied as RBE model.

The median brainstem $D_{\mathrm{LEM\ I|1\%}}$ was 23.7 Gy (range, 11.2–31.3 (RBE)), which corresponded to only 12.4 Gy (range, 5.5–21.8 (RBE)) in D_{MKM}, highlighting the restraining effect of the original CNAO constraint in achieving optimal CIRT treatments.

Only four of the brainstems received D_{MKM} >30 Gy (RBE), each of them to a volume smaller than 0.05 cm^3. As seen in **Figures 1B, D**, the highest $D_{\mathrm{LEM\ I}}$ to the brainstem volumes 0.7 and 0.1 cm^3 were 29 Gy (RBE) and 35 Gy (RBE), respectively, corresponding to 17 Gy (RBE) and 25 Gy (RBE) in D_{MKM}. These modest doses resulted in a very low probability of asymptomatic (grade 1) brainstem injury according to the NTCP model published by Shirai et al. (14): One patient had an NTCP of 2%, while the NTCPs of the remaining 29 patients were close to 0%, see **Figure 2**.

For each patient, the brainstem dose metrics $D_{\mathrm{LEM\ I|0.7\ cm^3}}$ and $D_{\mathrm{LEM\ I|0.1\ cm^3}}$ were plotted against the corresponding dose metric in D_{MKM} (**Figure 3**). With the assumption that the intercept should be at origin ($D_{\mathrm{LEM}} = 0$ Gy (RBE) when $D_{\mathrm{MKM}} = 0$ Gy (RBE)), we found that the quadratic regression model

$$D_{MKM} = (b1 \times D_{LEM\ \ I}) + (b2 \times [D_{LEM\ \ I}]^2)$$

adequately fit both sets of data (coefficients of determination, $R^2 \geq 0.918$). Extrapolation of the models to the relevant dose levels revealed that a $D_{\mathrm{MKM|0.7\ cm^3}}$ of 30 Gy (RBE) and a $D_{\mathrm{MKM|0.1\ cm^3}}$ of 40 Gy (RBE) translates into a $D_{\mathrm{LEM\ I|0.7\ cm^3}}$ of 41 Gy (RBE) (95% CI, 38–44 Gy (RBE)) and a $D_{\mathrm{LEM\ I|0.1\ cm^3}}$ of 49 Gy (RBE) (95% CI, 46–52 Gy (RBE)), respectively.

Subsequently, we reoptimized five of the treatment plans in which the old brainstem constraint ($D_{\mathrm{LEM\ I|1\%}}$ <30 Gy (RBE)) caused suboptimal CTV dose coverage. For the reoptimization, new brainstem constraints within the lower half of the 95% CI of the dose translation estimates were applied, *i.e.*, $D_{\mathrm{LEM\ I|0.7\ cm^3}}$ <38–41 Gy (RBE) and $D_{\mathrm{LEM\ I|\ cm^3}}$ <46–49 Gy (RBE). The relationship of $D_{\mathrm{LEM\ I}}$ to D_{MKM} for the dose metrics $D_{0.7\ \mathrm{cm^3}}$ and $D_{0.1\ \mathrm{cm^3}}$ from the reoptimized plans are plotted as open circles in the scatterplots of **Figure 3**. As can be seen, the values of these data pairs agree with the prediction of the dose translation model. To demonstrate the potential clinical impact of relaxing the constraints, a comparison of the original and reoptimized plans, displayed in both $D_{\mathrm{LEM\ I}}$ and $D_{\mathrm{MKM,}}$ is presented in **Figure 4**. For this patient, the proportion of the CTV receiving >95% of the prescription dose increased from 74 to 95%.

DISCUSSION

For the implementation of CIRT at CNAO, the goal has been to replicate the successful results achieved at Japanese CIRT centers, by translating NIRS prescription doses into

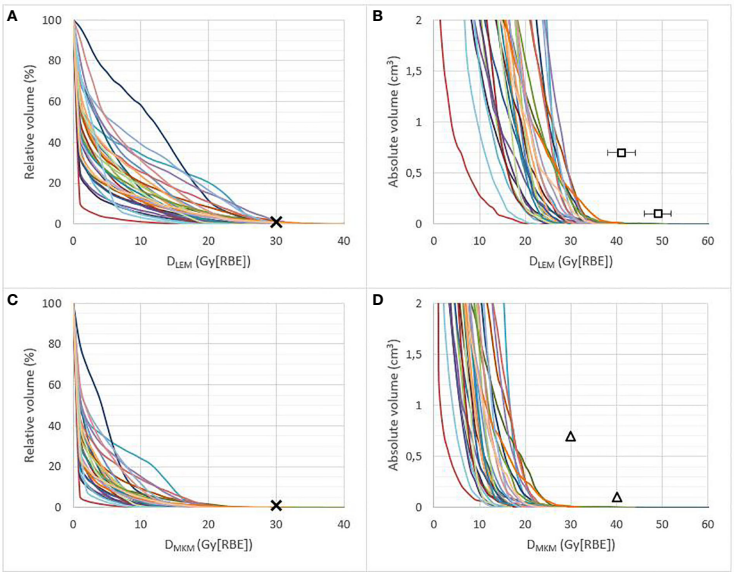

FIGURE 1 | Brainstem DVHs in relative **(A, C)** and absolute volume (≤2 cm^3) **(B, D)** of 30 patients treated at CNAO, presented in $D_{LEM\ I}$ **(A, B)** and D_{MKM} **(C**, **D)**. Crosses represent the former CNAO and NIRS dose constraint of $D_{1\%}$ ≤30 Gy (RBE). Triangles represent the new D_{MKM} constraints $V_{40\ Gy\ (RBE)}$ <0.1 cm^3 and $V_{30\ Gy\ (RBE)}$ <0.7 cm^3 as defined by Shirai et al. (14). Squares in **(B)** represent the possible new $D_{LEM\ I}$ constraints (error bars, 95% CI) resulting from the dose translation model presented in this work, see **Figure 3**.

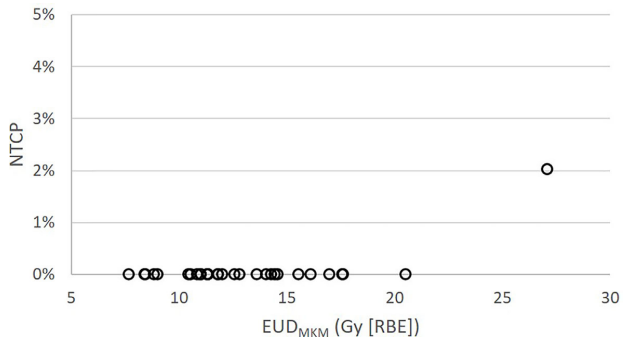

FIGURE 2 | Brainstem NTCP for the 30 patients treated at CNAO as function of EUD_{MKM} according to the NTCP model published by Shirai et al. (14).

equiefficient doses within the LEM I dose prescription system (9, 10). However, initially the OAR dose constraints were not adjusted correspondingly. This study clearly shows that the original brainstem dose constraint applied at CNAO is too conservative compared with the clinical practice in Japanese centers. In a recent publication on skull base chordomas treated at CNAO, Iannalfi et al. found that 92% of the local recurrences were attributable to suboptimal target dose in regions close to the brainstem or optic pathways (19). The estimated 5-year local control (LC) rate was 71%. This is inferior to the results reported by Japanese centers, where 5-year LC rates within the range 76–92% have been reported (20, 21).

Consequently, updated constraints for LEM I-optimized CIRT are urgently needed. In our opinion, due to the lack of publications

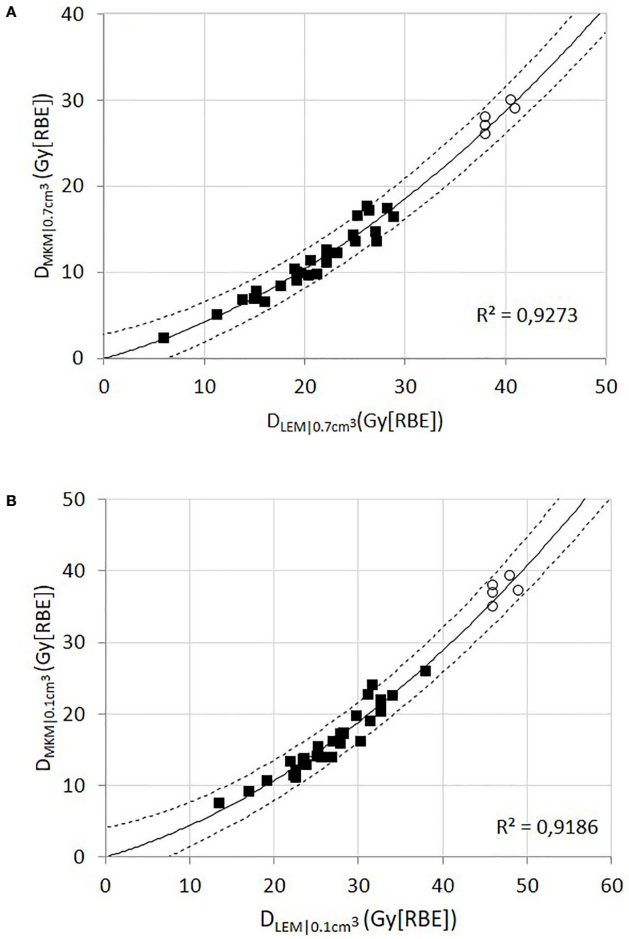

FIGURE 3 | Black squares represent the relationship of $D_{LEM\ I}$ to D_{MKM} for the dose metrics $D_{0.7\ cm^3}$ **(A)** and $D_{0.1\ cm^3}$ **(B)** for each individual brainstem. The solid line represents the quadratic function providing the best fit to the data points (black squares), assuming that the intercept should be in the origin. The dashed lines represent the 95% CI. The open circles represent the data collected from the reoptimized plans; these data points were not used for the curve fitting procedure.

addressing brainstem NTCP for LEM I-optimized CIRT, this aim was only achievable by making use of D_{MKM}-validated dose constraints. Relating the CNAO DVHs to the new D_{MKM} constraints defined by Shirai et al. (**Figure 1D**) suggests that doses to the brainstem volumes 0.7 and 0.1 cm^3 potentially could be increased by 13 Gy (RBE) and 15 Gy (RBE) in D_{MKM}, respectively, compared with the former practice at CNAO. According to our dose constraint translation, the corresponding increase in $D_{LEM\ I}$ would be approximately 12 Gy (RBE) (95% CI, 9–15 Gy (RBE)) and 14 Gy (RBE) (95% CI, 11–17 Gy (RBE)). This unveils an opportunity for improved target dose coverage, and thus improved treatment outcome, as demonstrated in **Figure 4**.

Recently, the European Particle Therapy Network (EPTN) released a consensus paper for dose constraints to various OARs (22), suggesting a general constraint of $D_{0.03\ cm^3} \leq 54$ Gy (RBE) to the brainstem, with an option to allow for $D_{0.03\ cm^3} \leq 60$ Gy (RBE) to the brainstem surface. Both constraints were expressed in *equivalent dose in 2 Gy fractions* (EQD2), with an assumed α/β ratio of 2 Gy. These guidelines are based on photon and proton RT toxicity data and are not necessarily applicable for CIRT due

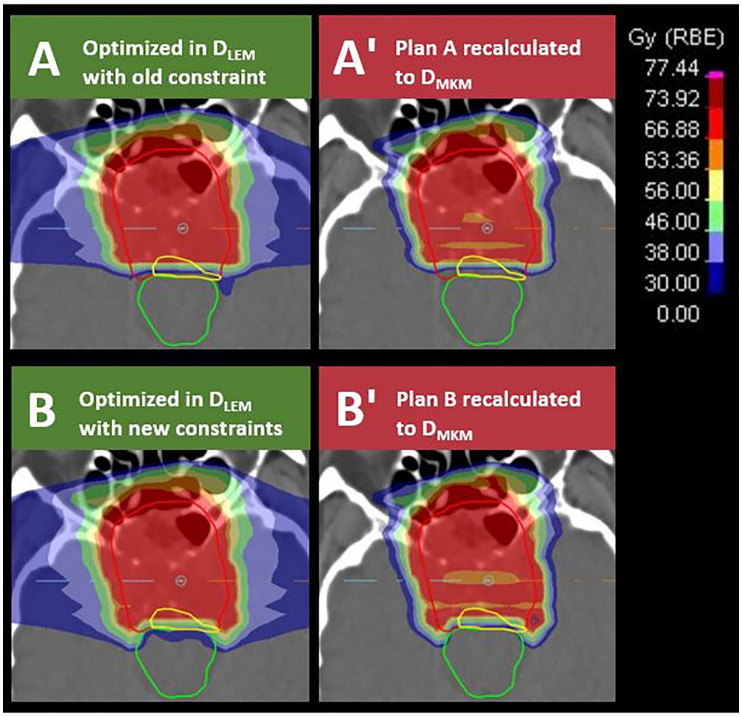

FIGURE 4 | Transversal sections of $D_{LEM\ I}$-optimized treatment plans applying brainstem (green contour) constraints of $D_{LEM\ I|1\%}$ <30 Gy (RBE) in plan **(A)** or $D_{LEM\ I|0.7\ cm^3}$ <38 Gy (RBE) and $D_{LEM|0.1\ cm^3}$ <46 Gy (RBE) in plan **B)**. The dose constraint levels are illustrated by dark blue, light blue, and light green isodose, respectively. Plans were subsequently recalculated to D_{MKM} **(A′, B′)**. Red isodose in plan **(A, B)** represents 95% of the target dose (70.4 Gy (RBE) in $D_{LEM\ I}$). Note the improved dose coverage to the CTV (red contour) and to the part of the CTV in which the tumor recurred (yellow contour) in plan B compared with plan A. Dose to the brainstem remains compliant with the constraints defined by Shirai et al. when evaluated in D_{MKM} **(B′)**.

to the larger uncertainties involved in the prediction of the RBE. However, similar constraints are used for CIRT at the *Heidelberg Ion Beam Therapy Center* (HIT) in Germany (23), building on previous clinical experience of the GSI. Various publications from this institution explicitly report an absence of brainstem toxicity (24, 25). Consequently, these constraints are considered safe for CIRT under HIT's current treatment paradigm, which consists of 20–22 fractions of 3.0–3.5 Gy (RBE) and 5–7 fractions per week. Although HIT also applies LEM I, these constraints may not be safely transferred to the 16 fraction/4 fractions per week treatment schedule of CNAO, as EQD2 conversion may not be sufficiently precise when fraction doses increase, due to uncertainties in the prediction of RBE.

That being said, it is interesting to observe that our translated constraints, when converted into EQD2, relate closely to the EQD2 constraints used in clinical practice at HIT (23), see **Figure 5**.

In 2010, as part of the *Quantitative Analysis of Normal Tissue Effects in the Clinic* (QUANTEC) effort, brainstem constraints and tolerance doses following photon and proton RT were summarized in Figure 1 in the organ-specific paper by Mayo et al. (26). Making use of the LQ model, tolerance doses from either normofractionated treatments or single fractionation stereotactic treatments were extrapolated to provide an approximation for the tolerance dose for hypofractionated treatments. The figure is reused in **Figure 6** of this paper, in which the $D_{LEM\ I|0.1\ cm^3}$ constraint we derived from this work has been superimposed as a red circle. Clearly, our constraint complies with the projections of the LQ model, supporting the capacity of the LEM I to predict the RBE of CIRT for this endpoint with sufficient accuracy.

An advantage of our dose translation approach is that the fractionation regimen at GHMC is similar to that of CNAO, and therefore the uncertainty related to EQD2 conversion can be avoided. Furthermore, both GHMC and CNAO have adopted the traditions of NIRS, in regard to the choice of beam number, angles, and strategies to achieve a robust treatment plan. Lastly, both centers are restricted to the use of fixed beam lines,

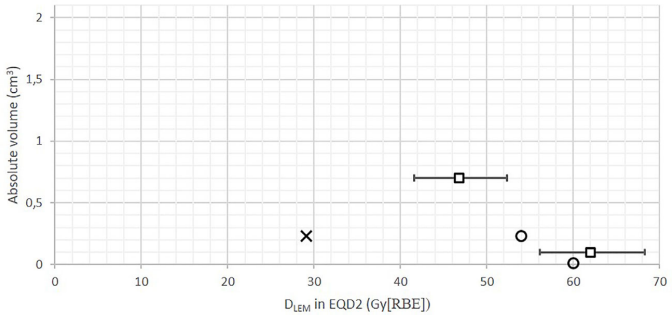

FIGURE 5 | Absolute volume DVH showing old CNAO $D_{\text{LEM I|1\%}}$ <30 Gy (RBE) constraint (cross) and the translated Shirai constraints $D_{\text{LEM I|0.7 cm}^3}$ <41 Gy (RBE) and $D_{\text{LEM I|0.1 cm}^3}$ <49 Gy (RBE) (squares, error bars = 95% CI), converted into EQD2 (assuming α/β ratio = 2 Gy) in comparison with the EQD2 constraints applied at HIT as reported by Nikoghosyan et al. (21): $D_{\text{LEM I|1\%}}$ <54 Gy (RBE) and $D_{\text{LEM I|max}}$ <60 Gy (RBE) (circles). As an approximation to the absolute volume relating to the $D_{1\%}$ constraints, the median brainstem volume in our data set (26 cm^3) was used. The translated constraints are more closely related to the constraints used at HIT than the old CNAO constraint.

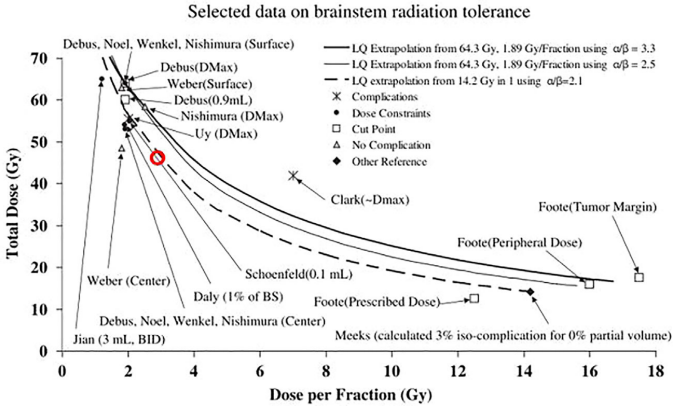

FIGURE 6 | Figure 1 from Mayo et al. (23) reprinted with permission, comparing selected data on brainstem tolerance and dose constraints from stereotactic RT or normofractionated photon or proton RT, compared with the linear quadratic (LQ) model extrapolations. Data points are marked with the corresponding author and dose parameter considered in parenthesis. The $D_{\text{LEM I|0.1 cm}^3}$ <46 Gy (RBE) constraint for a 16-fraction LEM I-optimized CIRT, estimated by dose translation of the corresponding D_{MKM} constraint is superimposed as a red circle on the original figure.

whichinevitably restricts the freedom of beam angles and consequently favors harmonization of the treatments at the two centers additionally.

However, our method is affected by unavoidable uncertainties. Firstly, transferring dose constraints from a center with passive scattering beam delivery (PS) to a center with pencil beam scanning (PBS) may be controversial. The beam delivery techniques will inevitably cause differences in the radiation quality (mixture of primary and secondary particles and their corresponding LET values) of the beams, and the distribution and weighting of Bragg peaks may be very dissimilar. However, two studies have confirmed that the biological effect of the carbon ion beams of NIRS, HIT, and CNAO are identical (27, 28).

Secondly, the D_{Abs} underlying the RBE-weighted dose is calculated by different beam models at the two institutions. It has been shown that the D_{Abs} of a given RBE-weighted dose could on average vary about 2.5% in the *target region* of head and neck treatments, depending on the beam model (9). Differences related to beam modeling in the *out-of-target* areas have not been investigated, but one would expect to find more profound deviations in D_{Abs} especially within the lateral penumbra dose fall-off. This region is certainly sensitive to how the lateral spread

of the beam is modeled. This is of importance, since the sharp lateral penumbra of the carbon ion beam typically is utilized to avoid high doses to the brainstem when it is located close to the tumor.

To conclude, these latter issues infer that the D_{MKM} that we reproduce in this work, based on the D_{Abs} of CNAO $D_{LEM\ I}$-optimized treatment plans, are not an exact replica of GHMC treatment plans. Nevertheless, our dose translation approach definitely provides guidance as to how much the $D_{LEM\ I}$ constraints at CNAO may be relaxed in order to match the Japanese constraints. As a measure of caution, we propose the lower bound of the 95% CI of the dose translation estimates, *i.e.*, $D_{LEM\ I|0.7\ cm^3}$ <38 Gy (RBE) and $D_{LEM\ I|0.1\ cm^3}$ <46 Gy (RBE), as possible brainstem constraints for LEM I-optimized CIRT in a 16-fraction schedule. These proposed constraint values imply $D_{LEM\ I}$/D_{MKM} conversion factors of 1.27 and 1.15 for D_{MKM} fraction doses of 1.88 Gy (RBE) and 2.5 Gy (RBE) respectively, which is quite modest compared with the target dose conversion factors found by Steinsträter et al. (29), where conversion factors for the respective fraction doses were found to be >1.44 and >1.21.

Finally, as our conclusions rely on the results of Shirai et al., the limitations described in their study also apply to our work (small number of events, single institution study, *etc.*). Another essential assumption for the application of these constraints is that asymptomatic MRI contrast enhancement does not necessarily evolve into necrosis and therefore constraints that safeguard against this event most certainly will prevent the more meaningful clinical endpoint. Mere contrast enhancement is regarded as evidence of increased permeability of the blood-brain barrier (BBB), which results from radiation-induced alterations in endothelial and glial cell function (30). However, increased permeability does not necessarily lead to parenchymal damage as demonstrated for the spinal cord in a rat model (31). This phenomenon has also been documented for radiation-induced injury of the brain following CIRT, and it is hypothesized that since smaller volumes of CNS tissue is irradiated by particle therapy in comparison with photon RT, the probability of recovery will be higher (32). The observation that the lesions reported by Shirai et al. were reversible or stable in the absence of therapeutic intervention further supports the argument that no real necrosis had occurred.

In this setting, applying the CTCAE term *CNS necrosis grade 1* when only contrast enhancement is evident, as done by Shirai et al., may be confusing and potentially discourage physicians from referring patients to CIRT. However, the CTCAE lacks a proper predefined term to discriminate increased permeability in the BBB from a necrotic process. Moreover, neither the *SOMA-LENT scale* (subterm *MRI* in the *Analytic* scale) (33) nor the *RTOG/EORTC Late Morbidity Scoring Schema* (subterm *Brain*) (34) exhibit sufficient granularity to encompass this distinction. We therefore suggest to apply the CTCAE term *Nervous system disorders—Other*, and specifying it as *Brainstem reaction* as an analogy to the *Temporal lobe reaction* term coined by Gilman et al. (35), in which contrast enhancement would be a grade 1 "reaction," thus avoiding the use of the misleading and more distressing term "necrosis."

CONCLUSIONS

Based on this work, these new constraints, $D_{LEM\ I|0.7\ cm^3}$ <38 Gy (RBE) and $D_{LEM\ I|0.1\ cm^3}$ <46 Gy (RBE), have been implemented in the prospective treatment protocols of CNAO since October 2018. They can serve as constraints also for other centers applying LEM I within CIRT schedules of 16 fractions. Indeed, these constraints have also been selected as the most optimal constraints available and have therefore recently been implemented in clinical practice at the MedAustron Ion Therapy Center (Wiener-Neustadt, Austria) for 16 fractions of CIRT treatment of skull base tumors optimized with LEM I.

This paper highlights a challenge that is unique for CIRT compared with other external beam RT modalities: the exchange of experience between Japanese and European CIRT facilities is severely hampered by the use of disparate RBE models. Fortunately, we anticipate that the recalculation of treatment plans to the alternative RBE model will become substantially less time consuming due to the introduction of such functionality in commercial TPSs. We therefore hope to see future CIRT publications reporting OAR toxicity, NTCP, and related dose metrics in both D_{MKM} and $D_{LEM\ I}$, as our group recently has done for the optic nerve (36). This would accelerate the much needed validation of OAR constraints for both RBE models.

DATA AVAILABILITY STATEMENT

The datasets generated for this study are available on request to the corresponding author.

ETHICS STATEMENT

The patients analyzed in the study cannot be identified as all the research has been conducted with anonymized data. All patients enrolled in the clinical trials at CNAO gave their free informed consent to the treatment and the use of their anonymized data for research purposes. The anonymized patient data used for this study originated from the clinical trials "CNAO S9/2012/C", "CNAO S12/2012/C" and "CNAO S15/2012/C" approved by the CNAO Ethics Committee.

AUTHORS CONTRIBUTIONS

The manuscript was mainly authored by JD with support from PF, SM, OD, TO, and BV. JD performed data analysis. Clinical treatment plans were optimized by medical physicists SM, GM, and AM with FV, MB, VV, BV, and PF as the responsible radiation oncologists. Clinical data were collected by VV, MB, BV, AH, and PF. JD, SM, and GM performed the recalculation of all treatment plans. FV, VV, and BV are

responsible for the treatment protocols and analyzed patient follow-up together with MB and PF. JD, SM, OD, AM, TO, AH, and PF contributed to the development of the study methodology. All authors critically reviewed the manuscript. All authors contributed to the article and approved the submitted version.

FUNDING

This work was supported by grants (grant no: BFS2015PAR02) from the Trond Mohn Foundation, Ytrebygdsvegen 215, Kokstad, Postboks 7150, 5020 BERGEN, Norway, tlf: +47 479 00 111, org.nr: 988 029 327.

REFERENCES

1. Kanai T, Endo M, Minohara S, Miyahara N, Koyama-ito H, Tomura H, et al. Biophysical characteristics of HIMAC clinical irradiation system for heavy-ion radiation therapy. *Int J Radiat Oncol Biol Phys* (1999) 44(1):201–10. doi: 10.1016/S0360-3016(98)00544-6
2. Inaniwa T, Kanematsu N, Matsufuji N, Kanai T, Shirai T, Noda K, et al. Reformulation of a clinical-dose system for carbon-ion radiotherapy treatment planning at the National Institute of Radiological Sciences, Japan. *Phys Med Biol* (2015) 60(8):3271–86. doi: 10.1088/0031-9155/60/8/3271
3. Hawkins RB. A Microdosimetric-Kinetic Model for the Effect of Non-Poisson Distribution of Lethal Lesions on the Variation of RBE with LET. *J Radiat Res* (2003) 160(1):61–69, 9. doi: 10.1667/RR3010
4. Hawkins RB. A microdosimetric-kinetic model of cell death from exposure to ionizing radiation of any LET, with experimental and clinical applications. *Int J Radiat Biol* (1996) 69(6):739–55. doi: 10.1080/095530096145481
5. Hawkins RB. A statistical theory of cell killing by radiation of varying linear energy transfer. *Radiat Res* (1994) 140(3):366–74. doi: 10.2307/3579114
6. Scholz M, Kellerer MA, Kraft-Weyrather W, Kraft G. Computation of cell survival in heavy ion beams for therapy. *Radiat Environ Biophys* (1997) 36 (1):59–66. doi: 10.1007/s004110050055
7. Kramer M, Scholz M. Treatment planning for heavy-ion radiotherapy: calculation and optimization of biologically effective dose. *Phys Med Biol* (2000) 45(11):3319–30. doi: 10.1088/0031-9155/45/11/314
8. Rossi S. The National Centre for Oncological Hadrontherapy (CNAO): Status and perspectives. *Phys Med* (2015) 31(4):333–51. doi: 10.1016/j.ejmp.2015.03.001
9. Molinelli S, Magro G, Mairani A, Matsufuji N, Kanematsu N, Inaniwa T, et al. Dose prescription in carbon ion radiotherapy: How to compare two different RBE-weighted dose calculation systems. *Radiother Oncol* (2016) 120(2):307–12. doi: 10.1016/j.radonc.2016.05.031
10. Fossati P, Molinelli S, Matsufuji N, Ciocca M, Mirandola A, Mairani A, et al. Dose prescription in carbon ion radiotherapy: a planning study to compare NIRS and LEM approaches with a clinically-oriented strategy. *Phys Med Biol* (2012) 57(22):7543–54. doi: 10.1088/0031-9155/57/22/7543
11. Magro G, Dahle T, Molinelli S, Ciocca M, Fossati P, Ferrari A, et al. The FLUKA Monte Carlo code coupled with the NIRS approach for clinical dose calculations in carbon ion therapy. *Phys Med Biol* (2017) 62(9):3814–27. doi: 10.1088/1361-6560/aa642b
12. Koto M, Hasegawa A, Takagi R, Sasahara G, Ikawa H, Mizoe JE, et al. Feasibility of carbon ion radiotherapy for locally advanced sinonasal adenocarcinoma. *Radiother Oncol* (2014) 113(1):60–5. doi: 10.1016/j.radonc.2014.09.009
13. Ohno T, Kanai T, Yamada S, Yusa K, Tashiro M, Shimada H, et al. Carbon Ion Radiotherapy at the Gunma University Heavy Ion Medical Center: New Facility Set-up. *Cancers* (2011) 3(4):4046–60. doi: 10.3390/cancers3044046
14. Shirai K, Fukata K, Adachi A, Saitoh JI, Musha A, Abe T, et al. Dose-volume histogram analysis of brainstem necrosis in head and neck tumors treated using carbon-ion radiotherapy. *Radiother Oncol* (2017) 125(1):36–40. doi: 10.1016/j.radonc.2017.08.014
15. Lyman JT. Complication probability as assessed from dose-volume histograms. *Radiat Res Suppl* (1985) 8:S13–9. doi: 10.2307/3583506
16. Burman C, Kutcher GJ, Emami B, Goitein M. Fitting of normal tissue tolerance data to an analytic function. *Int J Radiat Oncol Biol Phys* (1991) 21(1):123–35. doi: 10.1016/0360-3016(91)90172-Z
17. Niemierko A. Reporting and analyzing dose distributions: a concept of equivalent uniform dose. *Med Phys* (1997) 24(1):103–10. doi: 10.1118/1.598063
18. Wieser H-P, Cisternas E, Wahl N, Ulrich S, Stadler A, Mescher H, et al. Development of the open-source dose calculation and optimization toolkit matRad. *Med Phys* (2017) 44(6):2556–68. doi: 10.1002/mp.12251
19. Iannalfi A, D'Ippolito E, Riva G, Molinelli S, Gandini S, Viselner G, et al. Proton and carbon ions radiotherapy in skull base chordomas: a prospective study based on a dual particle and a patient-customized treatment strategy. *Neuro Oncol* (2020) 22(9):1348–58. doi: 10.1093/neuonc/noaa067
20. Takagi M, Demizu Y, Nagano F, Terashima K, Fujii O, Jin D, et al. Treatment outcomes of proton or carbon ion therapy for skull base chordoma: a retrospective study. *Radiat Oncol* (2018) 13(1):232. doi: 10.1186/s13014-018-1173-0
21. Koto M, Ikawa H, Kaneko T, Hagiwara Y, Hayashi K, Tsuji H, et al. Long-term outcomes of skull base chordoma treated with high-dose carbon-ion radiotherapy. *Head Neck* (2020) 42(9):2607–13. doi: 10.1002/hed.26307
22. Lambrecht M, Eekers DBP, Alapetite C, Burnet NG, Calugaru V, Coremans IEM, et al. Radiation dose constraints for organs at risk in neuro-oncology; the European Particle Therapy Network consensus. *Radiother Oncol* (2018) 128 (1):26–36. doi: 10.1016/j.radonc.2018.05.001
23. Nikoghosyan AV, Karapanagiotou-Schenkel I, Munter MW, Jensen AD, Combs SE, Debus J, et al. Randomised trial of proton vs. carbon ion radiation therapy in patients with chordoma of the skull base, clinical phase III study HIT-1-Study. *BMC Cancer* (2010) 10:607. doi: 10.1186/1471-2407-10-606
24. Schulz-Ertner D, Karger CP, Feuerhake A, Nikoghosyan A, Combs SE, Jakel O, et al. Effectiveness of carbon ion radiotherapy in the treatment of skull-base chordomas. *Int J Radiat Oncol Biol Phys* (2007) 68(2):449–57. doi: 10.1016/j.ijrobp.2006.12.059
25. Uhl M, Mattke M, Welzel T, Oelmann J, Habl G, Jensen AD, et al. High control rate in patients with chondrosarcoma of the skull base after carbon ion therapy: first report of long-term results. *Cancer* (2014) 120(10):1579–85. doi: 10.1002/cncr.28606
26. Mayo C, Yorke E, Merchant TE. Radiation associated brainstem injury. *Int J Radiat Oncol Biol Phys* (2010) 76(3 Suppl):S36–41. doi: 10.1016/j.ijrobp.2009.08.078
27. Uzawa A, Ando K, Koike S, Furusawa Y, Matsumoto Y, Takai N, et al. Comparison of biological effectiveness of carbon-ion beams in Japan and Germany. *Int J Radiat Oncol Biol Phys* (2009) 73(5):1545–51. doi: 10.1016/j.ijrobp.2008.12.021
28. Facoetti A, Vischioni B, Ciocca M, Ferrarini M, Furusawa Y, Mairani A, et al. In vivo radiobiological assessment of the new clinical carbon ion beams at CNAO. *Radiat Prot Dosimetry* (2015) 166(1-4):379–82. doi: 10.1093/rpd/ncv145
29. Steinstrater O, Grun R, Scholz U, Friedrich T, Durante M, Scholz M, et al. Mapping of RBE-weighted doses between HIMAC- and LEM-Based treatment planning systems for carbon ion therapy. *Int J Radiat Oncol Biol Phys* (2012) 84(3):854–60. doi: 10.1016/j.ijrobp.2012.01.038
30. Yuan H, Gaber MW, Boyd K, Wilson CM, Kiani MF, Merchant TE, et al. Effects of fractionated radiation on the brain vasculature in a murine model: blood-brain barrier permeability, astrocyte proliferation, and ultrastructural changes. *Int J Radiat Oncol Biol Phys* (2006) 66(3):860–6. doi: 10.1016/j.ijrobp.2006.06.043
31. Siegal T, Pfeffer MR. Radiation-induced changes in the profile of spinal cord serotonin, prostaglandin synthesis, and vascular permeability. *Int J Radiat Oncol Biol Phys* (1995) 31(1):57–64. doi: 10.1016/0360-3016(94)E0305-4
32. Kishimoto R, Mizoe JE, Komatsu S, Kandatsu S, Obata T, Tsujii H, et al. MR imaging of brain injury induced by carbon ion radiotherapy for head and neck tumors. *Magn Reson Med Sci* (2005) 4(4):159–64. doi: 10.2463/mrms.4.159
33. LENT SOMA tables. *Radiother Oncol* (1995) 35(1):17–60. doi: 10.1016/0167-8140(95)90055-1
34. Cox JD, Stetz J, Pajak TF. Toxicity criteria of the Radiation Therapy Oncology Group (RTOG) and the European Organization for Research

and Treatment of Cancer (EORTC). *Int J Radiat Oncol Biol Phys* 1995 31 (5):1341–6.

35. Gillmann C, Lomax AJ, Weber DC, Jakel O, Karger CP. Dose-response curves for MRI-detected radiation-induced temporal lobe reactions in patients after proton and carbon ion therapy: Does the same RBE-weighted dose lead to the same biological effect? *Radiother Oncol* (2018) 128(1):109–14. doi: 10.1016/j.radonc.2018.01.018
36. Dale JE, Molinelli S, Vitolo V, Vischioni B, Bonora M, Magro G, et al. Optic nerve constraints for carbon ion RT at CNAO - Reporting and relating outcome to European and Japanese RBE. *Radiother Oncol* (2019) 140:175–81. doi: 10.1016/j.radonc.2019.06.028

Conflict of Interest: The authors declare that the research was conducted in the absence of any commercial or financial relationships that could be construed as a potential conflict of interest.

Errata for
Dose Constraints for important Organs at Risk in the Head and Neck Region for Carbon Ion Radiotherapy optimized with the Local Effect Model I (LEM I)

Jon Espen Dale

Thesis for the degree philosophiae doctor (PhD)
at the University of Bergen

15. 02. 2021

(date and sign. of candidate)

(date and sign. of faculty)

Errata

Page 4 Misspelling: “Hadrontherapay” – corrected to “Hadrontherapy”

Page 5 Misspelling: “reseach” – corrected to “research”

Page 5 Misspelling: “the the” – corrected to “the”

Page 5 Misspelling: “You” – corrected to “Your”

Page 5 Misspelling: “cantine” – corrected to “canteen”

Page 6 Misspelling: “colleauges” – corrected to “colleagues”

Page 8 Misspelling: “Quanititative” – corrected to “Quantitative”

Page 8 Misspelling: “Effectivness” – corrected to “Effectiveness”

Page 10 Consistency of language: “analysed” – corrected to “analyzed”

Page 16 Consistency of language: “tumours” – corrected to “tumors”

Page 16 Consistency of language: “tumour” – corrected to “tumor”

Page 17 Consistency of language: “tumour” – corrected to “tumor”

Page 17 Consistency of language: “tumours” – corrected to “tumors”

Page 21 Misspelling: “buildup” – corrected to “build-up”

Page 22 Misspelling: “becomming” – corrected to “becoming”

Page 23 Misspelling: “gray” – corrected to “Gray”

Page 26 (Figure 7) Misspelling: “plottet” – corrected to “plotted”

Page 27 Consistency of language: “tumours” – corrected to “tumors”

Page 28 Misspelling: “Thererfore” – corrected to “Therefore”

Page 28 Misspelling: “scheduels” – corrected to “schedules”

Page 29 Misspelling: “*Quanititative*” – corrected to “*Quantitative*”

Page 35 Consistency of language: “tumours” – corrected to “tumors”

Page 35 Consistency of language: “tumour” – corrected to “tumor”

Page 37 (Figure 14) Misspelling: “reponse” – corrected to “response”

Page 39 Incorrect figure citation: “Figure 4.1.” – corrected to “Figure 15”

Page 44 Consistency of language: "tumours" – corrected to "tumors"

Page 44 Consistency of language: "tumour" – corrected to "tumor"

Page 45 Incorrect figure citation: "Figure 6.1." – corrected to "Figure 18."

Page 46 Consistency of language: "favourable" – corrected to "favorable"

Page 51 Grammatical error: "have" – corrected to "has"

Page 51 Consistency of language: "tumour" – corrected to "tumor"

Page 55 Consistency of language: "tumour" – corrected to "tumor"

Page 55 Consistency of language: "tumours" – corrected to "tumors"

Page 55 Consistency of language: "haemorrhage" – corrected to "hemorrhage"

Page 60 Consistency of language: "tumour" – corrected to "tumor"

Page 60 Consistency of language: "haemorrhage" – corrected to "hemorrhage"

Page 62 Consistency of language: "tumours" – corrected to "tumors"

Page 63 Misspelling: "supressing" – corrected to "suppressing"

Page 68 Grammatical error: A misplaced comma deleted after sentence "….in order to produce a dose translation model."

Page 69 Consistency of language: "analysed" – corrected to "analyzed"

Page 75 (Table 6) Table 6 was incorrectly named "Table 1" – corrected.

Page 78 (Table 7) Misspelling: "Case nr." – corrected to "Case no."

Page 78 (Table 7) Misspelling: "Cordoma." – corrected to "Chordoma"

Page 80 Incorrect figure citation: "figure…." – corrected to "Figure 33b".

Page 85 Misspelling: "uncertaintites" – corrected to "uncertainties".

Page 85 Incorrect reference: "…see section 5.1.2." – corrected to "…see section 10.1.2."

Page 85 Misspelling: "totalt" – corrected to "total"

Page 85 Consistency of language: "analyse" corrected to "analyze"

Page 86 Consistency of language: "haemorrhage" – corrected to "hemorrhage"

Page 86 Consistency of language: "favourable" – corrected to "favorable"

Page 87 Undefined abbreviation: "reRT" – corrected to "the reirradiation"

Page 87 Consistency of language: "favourable" – corrected to "favorable"

Page 87 Consistency of language: "haemorrhage" – corrected to "hemorrhage"

Page 87 Consistency of language: "centre" – corrected to "center"

Page 88 Consistency of language: "haemorrhage" – corrected to "hemorrhage"

Page 88 Consistency of language: "tumour" – corrected to "tumor"

Page 89 Consistency of language: "tumour" – corrected to "tumor"

Page 90 Consistency of language: "tumour" – corrected to "tumor"

Page 90 Consistency of language: "tumours" – corrected to "tumors"

Page 91 Consistency of language: "centre" – corrected to "center"

Page 92 Misplaced full stop: "Hasegawa et. al" – corrected to "Hasegawa et al."

Page 92 Misspelling: "and and" – corrected to "and"

Page 95 Consistency of language: "tumours" – corrected to "tumors"

Page 95 Consistency of language: "tumour" – corrected to "tumor"

Page 95 Grammatical error: "However, there were no events brainstem damage in this cohort either" – corrected to "However, there were no events of brainstem damage in this cohort either"

Page 95 Misspelling: "by by" – corrected to "by"

Page 99 Misspelling: "constrainst" – corrected to "constraints"

Page 100 Consistency of language: "tumour" – corrected to "tumor"

Page 101 Consistency of language: "multicentre" – corrected to "multicenter"

Graphic design: Communication Division, UiB / Print: Skipnes Kommunikasjon AS

uib.no

ISBN: 9788230854396 (print)
9788230865613 (PDF)